

1510 **Chapter 3**  
1511 **Classical Cyclotron**

1512 **Abstract** This chapter introduces the classical cyclotron, and the theoretical material  
1513 needed for the simulation exercises. It begins with a brief reminder of the historical  
1514 context, and continues with beam optics and with the principles and methods which  
1515 the classical cyclotron leans on, including  
1516 - ion orbit in a cyclic accelerator,  
1517 - weak focusing and periodic transverse motion,  
1518 - revolution period and isochronism,  
1519 - voltage gap and resonant acceleration,  
1520 - the cyclotron equation.

1521 The simulation of a cyclotron dipole will either resort to an analytical model of the  
1522 field: the optical element DIPOLE, or will resort to using a field map together with  
1523 the keyword TOSCA to handle it and raytrace through. An additional accelerator  
1524 device needed in the exercises, CAVITE, simulates a local oscillating voltage. Run-  
1525 ning a simulation generates a variety of output files, including the execution listing  
1526 zgoubi.res, always, and other zgoubi.plt, zgoubi.CAVITE.out, zgoubi.MATRIX.out,  
1527 etc., aimed at looking up program execution, storing data for post-treatment, produc-  
1528 ing graphs, etc. Additional keywords are introduced as needed, such as the matching  
1529 procedure FIT[2]; FAISCEAU and FAISTORE which log local particle data in  
1530 zgoubi.res or in a user defined ancillary file; MARKER; the 'system call' command  
1531 SYSTEM; REBELOTE, a 'do loop'; and some more. This chapter introduces in addi-  
1532 tion to spin motion in accelerator magnets; dedicated simulation exercises include a  
1533 variety of keywords: SPNTRK, a request for spin tracking, SPNPRT or FAISTORE,  
1534 to log spin vector components in respectively zgoubi.res or some ancillary file, and  
1535 the "IL=2" flag to log stepwise particle data, including spin vector, in zgoubi.plt file.  
1536 Simulations include deriving transport matrices, beam matrix, optical functions and  
1537 their transport, from rays, using MATRIX and TWISS keywords.

1538 **Notations used in the Text**

$B; B_0$	magnetic field; at a reference radius $R_0$
$\mathbf{B}; B_R; B_y$	field vector; radial component; axial component
$BR = p/q$	magnetic rigidity
$C; C_0$	orbit length, $C = 2\pi R$ ; reference, $C_0 = 2\pi R_0$
$E$	ion energy, $E = \gamma m_0 c^2$
$f_{\text{rev}}, f_{\text{rf}}$	revolution and RF voltage frequencies
$G$	gyromagnetic anomaly, $G = 1.7928$ for proton, $-4.184$ for helion
$h$	harmonic number, an integer, $h = f_{\text{rf}}/f_{\text{rev}}$
$k = \frac{R}{B} \frac{dB}{dR}$	radial field index
$m; m_0; M$	ion mass; rest mass; in units of $\text{MeV}/c^2$
$\mathbf{p}; p; p_0$	ion momentum vector; its modulus; reference
$q$	ion charge
$R; R_0; R_E$	equilibrium orbit radius; reference, $R(p_0)$ ; at energy $E$
$RF$	Radio-Frequency
1539 $s$	path variable
$T_{\text{rev}}, T_{\text{rf}}$	revolution and accelerating voltage periods
$\mathbf{v}; v$	ion velocity vector; its modulus
$V(t); \hat{V}$	oscillating voltage; its peak value
$W$	kinetic energy, $W = \frac{1}{2}mv^2$
$x, x', y, y'$	radial and axial coordinates $\left[ (*)' = \frac{d(*)}{ds} \right]$
$\alpha$	trajectory deviation, or momentum compaction
$\beta = \frac{v}{c}; \beta_0; \beta_s$	normalized ion velocity; reference; synchronous
$\gamma = E/m_0c^2$	Lorentz relativistic factor
$\Delta p, \delta p$	momentum offset
$\varepsilon_u$	Courant-Snyder invariant ( $u : x, r, y, l, Y, Z, s, \text{etc.}$ )
$\theta$	azimuthal angle
$\phi$	RF phase at ion arrival at the voltage gap

1540 **3.1 Introduction**

1541 Cyclotrons are the most widespread type of accelerator, today, used by thousands,  
 1542 with the production of isotopes as the dominant application. This chapter is devoted  
 1543 to the first cyclic accelerator: the early 1930s *classical* cyclotron which its concept  
 1544 limited to low energy, a few 10s of  $\text{MeV}/\text{nucleon}$ . This limitation overcome a decade  
 1545 later by the azimuthally varying field (AVF) technique, this is the subject of the next  
 1546 chapter.

1547 The classical cyclotron is based on four main principles:

1548 (i) the use of a cylindrical-symmetry magnetic field in the gap of an electromagnet  
 1549 (Fig. 3.1) to maintain ions on a circular trajectory

- 1550 (ii) transverse vertical confinement of the beam obtained by a slow radial decrease  
 1551 of the magnetic field. A technique known as weak focusing, applied over the years  
 1552 in all cyclic accelerators: microtron, betatron, synchrocyclotron, synchrotron. These  
 1553 weak focusing accelerator species all are still part of the landscape today  
 1554 (iii) resonant acceleration by synchronization of a fixed-frequency accelerating volt-  
 1555 age on the quasi-constant revolution time (Fig. 3.1). and  
 1556 (iv) use of high voltage, to mitigate the effect of the turn-by-turn RF phase slip.

1557 Resonant acceleration has the advantage that a small gap voltage is enough to  
 1558 accelerate with, in principle, no energy limitation, by contrast with the electrostatic  
 1559 techniques developed at the time, which required the generation of the full voltage,  
 1560 such as the Van de Graaf which was limited by sparking at a few tens of megavolts.

1561 The cyclotron concept goes back to the late 1920s [1], yet it was not until the early  
 1562 1930s when a cyclotron was first brought to operation [2]. The principles are sum-  
 1563 marized in Fig. 3.1: an oscillating voltage is applied on a pair of electrodes (“dees”)  
 1564 forming an accelerating gap and placed between the two poles of an electromagnet.  
 1565 Ions reaching the gap during the acceleration phase of the voltage wave experience  
 1566 an energy boost; no field is experienced inside the dees. Under the effect of energy  
 1567 increase at the gap every half-revolution, they spiral out in the quasi-constant field  
 of the dipole.

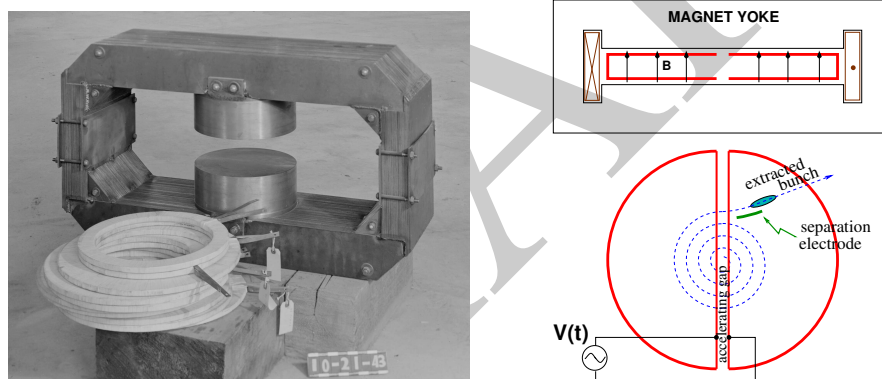


**Fig. 3.1** Left: a cyclotron electromagnet, namely here that used for a model of Berkeley’s 184-inch cyclotron in the early 1940s [3]. Magnetic field in the gap decreases with radius. Right: a schematic of the resonant acceleration motion; gap after gap, accelerated ions spiral out (bottom) in the quasi-uniform field (top). A double-dee (or, a variant, a single-dee facing a slotted electrode) forms an accelerating gap. The fixed-frequency oscillating voltage  $V(t)$  applied is a harmonic of the revolution frequency. Ions experiencing proper voltage phase at the gap, turn by turn, are accelerated. A septum electrode allows beam extraction

1568 The first cyclotron achieved acceleration of  $H_2^+$  hydrogen ions to 80 keV [2], at  
 1569 Berkeley in 1931. The apparatus used a dee-shaped electrode vis-à-vis a slotted  
 1570 electrode forming a voltage gap, the ensemble housed in a 5 in diameter vacuum  
 1571 chamber and placed in the 1.3 Tesla field of an electromagnet. A  $\approx 12$  MHz vacuum  
 1572 tube oscillator provided 1 kVolt gap voltage.  
 1573

1574 One goal foreseen in developing this technology was the acceleration of protons  
 1575 to MeV energy range for the study of atom nucleus. And in background, a wealth  
 1576 of potential applications. An 11 in cyclotron followed which delivered a  $0.01 \mu\text{A}$   
 1577  $\text{H}_2^+$  beam at 1.22 MeV [4], and a 27 in cyclotron later reached 6 MeV (Fig. 3.2) [5].  
 1578 Targets were mounted at the periphery of the 11-inch cyclotron, disintegrations were  
 1579 observed in 1932. And, in 1933: *'The neutron had been identified by Chadwick*  
 1580 *in 1932. By 1933 we were producing and observing neutrons from every target*  
 1581 *bombarded by deuterons.'* [5, M.S. Livingston, p. 22].

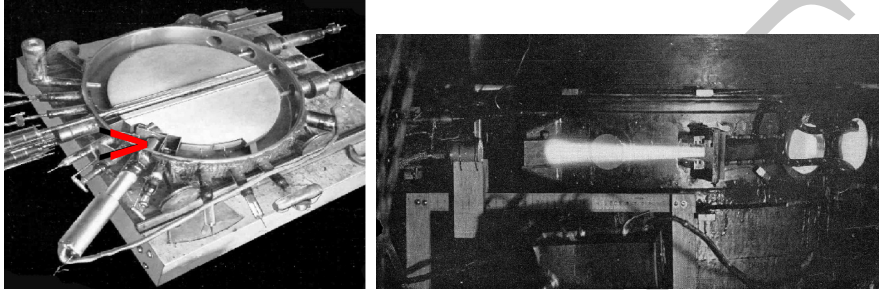
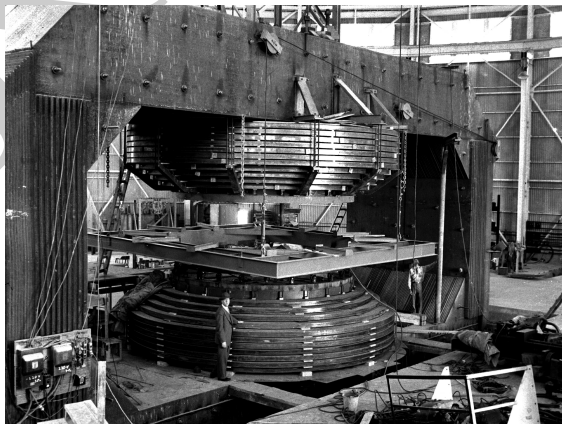


**Fig. 3.2** Berkeley 27-inch cyclotron, brought to operation in 1934, accelerated deuterons up to 6 MeV. Left: a double-dee (seen in the vacuum chamber, cover off), 22 in diameter, creates an accelerating gap: 13 kV, 12 MHz radio frequency voltage is applied for deuterons for instance (through two feed lines seen at the top right corner). This apparatus was dipped in the 1.6 Tesla dipole field of a 27 in diameter, 75 ton, electromagnet. A slight decrease of the dipole field with radius, from the center of the dipole, ensures axial beam focusing. With their energy increasing, ions spiral out from the center to eventually strike a target (red arrow). Right: ionization of the air by the extracted beam (1936); the view also shows the vacuum chamber squeezed between the pole pieces of the electromagnet [3]

**Fig. 3.3** Berkeley 184 in diameter, 4,000 ton cyclotron during construction [3]. The coil windings around both of the magnetic poles are clearly visible. Following the invention of longitudinal focusing it was actually operated as a synchrocyclotron, in 1946. The man on the right gives the scale





1582 A broad range of applications were foreseen: “*At this time biological experiments*  
1583 *were started. [...] Also at about this same time the first radioactive tracer experiments*  
1584 *on human beings were tried [...] simple beginnings of therapeutic use, coming a*  
1585 *little bit later, in which neutron radiation was used, for instance, in the treatment*  
1586 *of cancer. [...] Another highlight from 1936 was the first time that anyone tried*  
1587 *to make artificially a naturally occurring radio-nuclide. (a bismuth isotope) [5,*  
1588 *McMillan, p. 26].*

1589 Berkeley’s 184 in cyclotron, the largest (Fig. 3.3), commissioned in 1941, was to  
1590 accelerate Deuterons to 100 MeV for meson production. It’s magnet however was  
1591 diverted to the production of uranium for the atomic bomb during the second world  
1592 war years [1]. Re-started in 1946, as a consequence of the discovery of phase focusing  
1593 the accelerator was actually operated as a synchrocyclotron (an accelerator species  
1594 addressed in Chap. 7).

### 1595 *Limitation in energy*

1596 The understanding of the dynamics of ions in the classical cyclotron took some time,  
1597 and brought two news, a bad one and a good one,

1598 (i) the bad one first: the energy limitation. A consequence of the loss of isochro-  
1599 nism resulting from the relativistic increase of the ion mass so that “[...] *it seems*  
1600 *useless to build cyclotrons of larger proportions than the existing ones [...] an accel-*  
1601 *erating chamber of 37 in radius will suffice to produce deuterons of 11 MeV energy*  
1602 *which is the highest possible [...] [6], or in a different form: “If you went to graduate*  
1603 *school in the 1940s, this inequality ( $-1 < k < 0$ ) was the end of the discussion of*  
1604 *accelerator theory” [7].*

1605 (ii) the good news now: the energy limit which results from the mass increase can  
1606 be removed by splitting the magnetic pole into valley and hill field sectors. This is  
1607 the azimuthally varying field (AVF) cyclotron technology, due to L.H. Thomas in  
1608 1938 [8]. It took some years to see effects of this breakthrough (Fig. 3.4). The AVF  
1609 is the object of Chap. 4.

1610 With the progress in magnet computation tools, in computer speed and in beam  
1611 dynamics simulations, the AVF cyclotron ends up being essentially as simple to  
1612 design and build: it has in a general manner supplanted the classical cyclotron in all  
1613 energy domains (Fig. 3.4).

## 1614 **3.2 Basic Concepts and Formulæ**

1615 The cyclotron was conceived as a means to overcome the technological difficulty of  
1616 a long series of high electrostatic voltage electrodes in a linear layout, by, instead,  
1617 repeated recirculation through a single accelerating gap in synchronism with an  
1618 oscillating voltage (Fig. 3.5). As the accelerated bunch spirals out in the uniform  
1619 magnetic field, the velocity increase comes with an increase in orbit length; the

**Fig. 3.4** Evolution of the number of the various cyclotron species, over the years [9]. From the 1950s on the AVF cyclotron rapidly supplanted the 1930s' classical cyclotron

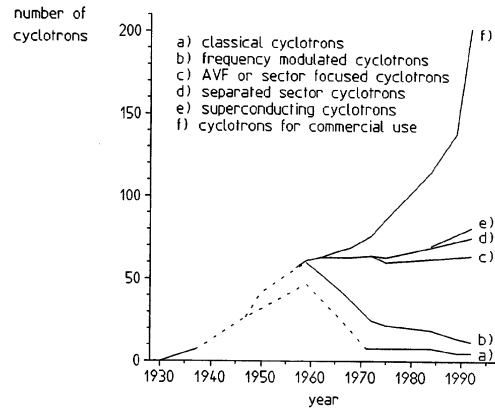


**Fig. 3.5** Resonant acceleration: in an  $h = 1$  configuration an ion bunch meets an oscillating field  $\mathbf{E}$  across gap A, at time  $t$ , at an accelerating phase; it meets again, half a turn later, at time  $t + T_{rev}/2$ , the accelerating phase across gap A', and so on: the magnetic field recirculates the bunch through the gap, repeatedly. Higher harmonic allows more bunches: the next possibility in the present configuration is  $h=3$ , and 3 bunches, 120 degrees apart, in synchronism with  $\mathbf{E}$

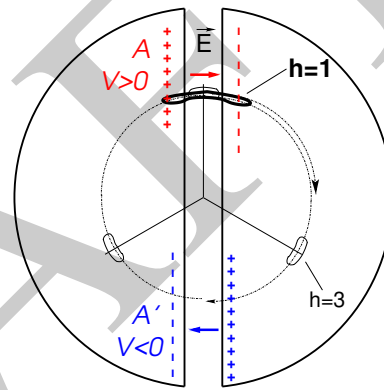
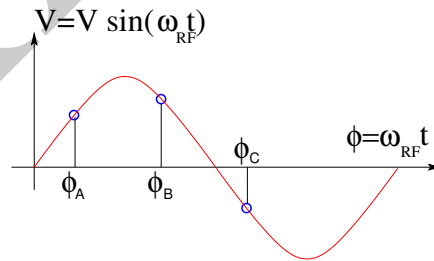


**Fig. 3.6** An ion which reaches the double-dee gap at the RF phase  $\omega_{rf}t = \phi_A$  or  $\omega_{rf}t = \phi_B$  is accelerated. If it reaches the gap at  $\omega_{rf}t = \phi_C$  it is decelerated



1620 net result is a slow increase of the revolution period  $T_{\text{rev}}$  with energy, yet, with  
 1621 appropriate fixed  $f_{\text{rf}} \approx h/T_{\text{rev}}$  the revolution motion and the oscillating voltage can  
 1622 be maintained in sufficiently close synchronism,  $T_{\text{rev}} \approx T_{\text{rf}}/h$ , that the bunch will  
 1623 transit the voltage gap at an accelerating phase (Fig. 3.6) over a large enough number  
 1624 of turns that it acquires a significant energy boost.

1625 The orbital motion quantities: radius  $R$ , ion rigidity  $BR$ , revolution frequency  
 1626  $f_{\text{rev}}$ , satisfy

$$BR = \frac{p}{q}, \quad 2\pi f_{\text{rev}} = \omega_{\text{rev}} = \frac{v}{R} = \frac{qB}{m} = \frac{qB}{\gamma m_0} \quad (3.1)$$

1627 These relationships hold at all  $\gamma$ , so covering the *classical* cyclotron domain ( $v \ll c$ ,  
 1628  $\gamma \approx 1$ ) as well as the *isochronous* cyclotron (in which the ion energy increase is  
 1629 commensurate with its mass). To give an idea of the revolution frequency, in the  
 1630 limit  $\gamma = 1$ , for protons, one has  $f_{\text{rev}}/B = q/2\pi m = 15.25 \text{ MHz/T}$ .

1631 The cyclotron design sets the constant RF frequency  $f_{\text{rf}} = \omega_{\text{rf}}/2\pi$  at an interme-  
 1632 diate value of  $hf_{\text{rev}}$  along the acceleration cycle. The energy gain, or loss, by the ion  
 1633 when transiting the gap, at time  $t$ , is

$$\Delta W(t) = q\hat{V} \sin \phi(t) \quad \text{with} \quad \phi(t) = \omega_{\text{rf}}t - \omega_{\text{rev}}t + \phi_0 \quad (3.2)$$

1634 with  $\phi$  its phase with respect to the RF signal at the gap (Fig. 3.6),  $\phi_0 = \phi(t=0)$ ,  
 1635 and  $\omega_{\text{rev}}t$  the orbital angle. Assuming constant field  $B$ , the increase of the revolution  
 1636 period with ion energy satisfies

$$\frac{\Delta T_{\text{rev}}}{T_{\text{rev}}} = \gamma - 1 \quad (3.3)$$

1637 The mis-match so induced between the RF and cyclotron frequencies is a turn-by-turn  
 1638 cumulative effect and sets a limit to the tolerable isochronism defect,  $\Delta T_{\text{rev}}/T_{\text{rev}} \approx$   
 1639  $2 - 3\%$ , or highest velocity  $\beta = v/c \approx 0.22$ . This results for instance in a practical  
 1640 limitation to  $\approx 25 \text{ MeV}$  for protons, and  $\approx 50 \text{ MeV}$  for D and  $\alpha$  particles, a limit  
 1641 however dependent on energy gain per turn.

1642 Over time multiple-gap accelerating structures were developed, whereby a  
 1643 “multiple- $\Delta$ ” electrode pattern substitutes to a “double-D”. An example is GANIL  
 1644 C0 injector with its 4 accelerating gaps and  $h = 4$  and  $h = 8$  RF harmonic opera-  
 1645 tion [10].

### 1646 3.2.1 Fixed-Energy Orbits, Revolution Period

In a laboratory frame (O;x,y,z), with (O;x,z) the bend plane (Fig. 3.7), assume  
 $\mathbf{B}|_{y=0} = \mathbf{B}_y$ , constant. An ion is launched from the origin with a velocity

$$\mathbf{v} = \left( \frac{dx}{dt}, \frac{dy}{dt}, \frac{dz}{dt} \right) = (v \sin \alpha, 0, v \cos \alpha)$$

at an angle  $\alpha$  from the  $z$ -axis. Solving

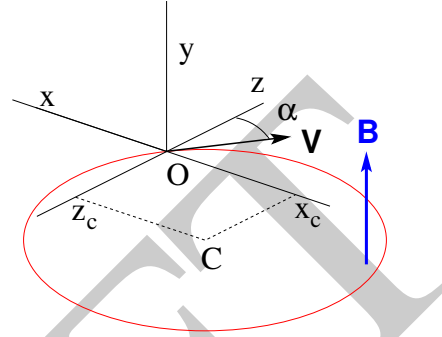


**Fig. 3.7** Circular motion of an ion in the plane normal to a uniform magnetic field  $\mathbf{B}$ . The orbit is centered at  $x_C = -v \cos \alpha / \omega_{\text{rev}}$ ,  $z_C = v \sin \alpha / \omega_{\text{rev}}$ , its radius is  $v / \omega_{\text{rev}}$

1647

$$m\dot{\mathbf{v}} = q\mathbf{v} \times \mathbf{B} \quad (3.4)$$

1648 with  $\mathbf{B} = (0, B_y, 0)$  yields the parametric equations of motion

$$\begin{cases} x(t) = \frac{v}{\omega_{\text{rev}}} \cos(\omega_{\text{rev}}t - \alpha) - \frac{v \cos \alpha}{\omega_{\text{rev}}} \\ y(t) = \text{constant} \\ z(t) = \frac{v}{\omega_{\text{rev}}} \sin(\omega_{\text{rev}}t - \alpha) + \frac{v \sin \alpha}{\omega_{\text{rev}}} \end{cases} \quad (3.5)$$

1649 which result in

$$\left(x + \frac{v \cos \alpha}{\omega_{\text{rev}}}\right)^2 + \left(z - \frac{v \sin \alpha}{\omega_{\text{rev}}}\right)^2 = \left(\frac{v}{\omega_{\text{rev}}}\right)^2 \quad (3.6)$$

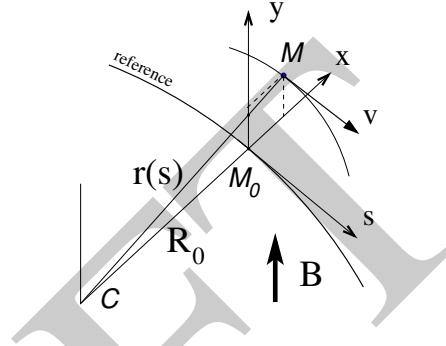
1650 a circular trajectory of radius  $R = v / \omega_{\text{rev}}$  centered at  $(x_C, z_C) = \left(-\frac{v \cos \alpha}{\omega_{\text{rev}}}, \frac{v \sin \alpha}{\omega_{\text{rev}}}\right)$ .

1651 *Stability of the cyclic motion* - The initial velocity vector defines a reference closed  
 1652 orbit in the median plane of the cyclotron dipole; a small perturbation in  $\alpha$  or  $v$   
 1653 results in a new orbit *in the vicinity* of the reference. An axial velocity component  $v_y$   
 1654 on the other hand, causes the ion to drift away from the reference, vertically, linearly  
 1655 with time, as there is no axial restoring force. The next Section will investigate the  
 1656 necessary field property to ensure both horizontal and vertical confinement of the  
 1657 cyclic motion in the vicinity of a reference orbit in the median plane.

### 1658 3.2.2 Weak Focusing

1659 In the early accelerated turns in a classical cyclotron (central region of the electro-  
 1660 magnet, energy up to tens of keV/u), the accelerating electric field provides vertical  
 1661 focusing for particles with proper RF phase [11, Sect. 8], whereas a flat magnetic  
 1662 field with uniformity  $dB/B < 10^{-4}$  is sufficient to maintain isochronism. Beyond  
 1663 this low energy region however, at greater radii, a magnetic field gradient must be  
 1664 introduced to ensure transverse stability: field must decrease with  $R$ .

**Fig. 3.8** Moving frame  $(M_0; s, x, y)$  along the reference circular orbit. The curvature  $1/R_0$  is constant along the orbit and  $(M_0; s, x, y)$  can be considered equivalent to the cylindrical frame  $(C; \theta, R_0, y)$



1665 Ion coordinates in the following are defined in the moving frame  $(M_0; s, x, y)$   
 1666 (Fig. 3.8), which moves along the reference orbit (radius  $R_0$ ), with its origin  $M_0$   
 1667 the projection of ion location  $M$  on the reference orbit; the  $s$  axis is tangent to the  
 1668 latter, the  $x$  axis is normal to  $s$ , the  $y$  axis is normal to the bend plane. Median-plane  
 1669 symmetry of the field is assumed, thus the radial field component  $B_R|_{y=0} = 0$  at all  
 1670  $R$  (Fig. 3.9).

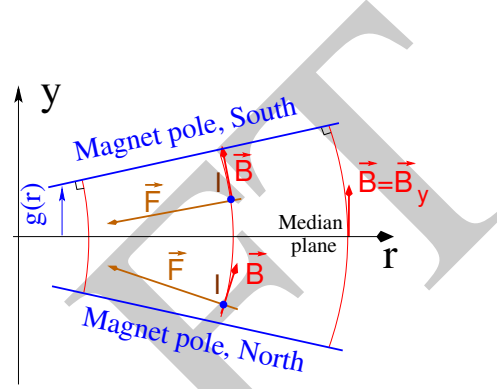
1671 Consider small motion excursions  $x(t) = r(t) - R_0 \ll R_0$ ; introduce Taylor  
 1672 expansion of the field components,

$$\begin{aligned}
 B_y(R_0 + x) &= B_y(R_0) + x \left. \frac{\partial B_y}{\partial R} \right|_{R_0} + \frac{x^2}{2!} \left. \frac{\partial^2 B_y}{\partial R^2} \right|_{R_0} + \dots \approx B_y(R_0) + x \left. \frac{\partial B_y}{\partial R} \right|_{R_0} \\
 B_R(0 + y) &= y \underbrace{\left. \frac{\partial B_R}{\partial y} \right|_0}_{= \left. \frac{\partial B_y}{\partial R} \right|_{R_0}} + \frac{y^3}{3!} \left. \frac{\partial^3 B_R}{\partial y^3} \right|_0 + \dots \approx y \left. \frac{\partial B_y}{\partial R} \right|_{R_0}
 \end{aligned} \quad (3.7)$$

1673 Using these, and noting  $(\dot{*}) = d(*)/dt$ , the linear approximation of the differential  
 1674 equations of motion in the moving frame writes

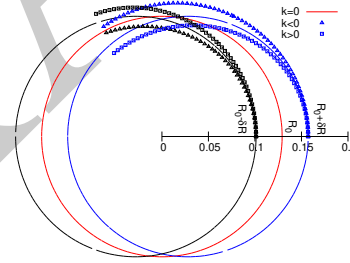
$$\begin{aligned}
 F_x = m\ddot{x} &= -qvB_y(R) + \frac{mv^2}{R_0 + x} \approx -qv \left( B_y(R_0) + \left. \frac{\partial B_y}{\partial R} \right|_{R_0} x \right) + \frac{mv^2}{R_0} \left( 1 - \frac{x}{R_0} \right) \\
 \rightarrow m\ddot{x} &= -\frac{mv^2}{R_0^2} \left( \frac{R_0}{B_0} \left. \frac{\partial B_y}{\partial R} \right|_{R_0} + 1 \right) x \tag{3.8} \\
 F_y = m\ddot{y} &= qvB_R(y) = qv \left. \frac{\partial B_R}{\partial y} \right|_{y=0} y + \text{higher order} \rightarrow m\ddot{y} = qv \frac{\partial B_y}{\partial R} y
 \end{aligned}$$

**Fig. 3.9** Axial motion stability requires proper shaping of field lines:  $B_y$  has to decrease with radius. The Laplace force pulls a positive charge with velocity pointing out of the page, at I, toward the median plane. Increasing the field gradient ( $k$  closer to -1, gap opening up faster) increases the focusing



1675

**Fig. 3.10** Geometrical focusing: take  $k=0$ ; two circular trajectories which start from  $r = R_0 \pm \delta R$  (solid lines, going counter-clockwise) undergo exactly one oscillation around the reference orbit  $r = R_0$ . A negative  $k$  (triangles), for axial focusing, decreases the radial convergence; a positive  $k$  (square markers) increases the radial convergence - and increases vertical divergence



1676

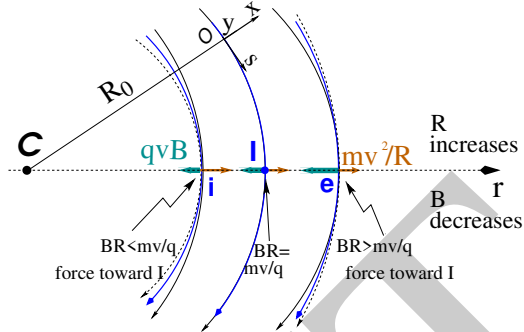
Note  $B_y(R_0) = B_0$  and introduce

$$\omega_R^2 = \omega_{\text{rev}}^2 \left( 1 + \frac{R_0}{B_0} \frac{\partial B_y}{\partial R} \right), \quad \omega_y^2 = -\omega_{\text{rev}}^2 \frac{R_0}{B_0} \frac{\partial B_y}{\partial R} \tag{3.9}$$

1677

substitute in Eqs. 3.8, this yields

**Fig. 3.11** Radial motion stability. Trajectory arcs at  $p = mv$  are represented: case of  $k = 0$  (thin black lines), of  $-1 < k < 0$  (thick blue lines), and of  $k = -1$  (dashed concentric circles).  $k$  decreasing towards  $-1$  reduces the geometrical focusing, increases axial focusing. The resultant of the Laplace and centrifugal forces,  $F_t = -qvB + mv^2/r$ , is zero at I, motion is stable if  $F_t$  is toward I at  $i$ , i.e.  $qvB_i < mv^2/R_i$ , and toward I as well at  $e$ , i.e.  $qvB_e > mv^2/R_e$



$$\ddot{x} + \omega_R^2 x = 0 \quad \text{and} \quad \ddot{y} + \omega_y^2 y = 0 \quad (3.10)$$

1678 A restoring force (linear terms in  $x$  and  $y$ , Eq. 3.10) arises from the radially varying  
1679 field, characterized by a field index

$$k = \frac{R_0}{B_0} \left. \frac{\partial B_y}{\partial R} \right|_{R=R_0, y=0} \quad (3.11)$$

1680 *Radial stability*: radially this force adds to the geometrical focusing (curvature term  
1681 “1” in  $\omega_R^2$ , Eq. 3.9, Fig. 3.10). In the weakly decreasing field  $B(R)$  an ion with mo-  
1682 mentum  $p = mv$  moving in the vicinity of the  $R_0$ -radius reference orbit experiences  
1683 in the moving frame a resultant force  $F_t = -qvB + m \frac{v^2}{r}$  (Fig. 3.11) of which the  
1684 (outward) component  $f_c = m \frac{v^2}{r}$  decreases with  $r$  at a higher rate than the decrease  
1685 of the Laplace (inward) component  $f_B = -qvB(r)$ . In other words, radial stability  
1686 requires  $BR$  to increase with  $R$ ,  $\frac{\partial BR}{\partial R} = B + R \frac{\partial B}{\partial R} > 0$ , this holds in particular at  $R_0$ ,  
1687 thus  $1 + k > 0$ .

1688 *Axial stability* requires a restoring force directed toward the median plane. Refer-  
1689 ring to Fig. 3.9, this means  $F_y = -a \times y$  (with  $a$  a positive quantity) and thus  $B_R < 0$ ,  
1690 at all  $(r, y \neq 0)$ . This is achieved by designing a guiding field which decreases with  
1691 radius,  $\frac{\partial B_R}{\partial y} < 0$ . Referring to Eq. 3.11 this means  $k < 0$ .

1692 From these radial and axial constraints the condition of “weak focusing” for  
1693 transverse motion stability around the circular equilibrium orbit results, namely,

$$-1 < k < 0 \quad (3.12)$$

1694 Note regarding the geometrical focusing: the focal distance associated with the  
1695 curvature of a magnet of arc length  $\mathcal{L}$  is obtained by integrating  $\frac{d^2 x}{ds^2} + \frac{1}{R_0^2} x = 0$  and  
1696 identifying with the focusing property  $\Delta x' = -x/f$ , namely,



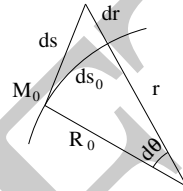
$$\Delta x' = \int \frac{d^2 x}{ds^2} ds \approx \frac{-x}{R^2} \int ds = \frac{-x \mathcal{L}}{R^2}, \text{ thus } f = \frac{R^2}{\mathcal{L}} \quad (3.13)$$

1697 *Isochronism*: the axial focusing constraint,  $B$  decreasing with  $R$ , contributes break-  
 1698 ing the isochronism (in addition to the effect of the mass increase) by virtue of  
 1699  $\omega_{\text{rev}} \propto B$ .

### 1700 Paraxial Transverse Coordinates

1701 Introduce the path variable  $s$  as the independent variable in Eq. 3.10 and neglect the  
 1702 transverse velocity components ( $1 + \frac{x}{R_0} \approx 1$ ,  $y \ll 0$ ) so that

$$ds = [r^2(s)d\theta^2 + dr^2 + dy^2]^{1/2} \approx |\mathbf{v}|dt \quad (3.14)$$



1703 thus the equations of motion in the moving frame (Eq. 3.10) take the form

$$\frac{d^2 x}{ds^2} + \frac{1+k}{R_0^2} x = 0 \quad \text{and} \quad \frac{d^2 y}{ds^2} - \frac{k}{R_0^2} y = 0 \quad (3.15)$$

1704 Given  $-1 < k < 0$  the motion is that of a harmonic oscillator, in both planes, with  
 1705 respective restoring constants  $(1+k)/R_0^2$  and  $-k/R_0^2$ , both positive quantities. The  
 1706 solution is a sinusoidal motion,

$$\begin{cases} r(s) - R_0 = x(s) = x_0 \cos \frac{\sqrt{1+k}}{R_0}(s - s_0) + x'_0 \frac{R_0}{\sqrt{1+k}} \sin \frac{\sqrt{1+k}}{R_0}(s - s_0) \\ r'(s) = x'(s) = -x_0 \frac{\sqrt{1+k}}{R_0} \sin \frac{\sqrt{1+k}}{R_0}(s - s_0) + x'_0 \cos \frac{\sqrt{1+k}}{R_0}(s - s_0) \end{cases} \quad (3.16)$$

$$\begin{cases} y(s) = y_0 \cos \frac{\sqrt{-k}}{R_0}(s - s_0) + y'_0 \frac{R_0}{\sqrt{-k}} \sin \frac{\sqrt{-k}}{R_0}(s - s_0) \\ y'(s) = -y_0 \frac{\sqrt{-k}}{R_0} \sin \frac{\sqrt{-k}}{R_0}(s - s_0) + y'_0 \cos \frac{\sqrt{-k}}{R_0}(s - s_0) \end{cases} \quad (3.17)$$

1708 Radial and axial wave numbers can be introduced,

$$\nu_R = \frac{\omega_R}{\omega_{\text{rev}}} = \sqrt{1+k} \quad \text{and} \quad \nu_y = \frac{\omega_y}{\omega_{\text{rev}}} = \sqrt{-k} \quad (3.18)$$

1709 *i.e.*, the number of sinusoidal oscillations of the paraxial motion about the reference  
 1710 circular orbit over a turn, respectively radial and axial. Both are less than 1: there  
 1711 is less than one sinusoidal oscillation in a revolution. In addition, as a result of the  
 1712 revolution symmetry of the field,

$$\nu_R^2 + \nu_y^2 = 1 \quad (3.19)$$

1713 *Off-Momentum Orbit*

In a structure with revolution symmetry, the equilibrium trajectory at momentum  $\begin{cases} p_0 \\ p = p_0 + \Delta p \end{cases}$  is at radius  $\begin{cases} R_0 \text{ with } B_0 R_0 = \frac{p_0}{q} \\ R \text{ with } BR = \frac{p}{q} \end{cases}$ , where  $\begin{cases} B = B_0 + \left(\frac{\partial B}{\partial x}\right)_0 \Delta x + \dots \\ R = R_0 + \Delta x \end{cases}$   
 On the other hand

$$BR = \frac{p}{q} \Rightarrow \left[ B_0 + \left(\frac{\partial B}{\partial x}\right)_0 \Delta x + \dots \right] (R_0 + \Delta x) = \frac{p_0 + \Delta p}{q}$$

1714 which, neglecting terms in  $(\Delta x)^2$ , and given  $B_0 R_0 = \frac{p_0}{q}$ , leaves  $\Delta x \left[ \left(\frac{\partial B}{\partial x}\right)_0 R_0 + B_0 \right] = \frac{\Delta p}{q}$ . With  $k = \frac{R_0}{B_0} \left(\frac{\partial B}{\partial x}\right)_0$  this yields

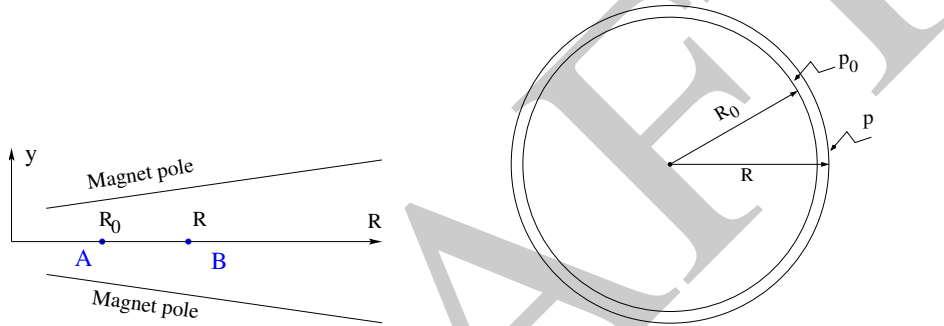


**Fig. 3.12** The equilibrium radius at location A is  $R_0$ , momentum is  $p_0$ , rigidity is  $B_0 R_0$ . The equilibrium radius at B is  $R$ , momentum  $p$ , rigidity  $BR$

1715

$$\Delta x = D \frac{\Delta p}{p_0} \quad \text{with} \quad D = \frac{R_0}{1+k} \quad \text{the dispersion function} \quad (3.20)$$

1716 The dispersion  $D$  is an  $s$ -independent quantity as a result of the revolution symmetry  
 1717 of the field ( $k$  and  $R=p/qB$  are  $s$ -independent).

1718 To the first order in the coordinates, the vertical coordinates  $y(s)$ ,  $y'(s)$  (Eq. 3.17)  
 1719 are unchanged under the effect of a momentum offset, the horizontal trajectory angle  
 1720  $x'(s)$  (Eq. 3.16) is unchanged as well (the circular orbits are concentric, Fig. 3.12)  
 1721 whereas  $x(s)$  satisfies

$$x(s, p_0 + \Delta p) = x(s, p_0) + \Delta p \left. \frac{\partial x}{\partial p} \right|_{s, p_0} = x(s, p_0) + D \frac{\Delta p}{p_0} \quad (3.21)$$

1722 *Orbit and revolution period lengthening*

1723 A  $\delta p$  momentum offset results in (Eq. 3.20)

$$\frac{\delta C}{C} = \frac{\delta R}{R} = \frac{\delta x}{R} = \alpha \frac{\delta p}{p} \quad \text{with} \quad \alpha = \frac{1}{1+k} = \frac{1}{\gamma^2 R} \quad (3.22)$$

1724 with  $\alpha$  the momentum compaction, a positive quantity: orbit length increases with  
1725 momentum. Substituting  $\frac{\delta \beta}{\beta} = \frac{1}{\gamma^2} \frac{\delta p}{p}$ , the change in revolution period  $T_{\text{rev}} = C/\beta c$   
1726 with momentum writes

$$\frac{\delta T_{\text{rev}}}{T_{\text{rev}}} = \frac{\delta C}{C} - \frac{\delta \beta}{\beta} = \left( \alpha - \frac{1}{\gamma^2} \right) \frac{\delta p}{p} \quad (3.23)$$

1727 Given that  $-1 < k < 0$  and  $\gamma \gtrsim 1$ , it results that  $\alpha - 1/\gamma^2 > 0$ : the revolution period  
1728 increases with energy, the increase in radius is faster than the velocity increase.

### 1729 3.2.3 Quasi-Isochronous Resonant Acceleration

1730 The energy  $W$  of an accelerated ion (in the non-relativistic energy domain of the  
1731 classical cyclotron) satisfies the frequency dependence

$$W = \frac{1}{2} m v^2 = \frac{1}{2} m (2\pi R f_{\text{rev}})^2 = \frac{1}{2} m \left( 2\pi R \frac{f_{\text{rf}}}{h} \right)^2 \quad (3.24)$$

1732 Observe in passing: given the cyclotron size (radius  $R$ ),  $f_{\text{rf}}$  and  $h$  set the limit for  
1733 the acceleration range. The revolution frequency decreases with energy and the  
1734 condition of synchronism with the oscillating voltage,  $f_{\text{rf}} = h f_{\text{rev}}$ , is only fulfilled  
1735 at that particular radius where  $\omega_{\text{rf}} = qB/m$  (Fig. 3.13-left). The out-phasing  $\Delta\phi$  of  
1736 the RF at ion arrival at the gap builds-up turn after turn, decreasing in a first stage  
1737 (towards lower voltages in Fig. 3.13-right) and then increasing back to  $\phi = \pi/2$  and  
1738 beyond towards  $\pi$ . Beyond  $\phi = \pi$  the RF voltage is decelerating.

1739 With  $\omega_{\text{rev}}$  constant between two gap passages, differentiating  $\phi(t)$  (Eq. 3.2) yields  
1740  $\dot{\phi} = \omega_{\text{rf}} - \omega_{\text{rev}}$ . Between two gap passages on the other hand,  $\Delta\phi = \dot{\phi}\Delta T = \dot{\phi}T_{\text{rev}}/2 =$   
1741  $\dot{\phi} \frac{\pi R}{v}$ , yielding a phase-shift of

$$\text{half-turn} \quad \Delta\phi = \pi \left( \frac{\omega_{\text{rf}}}{\omega_{\text{rev}}(R)} - 1 \right) = \pi \left( \frac{m\omega_{\text{rf}}}{qB(R)} - 1 \right) \quad (3.25)$$

1742 The out-phasing is thus a gap-after-gap, cumulative effect. Due to this the classical  
1743 cyclotron requires quick acceleration (small number of turns), which means high  
1744 voltage (tens to hundreds of kVolts). As expected, with  $\omega_{\text{rf}}$  and  $B$  constant,  $\phi$  presents  
1745 a minimum ( $\dot{\phi} = 0$ ) at  $\omega_{\text{rf}} = \omega_{\text{rev}} = qB/m$  where exact isochronism is reached  
1746 (Fig. 3.13). The upper limit to  $\phi$  is set by the condition  $\Delta W > 0$ : acceleration.

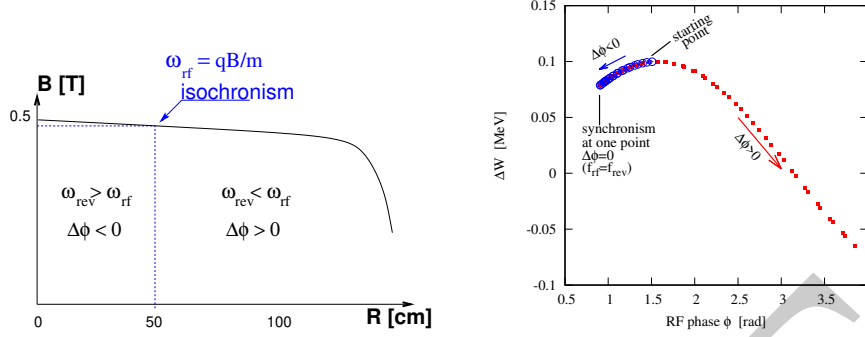
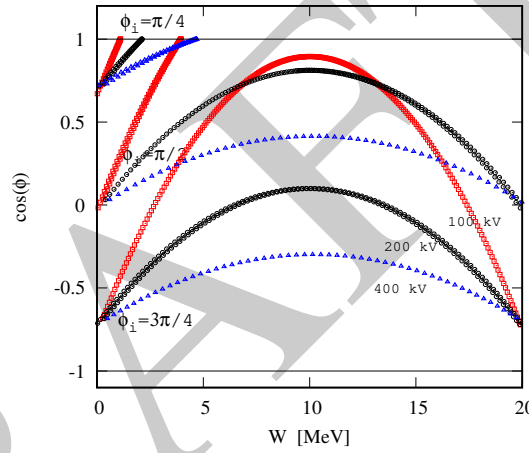


**Fig. 3.13** Left: a sketch of the synchronism condition at one point ( $h=1$  assumed). Right: the span in phase of the energy gain  $\Delta W = q\hat{V} \sin \phi$  (Eq. 3.2) over the acceleration cycle

**Fig. 3.14** A graph of the cyclotron equation (Eq. 3.26), for three different accelerating voltages: 100, 200 and 400 kV/gap (respectively square, circle and triangle markers). The sole settings resulting in  $-1 < \cos \phi(E) < 1$ ,  $\forall E$ , allow complete acceleration to top energy.  $\phi_i = \pi/4$  at injection for instance, does not (upper three curves).  $\phi_i = 3\pi/4$  works (lower three curves), with as low as 100 kV/gap



1747 The cyclotron equation determines the achievable energy range, depending on  
 1748 the injection energy  $E_i$ , the RF phase at injection  $\phi_i$ , the RF frequency  $\omega_{rf}$  and gap  
 1749 voltage  $\hat{V}$ . It writes [12]

$$\cos \phi = \cos \phi_i + \pi \left[ 1 - \frac{\omega_{rf}}{\omega_{rev}} \frac{E + E_i}{2M} \right] \frac{E - E_i}{q\hat{V}} \quad (3.26)$$

1750 Equation 3.26 is represented in Fig. 3.14 for various values of the peak voltage  
 1751 and phase at injection  $\phi_i$ .  $M$  [ $eV/c^2$ ] and  $E$  [ $eV$ ] are respectively the rest mass and  
 1752 relativistic energy,  $q\hat{V}$  is expressed in electron-volts, the index  $i$  denotes injection  
 1753 parameters.

### 1754 3.2.4 Beam Extraction

1755 From  $R = p/qB$  and assuming  $B(R) \approx \text{constant}$  (this is legitimate as  $k$  is normally  
1756 small), in the non-relativistic approximation ( $W \ll M$ ,  $W = p^2/2M$ ) one gets

$$\frac{dR}{R} = \frac{1}{2} \frac{dW}{W} \quad (3.27)$$

1757 Integrating yields

$$R^2 = R_i^2 \frac{W}{W_i} \quad (3.28)$$

1758 with  $R_i, W_i$  initial conditions. From Eqs. 3.27, 3.28, assuming  $W_i \ll W$  and constant  
1759 acceleration rate  $dW$  such that  $W = n dW$  after  $n$  turns, one gets the scaling laws

$$R \propto \sqrt{n}, \quad dR \propto \frac{R}{W} \propto \frac{1}{R} \propto dW, \quad \frac{dR}{dn} = \frac{R}{2n} \quad (3.29)$$

1760 The turn separation  $dR$  is proportional to the energy gain per turn and inversely  
1761 proportional to the orbit radius.

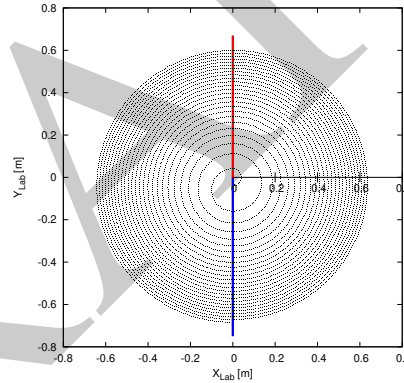


**Fig. 3.15** The radial distance between successive turns decreases with energy, in inverse proportion to the orbit radius. The red and blue segments here figure the accelerating gap

1762 The radial distance between successive turns decreases with energy, toward zero  
1763 (Fig. 3.15), eventually resulting in insufficient spacing for insertion of an extraction  
1764 septum.

#### 1765 *Orbit modulation*

1766 Consider an ion bunch injected in the cyclotron with some  $(x_0, x'_0)$  conditions in  
1767 the vicinity of the reference orbit, and assume slow acceleration. While accelerated  
1768 the bunch undergoes an oscillatory motion around the equilibrium orbit (Eq. 3.16).  
1769 Observed at the extraction septum this oscillation modulates the distance of the

1770 bunch to the local equilibrium orbit, moving it outwards or inwards depending on  
 1771 the turn number, which modulates the distance between the accelerated turns. This  
 1772 effect can be resorted to, so to increase the separation between the final two turns  
 1773 and so enhance the extraction efficiency [9].

### 1774 3.2.5 Spin Dance

1775 “Much of the physics of spin motion can be illustrated using the simplest model of a  
 1776 storage ring consisting of uniform horizontal bending and no straight sections.” [13].

1777 By virtue of this statement, a preliminary introduction to spin motion in magnetic  
 1778 fields is given in the present chapter. In support to this in addition, comes the fact that  
 1779 cyclotrons happened to be the first circular machines to accelerate polarized beams  
 1780 (first acceleration of polarized beams had happened earlier in the 1960s, using  
 1781 electrostatic columns at voltage generators, when polarized proton and deuteron  
 1782 sources began operating [14]).

1783 The magnetic field  $\mathbf{B}$  of the cyclotron dipole exerts a torque on the spin angular  
 1784 momentum  $\mathbf{S}$  of an ion, causing it to precess following the Thomas-BMT differential  
 1785 equation [15]

$$\frac{d\mathbf{S}}{dt} = \mathbf{S} \times \underbrace{\frac{q}{m} [(1+G)\mathbf{B}_{\parallel} + (1+G\gamma)\mathbf{B}_{\perp}]}_{\omega_{\text{sp}}} \quad (3.30)$$

1786 where  $t$  is the time;  $\omega_{\text{sp}}$  the precession vector: a combination of  $\mathbf{B}_{\parallel}$  and  $\mathbf{B}_{\perp}$  compo-  
 1787 nents of  $\mathbf{B}$  respectively parallel and orthogonal to the ion velocity vector.  $G$  is the  
 1788 gyromagnetic anomaly,

1789  $G=1.7928474$  (proton),  $-0.178$  (Li),  $-0.143$  (deuteron),  $-4.184$  ( $^3\text{He}$ ) ...

1790  $\mathbf{S}$  in this equation is in the ion rest frame, all other quantities are in the laboratory  
 1791 frame.

1792 In the case of an ion moving in the median plane of the dipole,  $\mathbf{B}_{\parallel} = 0$ , thus the  
 1793 precession axis is parallel to the magnetic field vector,  $\mathbf{B}_y$ , so that  $\omega_{\text{sp}} = \frac{q}{m} (1 +$   
 1794  $G\gamma)\mathbf{B}_y$ . The spin precession angle over a trajectory arc  $\mathcal{L}$  is

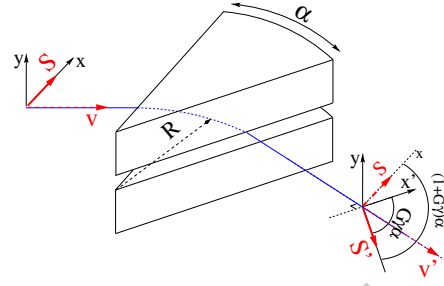
$$\theta_{\text{sp, Lab}} = \frac{1}{v} \int_{(\mathcal{L})} \omega_{\text{sp}} ds = (1+G\gamma) \frac{\int_{(\mathcal{L})} B ds}{BR} = (1+G\gamma)\alpha \quad (3.31)$$

1795 with  $\alpha$  the velocity vector precession (Fig. 3.16). The precession angle in the moving  
 1796 frame (the latter rotates by an angle  $\alpha$  along  $\mathcal{L}$ ) is

$$\theta_{\text{sp}} = G\gamma\alpha \quad (3.32)$$

1797 thus the number of  $2\pi$  spin precessions per ion orbit around the cyclotron is  $G\gamma$ . By  
 1798 analogy with the wave numbers (Eq. 3.18) this defines the “spin tune”

**Fig. 3.16** Spin and velocity vector precession in a constant field, from  $\mathbf{S}$  to  $\mathbf{S}'$  and  $\mathbf{v}$  to  $\mathbf{v}'$  respectively. In the moving frame the spin precession along the arc  $\mathcal{L} = R\alpha$  is  $G\gamma\alpha$ , in the laboratory frame the spin precesses by  $(1 + G\gamma)\alpha$



$$v_{\text{sp}} = G\gamma$$

(3.33)

DRAFT



### 1799 3.3 Exercises

1800 Note: some of the input data files for these simulations are available in zgoubi  
1801 sourceforge repository at

[https://sourceforge.net/p/zgoubi/code/HEAD/tree/branches/exemples/book/zgoubiMaterial/cyclotron\\_classical/](https://sourceforge.net/p/zgoubi/code/HEAD/tree/branches/exemples/book/zgoubiMaterial/cyclotron_classical/)

#### 1803 3.1 Modeling a Cyclotron Dipole: Using a Field Map

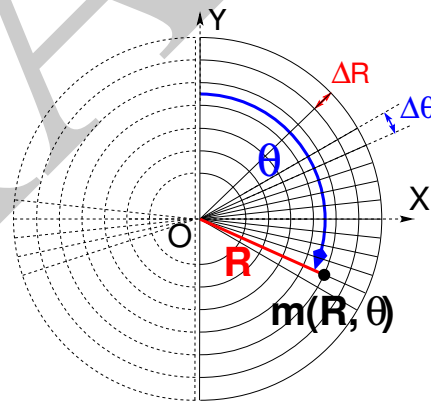
1804 Solution: page 71

1805 In this exercise, ion trajectories are ray-traced, various optical properties addressed  
1806 in the foregoing are recovered, using a field map to simulate the cyclotron dipole.  
1807 Fabricating that field map is a preliminary step of the exercise.

1808 The interest of using a field map is that it is an easy way to account for fancy  
1809 magnet geometries and fields, including field gradients and possible defects. A  
1810 field map can be generated using mathematical field models, or from magnet com-  
1811 putation codes, or from magnetic measurements. The first method is used, here.  
1812 TOSCA[MOD.MOD1=22.1] keyword [16, cf. INDEX] is used to ray-trace through  
1813 the map.

1814 *Working hypotheses:* A 2-dimensional  $m(R, \theta)$  polar meshing of the median plane  
1815 is considered (Fig. 3.17). It is defined in a  $(O; X, Y)$  frame and covers an angular  
1816 sector of a few tens of degrees. The mid-plane field map is the set of values  $B_Z(R, \theta)$   
1817 at the nodes of the mesh. During ray-tracing, TOSCA[MOD.MOD1=22.1] extrapolates  
1818 the field along 3D space  $(R, \theta, Z)$  ion trajectories from the 2D polar map [16].

**Fig. 3.17** Principle of a 2D field map in polar coordinates, covering a  $180^\circ$  sector (over the right hand side dee). The mesh nodes  $m(R, \theta)$  are distant  $\Delta R$  radially,  $\Delta\theta$  azimuthally. The map is used twice to cover the  $360^\circ$  cyclotron dipole as sketched here, while allowing insertion of an accelerating gap between the two dees



1819 (a) Construct a  $180^\circ$  two-dimensional map of a median plane field  $B_Z(R, \theta)$ ,  
1820 proper to simulate the field in a cyclotron as sketched in Fig. 3.1. Use one of  
1821 the following two methods: either (i) write an independent program, or (ii) use  
1822 zgoubi and its analytical field model DIPOLE, together with the keyword OP-  
1823 TIONS[CONSTY=ON] [16, cf. INDEX].

1824 Besides: use a uniform mesh (Fig. 3.17) covering from  $R_{\min}=1$  to  $R_{\max}=76$  cm,  
1825 with radial increment  $\Delta R = 0.5$  cm, azimuthal increment  $\Delta\theta = 0.5$  [cm]/ $R_0$  with  $R_0$

1826 some reference radius (say, 50 cm, in view of subsequent exercises), and constant  
 1827 axial field  $B_Z = 5$  kG. The appropriate 6-column formatting of the field map data  
 1828 for TOSCA[MOD.MOD1=22.1] to read is the following:

1829  $R \cos \theta, Z, R \sin \theta, BY, BZ, BX$

1830 with  $\theta$  varying first,  $R$  varying second;  $Z$  is the vertical direction (normal to the map  
 1831 mesh),  $Z \equiv 0$  in the present case. Note that proper functioning of TOSCA requires  
 1832 the field map to begin with the following line of numerical values:

1833 Rmin [cm]  $\Delta R$  [cm]  $\Delta \theta$  [deg]  $Z$  [cm]

1834 Produce a graph of the  $B_Z(R, \theta)$  field map content.

1835 (b) Ray-trace a few concentric circular mid-plane trajectories centered on the  
 1836 center of the dipole, ranging in  $10 \leq R \leq 80$  cm. Produce a graph of these concentric  
 1837 trajectories in the  $(O; X, Y)$  laboratory frame.

1838 Initial coordinates can be defined using OBJET, particle coordinates along tra-  
 1839 jectories during the stepwise ray-tracing can be logged in zgoubi.plt by setting IL=2  
 1840 under TOSCA. In order to find the Larmor radius corresponding to a particular  
 1841 momentum, the matching procedure FIT can be used. In order to repeat the latter for  
 1842 a series of different momenta, REBELOTE[IOPT=1] can be used.

1843 Explain why it is possible to push the ray-tracing beyond the 76 cm radial extent  
 1844 of the field map.

1845 (c) Compute the orbit radius  $R$  and the revolution period  $T_{\text{rev}}$  as a function of  
 1846 kinetic energy  $W$  or rigidity  $BR$ . Produce a graph, including for comparison the  
 1847 theoretical dependence of  $T_{\text{rev}}$ .

1848 (d) Check the effect of the density of the mesh (the choice of  $\Delta R$  and  $\Delta \theta$  values,  
 1849 *i.e.*, the number of nodes  $N_\theta \times N_R = (1 + \frac{180^\circ}{\Delta \theta}) \times (1 + \frac{80 \text{ cm}}{\Delta R})$ ), on the accuracy of the  
 1850 trajectory and time-of-flight computation.

1851 (e) Check the effect of the integration step size on the accuracy of the trajectory  
 1852 and time-of-flight computation, by considering a small  $\Delta s = 1$  cm and a large  
 1853  $\Delta s = 10$  cm, at 200 keV and 5 MeV (proton), and comparing with theory.

1854 (f) Consider a periodic orbit, thus its radius  $R$  should remain unchanged after  
 1855 stepwise integration of the motion over a turn. However, the size  $\Delta s$  of the numerical  
 1856 integration step has an effect on the final value of the radius:

1857 For two different cases, 200 keV (a small orbit) and 5 MeV (a larger one), provide a  
 1858 graph of the dependence of the relative error  $\delta R/R$  after one turn, on the integration  
 1859 step size  $\Delta s$  (consider a series of  $\Delta s$  values in a range  $\Delta s : 0.1 \text{ mm} \rightarrow 20 \text{ cm}$ ).  
 1860 REBELOTE[IOPT=1] do-loop can be used to repeat the one-turn raytracing with  
 1861 different  $\Delta s$ .

### 1862 3.2 Modeling a Cyclotron Dipole: Using an Analytical Field Model

1863 Solution: page 80

1864 This exercise is similar to exercise 3.1, yet using the analytical modeling DIPOLE,  
 1865 instead of a field map. DIPOLE provides the  $Z$ -parallel median plane field  $\mathbf{B}(R, \theta, Z =$   
 1866  $0) \equiv \mathbf{B}_Z(R, \theta, Z = 0)$  at the projected  $m(R, \theta, Z = 0)$  ion location (Fig. 3.18), while  
 1867  $\mathbf{B}(R, \theta, Z)$  at particle location is obtained by extrapolation.

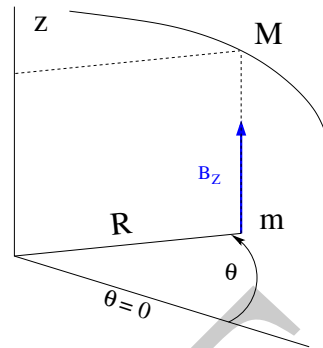


**Fig. 3.18** DIPOLE provides the value  $B_Z(m)$  of the median plane field at  $m$ , projection of particle position  $M(R, \theta, Z)$  in the median plane.  $\mathbf{B}(R, \theta, Z)$  is obtained by extrapolation

1868 (a) Simulate a  $180^\circ$  sector dipole; DIPOLE requires a reference radius [16,  
1869 Eqs. 6.3.19-21], noted  $R_0$  here; for the sake of consistency with other exercises, it is  
1870 suggested to take  $R_0 = 50$  cm. Take a constant axial field  $B_Z = 5$  kG.

1871 Explain the various data that define the field simulation in DIPOLE: geometry,  
1872 role of  $R_0$ , field and field indices, fringe fields, integration step size, etc.

1873 Produce a graph of  $B_Z(R, \theta)$ .

1874 (b) Repeat question (b) of exercise 3.1.

1875 (c) Repeat question (c) of exercise 3.1.

1876 (d) As in question (e) of exercise 3.1, check the effect of the integration step size  
1877 on the accuracy of the trajectory and time-of-flight computation.

1878 Repeat question (f) of exercise 3.1.

1879 (e) From the two series of results (exercise 3.1 and the present one), comment on  
1880 various pros and cons of the two methods, field map versus analytical field model.

### 1881 3.3 Resonant Acceleration

1882 Solution: page 84

1883 Based on the earlier exercises, using indifferently a field map (TOSCA) or an  
1884 analytical model of the field (DIPOLE), introduce a sinusoidal voltage between the  
1885 two dees, with peak value 100 kV. Assume that ion motion does not depend on RF  
1886 phase: the boost through the gap is the same at all passes, use CAVITE[IOPT=3] [16,  
1887 cf. INDEX] for that. Note that using CAVITE requires prior PARTICUL in order to  
1888 specify ion species and data, necessary to compute the energy boost (Eq. 3.2).

1889 (a) Accelerate a proton with initial kinetic energy 20 keV, up to 5 MeV, take  
1890 harmonic  $h=1$ . Produce a graph of the accelerated trajectory in the laboratory frame.

1891 (b) Provide a graph of the proton momentum  $p$  and total energy  $E$  as a function  
1892 of its kinetic energy, both from this numerical experiment (ray-tracing data can be  
1893 stored using FAISTORE) and from theory, all on the same graph.

1894 (c) Provide a graph of the normalized velocity  $\beta = v/c$  as a function of kinetic  
1895 energy, both numerical and theoretical, and in the latter case both classical and  
1896 relativistic.

1897 (d) Provide a graph of the relative change in velocity  $\Delta\beta/\beta$  and orbit length  $\Delta C/C$   
 1898 as a function of kinetic energy, both numerical and theoretical. From their evolution,  
 1899 conclude that the time of flight increases with energy.

1900 (e) Repeat the previous questions, assuming a harmonic  $h=3$  RF frequency.

### 1901 3.4 Spin Dance

1902 Solution: page 88

1903 Cyclotron modeling in the present exercise can use Exercise 3.1 or Exercise 3.2  
 1904 technique (*i.e.*, a field map or an analytical field model), indifferently.

1905 (a) Add spin transport, using SPNTRK [16, *cf.* INDEX]. Produce a listing  
 1906 (zgoubi.res) of a simulation, including spin outcomes.

1907 Note: PARTICUL is necessary here, for the spin equation of motion (Eq. 3.30) to  
 1908 be solved [16, Sect. 2]. SPNPRT can be used to have local spin coordinates listed in  
 1909 zgoubi.res (at the manner that FAISCEAU lists local particle coordinates).

1910 (b) Consider proton case, take initial spin longitudinal, compute the spin preces-  
 1911 sion over one revolution, as a function of energy over a range 12 keV  $\rightarrow$  5 MeV. Give  
 1912 a graphical comparison with theory.

1913 FAISTORE can be used to store local particle data, which include spin coord-  
 1914 inates, in a zgoubi.fai style output file. IL=2 [16, *cf.* INDEX] (under DIPOLE or  
 1915 TOSCA, whichever modeling is used) can be used to obtain a print out of particle  
 1916 and spin motion data to zgoubi.plt during stepwise integration.

1917 (c) Inject a proton with longitudinal initial spin  $S_i$ . Give a graphic of the lon-  
 1918 gitudinal spin component value as a function of azimuthal angle, over a few turns  
 1919 around the ring. Deduce the spin tune from this computation. Repeat for a couple of  
 1920 different energies.

1921 Place both FAISCEAU and SPNPRT commands right after the first dipole sector,  
 1922 and use them to check the spin rotation and its relationship to particle rotation, right  
 1923 after the first passage through that first sector.

1924 (d) Spin dance: the input data file optical sequence here is assumed to model a  
 1925 full turn. Inject an initial spin at an angle from the horizontal plane (this is in order  
 1926 to have a non-zero vertical component), produce a 3-D animation of the spin dance  
 1927 around the ring, over a few turns.

1928 (e) Repeat questions (b-d) for two additional ions: deuteron (much slower spin  
 1929 precession),  ${}^3\text{He}^{2+}$  (much faster spin precession).

### 1930 3.5 Synchronized Spin Torque

1931 Solution: page 94

1932 A synchronized spin kick is superimposed on orbital motion. An input data file for  
 1933 a complete cyclotron is considered as in question 3.4 (d), for instance six 60 degree  
 1934 DIPOLEs, or two 180 degree DIPOLEs.

1935 Insert a local spin rotation of a few degrees around the longitudinal axis, at the  
 1936 end of the optical sequence (*i.e.*, after one orbit around the cyclotron). SPINR can be  
 1937 used for that, rather than a local magnetic field, so to avoid any orbital effect. Track  
 1938 4 particles on their respective equilibrium orbit, with energies 0.2, 108.412, 118.878  
 1939 and 160.746 MeV.

1940 Produce a graph of the motion of the vertical spin component  $S_y$  along the circular  
1941 orbit.

1942 Produce a graph of the spin vector motion on a sphere.

### 1943 3.6 Weak Focusing

1944 Solution: page 97

1945 (a) Consider a  $60^\circ$  sector as in earlier exercises (building a field map and using  
1946 TOSCA as in exercise 3.1, or using DIPOLE as in exercise 3.2), construct the sector  
1947 accounting for a non-zero radial index  $k$  in order to introduce axial focusing, say  
1948  $k = -0.03$ , assume a reference radius  $R_0$  for a reference energy of 200 keV ( $R_0$  and  
1949  $B_0$  are required in order to define the index  $k$ , Eq. 3.11). Ray-trace that 200 keV  
1950 reference orbit, plot it in the lab frame: make sure it comes out as expected, namely,  
1951 constant radius, final and initial angles zero.

1952 (b) Using FIT[2], find and plot the radius dependence of orbit rigidity,  $BR(R)$ ,  
1953 from ray-tracing over a  $BR$  range covering 20 keV to 5 MeV; superpose the theoretical  
1954 curve. REBELOTE[IOPT=1] can be used to perform the scan.

1955 (c) Produce a graph of the paraxial axial motion of a 1 MeV proton, over a few  
1956 turns (use IL=2 under TOSCA, or DIPOLE, to have step by step particle and field  
1957 data logged in zgoubi.plt). Check the effect of the focusing strength by comparing  
1958 the trajectories for a few different index values, including close to -1 and close to 0.

1959 (d) Produce a graph of the magnetic field experienced by the ion along these  
1960 trajectories.

### 1961 3.7 Loss of Isochronism

1962 Solution: page 106

1963 Compare on a common graphic the revolution period  $T_{\text{rev}}(R)$  for a field index  
1964 value  $k \approx -0.95, -0.5, -0.03, 0^-$ . The scan method of exercise 3.6, based on  
1965 REBELOTE[IOPT=1] preceded by FIT[2], can be referred to.

### 1966 3.8 Ion Trajectories

1967 Solution: page 108

1968 In this exercise individual ion trajectories are computed. DIPOLE or TOSCA  
1969 magnetic field modeling can be used, indifferently. No acceleration here, ions circle  
1970 around the cyclotron at constant energy.

1971 (a) Produce a graph of the horizontal  $x(s)$  and vertical  $y(s)$  trajectory coordinates  
1972 of an ion with rigidity close to  $BR(R_0)$  ( $R_0$  is the reference radius in the definition of  
1973 the index  $k$ ), over a few turns around the cyclotron. From the number of turns, give  
1974 an estimate of the wave numbers. Check the agreement with the expected  $\nu_R(k)$ ,  
1975  $\nu_y(k)$  values (Eq. 3.18).

1976 (b) Consider now protons at 1 MeV and 5 MeV, far from the reference energy  
1977  $E(R_0)$ ; the wave numbers change with energy: consistency with theory can be  
1978 checked. Find their theoretical values, compare with numerical outcomes.

1979 (c) Consider proton, 200 keV energy, plot as a function of  $s$  the difference between  
1980  $x(s)$  from raytracing and its values from Eq. 3.16. Same for  $y(s)$  compared to Eq. 3.17.

1981 IL=2 can be used to store in zgoubi.plt the step-by-step particle coordinates across  
1982 DIPOLE.

1983 (d) Perform a scan of the wave numbers over 200 keV–5 MeV energy inter-  
1984 val, computed using OBJET[KOBJ=5] and MATRIX[IORD=1,IFOC=11], or OB-  
1985 JET[KOBJ=6] and MATRIX[IORD=2,IFOC=11], together with REBELOTE[IOPT=1]  
1986 to repeat MATRIX for a series of energy values.

### 1987 3.9 RF Phase at the Accelerating Gap

1988 Solution: page 114

1989 Consider the cyclotron model of exercise 3.6: field index  $k = -0.03$  defined at  
1990  $R_0 = 50$  cm, field  $B_0 = 5$  kG on that radius. two dees, double accelerating gap.

1991 Accelerate a proton from 1 to 5 MeV: get the turn-by-turn phase-shift at the gaps;  
1992 use CAVITE[IOPT=7] to simulate the acceleration. Compare the half-turn  $\Delta\phi$  so  
1993 obtained with the theoretical expectation (Eq. 3.25). Produce similar graphs  $B(R)$   
1994 and  $\Delta W(\phi)$  to Fig. 3.13.

1995 Accelerate over more turns, observe the particle decelerating.

### 1996 3.10 The Cyclotron Equation

1997 Solution: page 116

1998 The cyclotron model of exercise 3.3 is considered: two dees, double accelerating  
1999 gap, uniform field  $B = 5$  kG, no field gradient needed here (no vertical motion).

2000 (a) Set up an input data file for the simulation of a proton acceleration from  
2001 0.2 to 20 MeV. In particular, assume that  $\cos(\phi)$  reaches its maximum value at  
2002  $W_m = 10$  MeV; find the RF voltage frequency from  $d(\cos \phi)/dW = 0$  at  $W_m$ .

2003 (b) Give a graph of the energy-phase relationship (Eq. 3.26), for  $\phi_i = \frac{3\pi}{4}, \frac{\pi}{2}, \frac{\pi}{4}$ ,  
2004 from both simulation and theory.

### 2005 3.11 Cyclotron Extraction

2006 Solution: page 118

2007 (a) Acceleration of a proton in a uniform field  $B = 5$  kG is first considered (field  
2008 hypotheses as in exercise 3.3). RF phase is ignored: CAVITE[IOPT=3] can be used  
2009 for acceleration. Take a 100 kV gap voltage.

2010 Compute the distance  $\Delta R$  between turns, as a function of turn number and of  
2011 energy, over the range  $E : 0.02 \rightarrow 5$  MeV. Compare graphically with theoretical  
2012 expectation.

2013 (b) Assume a beam with Gaussian momentum distribution and *rms* momentum  
2014 spread  $\delta p/p = 10^{-3}$ . An extraction septum is placed half-way between two successive  
2015 turns, provide a graph of the percentage of beam loss at extraction, as a function of  
2016 extraction turn number. COLLIMA can be used for that simulation and for particle  
2017 counts, it also allows for possible septum thickness.

2018 (c) Repeat (a) and (b) considering a field with index: take for instance  $B_0 = 5$  kG  
2019 and  $k = -0.03$  at  $R_0 = R(0.2 \text{ MeV}) = 12.924888$  cm.

2020 (d) Investigate the effect of injection conditions ( $Y_i, T_i$ ) on the modulation of the  
2021 distance between turns.

2022 Try and confirm numerically that, with slow acceleration, the oscillation is mini-  
 2023 mized for an initial  $|T_i| = \left| \frac{x_0 v_R}{R} \right|$  (after Ref. [9, p. 133]).

### 2024 3.12 Acceleration and Extraction of a 6-D Polarized Bunch

2025 Solution: page 123

2026 The cyclotron simulation hypotheses of exercise 3.10-a are considered; account  
 2027 or  $k = -0.02$  field index.

2028 Add a short “high energy” extraction line, say 1 meter, following REBELOTE in  
 2029 the optical sequence, ending up with a “Beam\_Dump” MARKER for instance.

2030 (a) Create a 1,000 ion bunch with the following initial parameters:

2031 - random Gaussian transverse phase space densities, centered on the equilibrium  
 2032 orbit, truncated at 3 sigma, normalized *rms* emittances  $\varepsilon_Y = \varepsilon_Z = 1 \pi \mu\text{m}$ , both  
 2033 emittances matched to the 0.2 MeV orbit optics,

2034 - uniform bunch momentum density  $0.2 \times (1 - 10^{-3}) \leq p \leq 0.2 \times (1 + 10^{-3})$  MeV,  
 2035 matched to the dispersion, namely (Eq. 3.21),  $\Delta x = D \frac{\Delta p}{p}$ ,

2036 - random uniform longitudinal distribution  $-0.5 \leq s \leq 0.5$  mm,

2037 Note: two ways to create this object are, (i) using MCOBJET[KOBJ=3] which  
 2038 generates a random distribution, or (ii) using OBJET[KOBJ=3] to read an external  
 2039 particle coordinate file.

2040 Add spin tracking request (SPNTRK), all initial spins normal to the bend plane.

2041 Produce a graph of the three initial 2-D phase spaces: (Y,T), (Z,P),  $(\delta l, \delta p/p)$ ,  
 2042 matched to the 200 keV periodic optics. Provide Y, Z, dp/p,  $\delta l$  and  $S_Z$  histograms  
 2043 (HISTO can be used), check the distribution parameters.

2044 (b) Accelerate this polarized bunch to 20 MeV, using the following RF conditions:

2045 - 200 kV peak voltage,

2046 - RF harmonic 1,

2047 - initial RF phase  $\phi_i = \pi/4$ .

2048 Produce a graph of the three phase spaces as observed downstream of the extrac-  
 2049 tion line. Provide the Y, Z, dp/p,  $\delta l$  and  $S_Z$  histograms. Compare the distribution  
 2050 parameters with the initial values.

2051 What causes the spins to spread away from vertical?

## 2052 3.4 Solutions of Exercises of Chapter 3: Classical Cyclotron

### 2053 3.1 Modeling a Cyclotron Dipole: Using a Field Map

2054

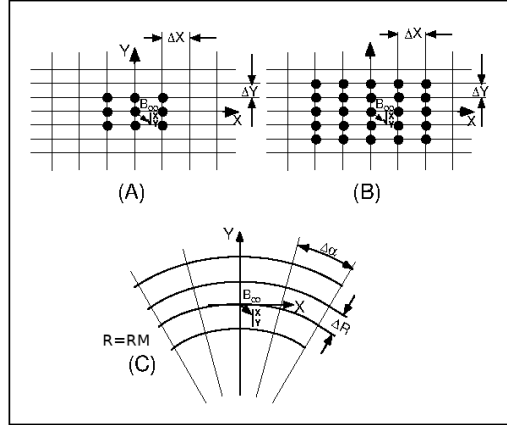
2055 (a) A field map of a  $180^\circ$  sector of a classical cyclotron magnet.

2056 The first option is retained here: a Fortran program, geneSectorMap.f, given in  
 2057 Tab. 3.1. constructs the required map of a field distribution  $B_Z(R, \theta)$ , to be subse-  
 2058 quently read and raytraced through using the keyword TOSCA [16, lookup INDEX].



2059 Regarding the second option: using the analytical model DIPOLE together with  
 2060 the keyword OPTIONS[CONSTY=ON] to fabricate a field map, examples can be  
 2061 found for instance in the FFAG chapter exercises (Chap. 10).

**Fig. 3.19** Principle 2-D field map mesh as used by TOSCA, and the (O;X,Y) coordinate system. (A), (B): Cartesian mesh in the (X,Y) plane, case of respectively 9-point and a 25-point interpolation grid; the mesh increments are  $\Delta X$  and  $\Delta Y$ . (C) : polar mesh and increments  $\Delta R$  and  $\Delta\alpha$  ( $\Delta\theta$  in the text), and (O;X,Y) frame moving along a reference arc of radius  $R_M$ . The field at particle location is interpolated from its values at the closest  $3 \times 3$  or  $5 \times 5$  nodes



2062 A polar mesh is retained (Fig. 3.19), rather than Cartesian, consistently with  
 2063 cyclotron magnet symmetry. The program can be compiled (*gfortran -o geneSectorMap geneSectorMap.f* will provide the executable, *geneSectorMap*) and run, as  
 2064 is. The field map is saved under the name *geneSectorMap.out*, excerpts of the expected content are given in Tab. 3.2. That name appears under TOSCA in *zgoubi*  
 2065 input data file for this simulation (Tab. 3.3). Figure 3.20 shows the field over the  
 2066  $180^\circ$  azimuthal extent (using a gnuplot script, bottom of Tab. 3.2).

2067 Note the following:

- 2068 (i) the field map azimuthal extent (set at  $180^\circ$  in *geneSectorMap*) can be changed,  
 2069 for instance to simulate a  $60^\circ$  sector instead;  
 2070 (ii) the field is vertical being the mid-plane field of dipole magnet. The field  
 2071 is taken constant in this exercise,  $\forall R, \forall \theta$  throughout the map mesh, whereas in  
 2072 upcoming exercises, a *focusing index* will be introduced, which will make  $B_Z \equiv$   
 2073  $B_Z(R)$  an R-dependent quantity (in Chap. 4 which addresses Thomas focusing and  
 2074 the isochronous cyclotron, exercises will further resort to  $B_Z \equiv B_Z(R, \theta)$ , an R- and  
 2075  $\theta$ -dependent quantity).

2076 This field map can be readily tested using the example of Tab. 3.3, which raytraces  
 2077  $E_k = 0.12, 0.2$  and  $5.52$  MeV protons on circular trajectories centered at the center  
 2078 of the field map. Trajectory radii, respectively  $R = 10.011, 12.924$  and  $67.998$  cm  
 2079 (Tab. 3.3), have been prior determined from

$$\text{Rigidity } B\rho = B_0 \times R \quad \text{and} \quad B\rho = p/c = \sqrt{E_k(E_k + 2M)}/c \quad (3.34)$$

2080 with  $B_0 = 0.5$  T (Tab. 3.1) and  $M = 938.272$  MeV/ $c^2$  the proton mass.

2081 The optical sequence for this particle raytracing uses the following keywords:

**Table 3.1** A Fortran program which generates a  $180^\circ$  mid-plane field map. This angle as well as field amplitude can be changed, a field index can be added. This program can be compiled and run, as is. The field map it produces is logged in geneSectorMap.out

```

C geneSectorMap.f program
  implicit double precision (a-h,o-z)
  parameter (pi=4.d0*atan(1.d0), BY=0.d0, BX=0.d0, Z=0.d0)

  open(unit=2,file='geneSectorMap.out')           ! Field map storage file.

C----- Hypotheses :
  AT = 180.d0 /180.d0*pi           ! Angular extent of field map. Can be changed 360, 60 deg, etc.).
  BZ=5.d0                           ! Field (kG).
  Rmi=1.d0; Rma=76.d0; RM=50.d0     ! cm. Radial extent of field map; reference radius to define mesh.
  dR = 0.5d0 ; NR = NINT((Rma - Rmi)/dR)+1 ! R-distance between nodes in mesh. Number of R-nodes.
C                                     RdA=RM*dA is the distance between two nodes along R=RM arc.
  RdA = 0.5d0 ! given angle increment dA (dA is the "Delta theta" quantity in the main text).
  NX= NINT(RM*AT /RdA) +1 ; RdA= RM*AT / DBLE(NX -1) ! exact mesh step at RM, corresponding to NX.
  dA = RdA / RM ; A1 = 0.d0 ; A2 = AT           ! corresponding delta_angle.
C-----
  write(2,*) Rmi,dR,pi*pi*180.d0,dZ,
  >' ! Rmi/cm, dR/cm, dA/deg, dZ/cm'
  write(2,*) '# Field map generated using geneSectorMap.f '
  write(2,fmt='(a)') '# AT/rd, AT/deg, Rmi/cm, Rma/cm, RM/cm,'
  >/' NR, dR/cm, NX, RdA/cm, dA/rd : '
  write(2,fmt='(a,1p,5(e16.8,1x),2(i3,1x,e16.8,1x),e16.8)')
  >' # ,AT, AT/pi*180.d0,Rmi, Rma, RM, NR, dR, NX, RdA, dA
  write(2,*) '# For TOSCA: ',NX,NR,' 1 22.1 1. ! IZ=1 -> 2D ; '
  >/' MOD=22 -> polar map ; .MOD2=-1 -> one map file'
  write(2,*) '# R*cosA Z=0, R*sinA'
  >/' BY BZ BX ix jr'
  write(2,*) '# cm cm cm '
  >/' kG kG kG '
  write(2,*) '# '
  do jr = 1, NR
    R = Rmi + dble(jr-1)*dR
    do ix = 1, NX
      A = A1 + dble(ix-1)*dA ; X = R * sin(A) ; Y = R * cos(A)
      write(2,fmt='(1p,6(e16.8),2(1x,i0))') Y,Z,X,BY,BZ,BX,ix,jr
    enddo
  enddo
  stop ' Job complete ! Field map stored in geneSectorMap.out.'
  end

```

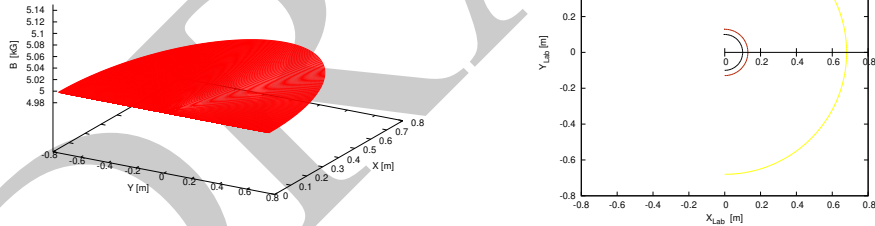


**Fig. 3.20** Left: map of a constant magnetic field over a 180 deg sector, 76 cm radial extent. Right: three circular trajectories, at respectively 0.12, 0.2 and 5.52 MeV, computed using that field map

**Table 3.2** First and last few lines of the field map file `geneSectorMap.out`. The file starts with an 8-line header, the first of which is effectively used by `zgoubi` (the following 7 are not used) and indicates, in that order: the minimum radius of the map mesh `Rmi`, the radial increment `dR`, the azimuthal increment `dA`, the axial increment `dZ` (null and not used in the present case of a two-dimensional field map), in units of, respectively, cm, cm, degree, cm. The additional 7 lines provide the user with various indications regarding numerical values used in, or resulting from, the execution of `geneSectorMap.f`. The first 5 numerical data in line 5 in particular are to be reported in `zgoubi` input data file under TOSCA keyword. The rest of the file is comprised of 8 columns, the first three give the node coordinates and the next three the field component values at that node, the last two columns are the (azimuthal and radial) node numbers, from (1,1) to (315,151) in the present case

```

1.00      0.500      0.57324840764331209      0.00      ! Rmi/cm, dR/cm, dA/deg, dZ/cm
# Field map generated using geneSectorMap.f
# AT/rd, AT/deg, Rmi/cm, Rma/cm, RM/cm, NR, dR/cm, NX, RdA/cm, dA/rd :
# 3.14159265E+00 1.800E+02 1.000E+00 7.600E+01 5.000E+01 151 5.000E-01 315 5.00253607E-01 1.00050721E-02
# For TOSCA:      315      151 1 22.1 1. !IZ=1 -> 2D; MOD=22 -> polar map; .MOD2=-1 -> one map file
#
# R*cosA      Z=0,      R*sinA      BY      BZ      BX      ix jr
# cm          cm          cm          kG          kG          kG
1.00000000E+00 0.00000000E+00 0.00000000E+00 0.00000000E+00 5.00000000E+00 0.00000000E+00 1 1
9.99949950E-01 0.00000000E+00 1.00049052E-02 0.00000000E+00 5.00000000E+00 0.00000000E+00 2 1
9.99799804E-01 0.00000000E+00 2.00088090E-02 0.00000000E+00 5.00000000E+00 0.00000000E+00 3 1
9.99549577E-01 0.00000000E+00 3.00107098E-02 0.00000000E+00 5.00000000E+00 0.00000000E+00 4 1
9.99199295E-01 0.00000000E+00 4.00096065E-02 0.00000000E+00 5.00000000E+00 0.00000000E+00 5 1
9.99199295E-01 0.00000000E+00 4.00096065E-02 0.00000000E+00 5.00000000E+00 0.00000000E+00 5 1
.....
-7.59391464E-01 0.00000000E+00 3.04073010E+00 0.00000000E+00 5.00000000E+00 0.00000000E+00 311 151
-7.59657679E-01 0.00000000E+00 2.28081394E+00 0.00000000E+00 5.00000000E+00 0.00000000E+00 312 151
-7.59847851E-01 0.00000000E+00 1.52066948E+00 0.00000000E+00 5.00000000E+00 0.00000000E+00 313 151
-7.59961962E-01 0.00000000E+00 7.60372797E-01 0.00000000E+00 5.00000000E+00 0.00000000E+00 314 151
-7.60000000E+01 0.00000000E+00 9.30731567E-15 0.00000000E+00 5.00000000E+00 0.00000000E+00 315 151

```

A gnuplot script to obtain a graph of  $B(X,Y)$ , Fig. 3.20:

```

# gnuplot_fieldMap.gnu
set key maxcol 1 ; set key t l ; set xtics mirror ; set ytics mirror ; cm2m = 0.01
set xlabel "Y [m]"; set ylabel "X [m]"; set zlabel "B [kG] \n" rotate by 90; set zrange [:5.15]
splot "geneSectorMap.out" u ($1 * cm2m):($3 * cm2m):($5) w l lc rgb "red" notit; pause 1

```

- 2084 (i) OBJET to define a (arbitrary) reference rigidity and initial particle coordinates  
2085 (ii) TOSCA, to read the field map and raytrace through (and TOSCA's 'IL=2'  
2086 flag to store step-by-step particle data into `zgoubi.plt`)  
2087 (iii) FAISCEAU to print out particle coordinates in `zgoubi.res` execution listing  
2088 (iv) SYSTEM to run a gnuplot script (Tab. 3.3) once raytracing is complete  
2089 (v) MARKER, to define two particular "LABEL\_1" type labels [16, *lookup INDEX*]  
2090 (#S\_halfDipole and #E\_halfDipole), to be used with INCLUDE in subsequent exer-  
2091 cises.

2092 Three circular trajectories in a dee, resulting from the data file of Tab. 3.3 are  
2093 shown in Fig. 3.20. Inspecting `zgoubi.res` execution listing one finds the D, Y, T, Z,  
2094 P, S particle coordinates under FAISCEAU, at OBJET (left) and current (right) after  
2095 a turn in the cyclotron (unchanged, as the trajectory forms a closed orbit):

```

2096 6 Keyword, label(s) : FAISCEAU IPASS= 1
2097
2098 TRACE DU FAISCEAU
2099 (follows element # 5)
2100 2 TRAJECTOIRES
2101
2102 OBJET FAISCEAU
2103 D Y(cm) T(mr) Z(cm) P(mr) S(cm) D-1 Y(cm) T(mr) Z(cm) P(mr) S(cm)
o 1 0.7746 10.011 0.000 0.000 0.000 0.0000 -0.2254 10.011 -0.000 0.000 0.000 3.145152E+01 1
o 1 5.2610 67.998 0.000 0.000 0.000 0.0000 4.2610 67.998 -0.000 0.000 0.000 2.136220E+02 2

```

2104 (b) Concentric trajectories in the median plane.

**Table 3.3** Simulation input data file `FieldMapSector.inc`: it is set to allow a preliminary test regarding the field map `geneSectorMap.out` (as produced by the Fortran program `geneSectorMap`, Tab. 3.1), by computing three circular trajectories centered on the center of the map. This file also defines the `INCLUDE` segment between the labels (LABEL1 type [16, Sect. 7.7]) `#S_halfDipole` and `#E_halfDipole`

```
FieldMapSector.inc
! Uniform field 180 deg sector. FieldMapSector.inc.
'MARKER' FieldMapSector_S ! Just for edition purposes.
'OBJET'
64.62444403717985 ! Reference Brho ("BORO" in the users' guide) -> 200keV proton.
2
3 1
10.011362 0. 0. 0. 0. 0.7745802 'a' ! p[MeV/c]= 15.007, Brho[kG.cm]= 50.057, kin-E[MeV]=0.12.
12.924888 0. 0. 0. 1. 'b' ! kin-E[MeV]=0.2.
67.997983 0. 0. 0. 5.2610112 'c' ! p[MeV/c]=101.926, Brho[kG.cm]=339.990, kin-E[MeV]=5.52.
1 1 1
'MARKER' #S_halfDipole
'TOSCA'
0 2 ! IL=2 to log step-by-step coordinates, spin, etc., to zgoubi.plt (avoid, if CPU time matters).
1. 1. 1. ! Normalization coefficients, for B, X, Y and Z coordinate values read from the map.
HEADER_8 ! The field map file starts with an 8-line header.
315 151 1 22.1 1. ! IZ=1 for 2D map; MOD=22 for polar frame; .MOD2=.1 if only one map file.
geneSectorMap.out
0 0 0 0 ! Possible vertical boundaries within the field map, to start/stop stepwise integration.
2
1. ! Integration step size. Small enough for orbits to close accurately.
2 ! Magnet positioning option.
0. 0. 0. 0. ! Magnet positioning.
'MARKER' #E_halfDipole
'FAISCEAU'
'SYSTEM' ! This SYSTEM command runs gnuplot, for a graph of the two trajectories.
1
gnuplot <./gnuplot_Zplt.gnu
'MARKER' FieldMapSector_E ! Just for edition purposes.
'END'
```

A `gnuplot` script to obtain a graph of the orbits, Fig. 3.20:

```
# gnuplot_Zplt.gnu
set key maxcol 1 ; set key t r ; set xtics ; set ytics ; cm2m = 0.01 ; unset colorbox
set xlabel "X_{Lab} [m]" ; set ylabel "Y_{Lab} [m]" ; set size ratio 1 ; set polar
plot for [orbit=1:3] "zgoubi.plt" u ($19==orbit ? $22 :1/0):($10 *cm2m):($19 w l lw 2 lc pal; pause 1
```

2105 The optical sequence for this exercise is given in Tab. 3.4. Compared to the  
 2106 previous sequence (Tab. 3.3), (i) the TOSCA segment has been replaced by an  
 2107 `INCLUDE`, for the mere interest of making the input data file for this simulation  
 2108 shorter, and (ii) additional keywords are introduced, including  
 2109 - `FIT`, which finds the circular orbit for a particular momentum,  
 2110 - `FAISCEAU`, a means to check local particle coordinates,  
 2111 - `REBELOTE`, which repeats the execution of the sequence (`REBELOTE` sends  
 2112 the execution pointer back to the top of the data file) for a new momentum value  
 2113 which `REBELOTE` itself defines, prior.

2114 In order to compute and then plot trajectories (Fig. 3.21), `zgoubi` proceeds as  
 2115 follows: orbit circles for a series of different radii taken in  $[10, 80]$  cm are searched,  
 2116 using `FIT` to find the appropriate momenta. `REBELOTE` is used to repeat that fitting  
 2117 on a series of different values of  $R$ ; prior to repeating, `REBELOTE` modifies the  
 2118 initial particle coordinate  $Y_0$  in `OBJET`. Stepwise particle data through the dipole  
 2119 field are logged in `zgoubi.plt`, due to `IL=2` under `TOSCA` keyword, at the first pass  
 2120 before `FIT`, and at the last pass following `FIT` completion. A key point here: a flag,

**Table 3.4** Simulation input data file: optical sequence to find cyclotron closed orbits at a series of different momenta. An INCLUDE inserts the #S\_halfDipole to #E\_halfDipole TOSCA segment of the sequence of Tab. 3.3

```

Uniform field 180 deg. sector. Find orbits.
'MARKER' FieldMapOrbits_S                               ! Just for edition purposes.
'OBJET'
64.62444403717985                                     ! Reference Brho ("BORO" in the users' guide) -> 200keV proton.
2
1 1                                                    ! Just one ion.
12.9248888074 0. 0. 0. 0. 1. 'm'                       ! This initial radius yields BR=64.6244440372 kG.cm.
1
'INCLUDE'                                             ! A half of the cyclotron dipole.
1
FieldMapSector.inc[#S_halfDipole:#E_halfDipole]
'FAISCEAU'
'INCLUDE'                                             ! A half of the cyclotron dipole.
1
FieldMapSector.inc[#S_halfDipole:#E_halfDipole]
'FIT'
1
2 35 0 6.                                             ! Vary momentum, to allow fulfilling the following constraint:
1
3.1 1 2 5 0. 1. 0                                     ! request same radius after a half-turn (i.e., after first 180 deg sector,
! this ensures centering of orbit on center of map).
'FAISCEAU' CHECK ! Allows quick check of particle coordinates, in zgoubi.res: final should = initial.

'REBELOTE'                                           ! Repeat what precedes,
15 0.1 0 1                                           ! 15 times.
1
OBJET 30 10:80 ! Prior to each repeat, first change the value of parameter 30 (i.e., Y) in OBJET.
'SYSTEM'
2
gnuplot <-./gnuplot_Zplt.gnu
cp gnuplot_Zplt_XYLab.eps gnuplot_Zplt_XYLab_stage1.eps
'MARKER' FieldMapOrbits_E                               ! Just for edition purposes.
'END'

```

A gnuplot script to obtain Fig. 3.21:

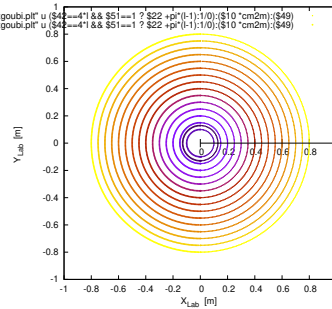
Note: removing the test '\$51==1 ?' on column 51 in zgoubi.plt, would add on the graph the orbit as it is before each FIT.

```

# gnuplot_Zplt.gnu
set key maxcol 1 ; set key t r ; set xtics ; set ytics ; set size ratio 1 ; set polar ; unset colorbox
set xlabel "X_{Lab} [m] \n" ; set ylabel "Y_{Lab} [m] \n" ; cm2m = 0.01 ; sector1=4 ; sector2=8 ; pi = 4.*atan(1.)
lmnt1 = 4 ; lmnt2=8 ## column numer in zgoubi.plt, $42: NOEL; $51: FITLST; $49: FIT number
plot for [l=lmnt1/4:lmnt2/4] "zgoubi.plt" u ($42==4*1 && $51==1 ? $22 +pi*(l-1):1/0):($10 *cm2m):($49) w p ps .3 lc pal
pause 1

```

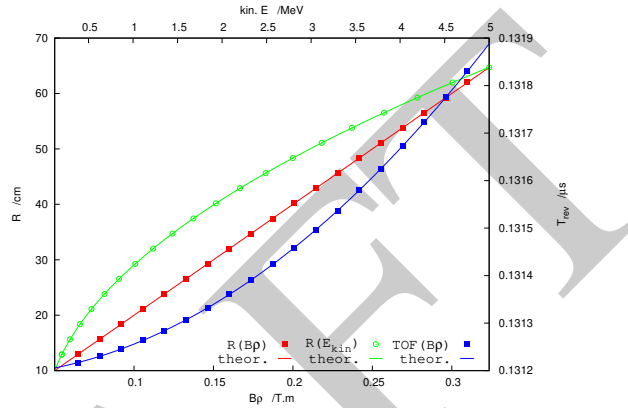
**Fig. 3.21** Circular trajectories in the cyclotron mid-plane, centered on the field map center. The outermost orbit is at  $R=80$  cm by hypothesis, thus  $BR = B_0 \times R = 0.4$  T m,  $E_k = 7.632$  MeV. These stepwise  $(R, \theta)$  data are read from zgoubi.plt, coordinates  $(Y, X)$  in zgoubi polar frame nomenclature [16, Sect.8.3]



2121 FITLST, recorded in column 51 in zgoubi.plt [16, Sect.8.3], is set to 1 at the last  
 2122 pass (the last pass follows the completion of the FIT execution and uses updated FIT  
 2123 variable values).

2124 At the bottom of zgoubi input data file, a SYSTEM command produces a graph  
 2125 of ion trajectories, by executing a gnuplot script (bottom of Tab. 3.4). Note the test  
 2126 on FITLST, which allows selecting the last pass following FIT completion. Graphic  
 2127 outcomes are given in Fig. 3.21.

**Fig. 3.22** Numerical (markers) and theoretical (solid lines) values of orbit radius,  $R$ , and revolution period,  $T_{\text{rev}}$ , versus kinetic energy (top scale) and rigidity (bottom scale). The mesh density here is  $N_\theta \times N_R = 315 \times 151$ . The integration step size is  $\Delta s = 1$  cm, so ensuring converged results (to  $\Delta R/R$  and  $\Delta T_{\text{rev}}/T_{\text{rev}} < 10^{-6}$ )



2128 The reason why it is possible to push the raytracing beyond the 76 cm radius field  
 2129 map extent, without loss of accuracy, is that the field is constant. Thus, referring to  
 2130 the polynomial interpolation technique used [16, Sect. 1.4], the extrapolation out of  
 2131 the map will leave the field value unchanged.

2132 (c) Energy and rigidity dependence of orbit radius and time-of-flight.

2133 The orbit radius  $R$  and the revolution time  $T_{\text{rev}}$  as a function of kinetic energy  $E_k$   
 2134 and rigidity  $BR$  are obtained by a similar scan to exercise (b). The results are shown  
 2135 in Fig. 3.22.

2136 A slow increase of revolution period with energy can be observed, which is due  
 2137 to the mass increase.

2138 Note that these results are converged for the step size, to high accuracy (see (d)),  
 2139 due to its value taken small enough, namely  $\Delta s = 1$  cm. This corresponds for instance  
 2140 to 80 steps to complete a revolution for the 120 keV,  $R = 12.9$  cm smaller radius  
 2141 trajectory in Fig 3.21.

2142 (d) Numerical convergence: mesh density.

2143 This question concerns the dependence of the numerical convergence of the  
 2144 solution of the differential equation of motion [16, Eq. 1.2.1] upon mesh density.

2145 The program used in (b) to generate a field map (Tab. 3.1) is modified to construct  
 2146 field maps of  $B_Z(R, \theta)$  with various radial and azimuthal mesh densities. Changing

**Fig. 3.23** Convergence versus mesh density and step size: a graph of orbit radius  $R$  (left axis), and revolution period,  $T_{\text{rev}}$  (right axis), versus kinetic energy (top scale) and rigidity (bottom scale). Solid markers are for  $\Delta s = 1$  cm and  $N_\theta \times N_R = 3 \times 3$  node mesh, large empty circles are for  $\Delta s = 10$  cm and  $N_\theta \times N_R = 106 \times 151$  node mesh. Solid lines are from theory and show convergence in the case  $3 \times 3$  nodes and  $\Delta s = 1$  cm

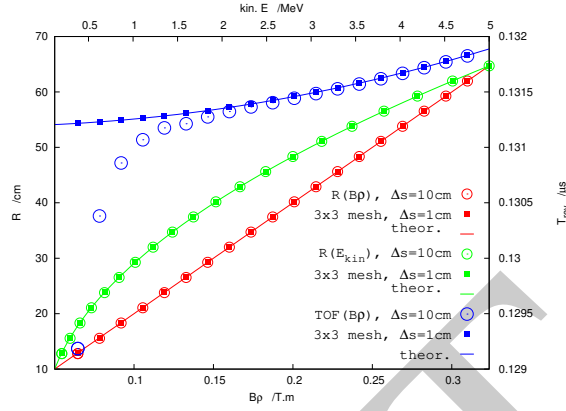


**Table 3.5** Field map of a  $60^\circ$  constant field sector as read by TOSCA. The field map is complete, with smallest possible  $NX \times NR = 3 \times 3 = 9$  number of nodes. The first line of the header is used by zgoubi (the following 7 are not used), namely, the minimum value of the radius in the map, radius increment, azimuthal increment, and vertical increment (null here, as this is a single, mid-plane map)

```

1.0 37.50 30.0 0. ! Rmi/cm, dR/cm, dA/deg, dZ/cm
# Field map generated using geneSectorMap.f
# AT/rd, AT/deg, Rmi/cm, Rma/cm, RM/cm, NR, dR/cm, NX, RdA/cm, dA/rd :
# 1.04719755E+00 60. 1. 76. 50. 3 37.5 3 26.1799388 0.523598776
# For TOSCA: 3 3 1 22.1 1. ! IZ=1 -> 2D ; MOD=22 -> polar map ; .MOD2=-1 -> one map file
#
# R*cosA Z=0, R*sinA BY BZ BX ix jr
# cm cm cm kG kG kG
1.00000000E+00 0.00000000E+00 0.00000000E+00 0.00000000E+00 5.00000000E+00 0.00000000E+00 1 1
8.66025404E-01 0.00000000E+00 5.00000000E-01 0.00000000E+00 5.00000000E+00 0.00000000E+00 2 1
5.00000000E-01 0.00000000E+00 8.66025404E-01 0.00000000E+00 5.00000000E+00 0.00000000E+00 3 1
3.85000000E-01 0.00000000E+00 0.00000000E+00 0.00000000E+00 5.00000000E+00 0.00000000E+00 1 2
3.33419780E-01 0.00000000E+00 1.92500000E+01 0.00000000E+00 5.00000000E+00 0.00000000E+00 2 2
1.92500000E+01 0.00000000E+00 3.33419780E-01 0.00000000E+00 5.00000000E+00 0.00000000E+00 3 2
7.60000000E-01 0.00000000E+00 0.00000000E+00 0.00000000E+00 5.00000000E+00 0.00000000E+00 1 3
6.58179307E-01 0.00000000E+00 3.80000000E-01 0.00000000E+00 5.00000000E+00 0.00000000E+00 2 3
3.80000000E-01 0.00000000E+00 6.58179307E-01 0.00000000E+00 5.00000000E+00 0.00000000E+00 3 3

```

Modified TOSCA keyword data, in the case of a  $60^\circ$  sector field map (compared to Tab. 3.3, the sole data line “3 3 1 22.1 1.” changes, from “315 151 1 22.1 1.” in that earlier  $180^\circ$  sector case):

```

'TOSCA'
0 2 ! IZ=2: log step-by-step coordinates, spin, etc., in zgoubi.plt (avoid if CPU time matters).
1. 1. 1. ! Normalization coefficients, for B, X, Y and Z coordinate values read from the map.
HEADER_8 ! The field map file starts with an 8-line header.
3 3 1 22.1 1. ! IZ=1 for 2D map; MOD=22 for polar frame; .MOD2=-1 if only one map file.
geneSectorMap.out
0 0 0 ! Possible vertical boundaries within the field map, to start/stop stepwise integration.
2
1. ! Integration step size. Small enough for orbits to close accurately.
2 ! Magnet positioning option.
0. 0. 0. 0. ! Magnet positioning.

```



2147 these is simply a matter of modifying the quantities  $dR$  (radius increment  $\Delta R$ ) and  
 2148  $R dA$  ( $R$  times the azimuth increment  $\Delta\theta$ ) in the program of Tab. 3.1. The field maps  
 2149 `geneSectorMap.out` so generated for various  $(dR, RdA)$  couples may be saved under  
 2150 different names, and used separately.

2151 Table. 3.5 shows the complete, 9 line, TOSCA field map, in the case of a  $60^\circ$   
 2152 sector covered in  $N_\theta \times N_R = \frac{60^\circ}{\Delta\theta} \times \frac{75 \text{ cm}}{\Delta R} = \frac{360^\circ}{120^\circ} \times \frac{75 \text{ cm}}{37.5 \text{ cm}} = 3 \times 3$  nodes. Six  
 2153 sectors are now required to cover the complete cyclotron dipole: `zgoubi` input data  
 2154 need be changed accordingly, namely stating TOSCA - possibly via an `INCLUDE` -  
 2155 six times, instead of just twice in the case of a 180 degree sector.

2156 The result to be expected: with a mesh reduced to as low as  $N_\theta \times N_R = 3 \times 3$ ,  
 2157 compared to  $N_\theta \times N_R = 106 \times 151$ , radius and time-of-flight should however remain  
 2158 unchanged. This shows in Fig. 3.23 which displays both cases, over a  $E_k : 0.12 \rightarrow$   
 2159  $5 \text{ MeV}$  energy span (assuming protons). The reason for the absence of effect of the  
 2160 mesh density is that the field is constant. As a consequence the field derivatives in the  
 2161 Taylor series based numerical integrator are all zero [16, Sect. 1.2]: only  $B_Z$  is left  
 2162 in evaluating the Taylor series, however  $B_Z$  is constant. Thus  $R$  remains unchanged  
 2163 when pushing the ion by a step  $\Delta s$ , and the cumulated path length - the closed orbit  
 2164 length - and revolution time - path length over velocity - end up unchanged. Note:  
 2165 this will no longer be the case when a radial field index is introduced in order to  
 2166 cause vertical focusing, in subsequent exercises.

2167 (e) Numerical convergence: integration step size

2168 Figure 3.23 displays two cases of step sizes,  $\Delta s \approx 1 \text{ cm}$  and  $\Delta s = 10 \text{ cm}$ .

2169 It has been shown (Fig. 3.22) that  $\Delta s \approx 1 \text{ cm}$  is small enough that the numerical  
 2170 integration is converged, agreement with theoretical expectation is quite good.

2171 The difference on the value of  $R$ , in the case  $\Delta s \approx 10 \text{ cm}$ , appears to be weak,  
 2172 only noticeable at the scale of the graph for  $R$  values small enough that the number  
 2173 of steps over one revolution goes as low as  $2\pi R/\Delta s \approx 2\pi \times 14.5/10 \approx 9$ . The change  
 2174 in time-of-flight due to the larger step size amounts to a relative  $10^{-3}$ .

2175 Step size is critical in the numerical integration, the reason is that the coefficients  
 2176 of the Taylor series that yield the new position vector  $\mathbf{R}(M_1)$  and velocity vector  
 2177  $\mathbf{v}(M_1)$ , from an initial location  $M_0$  after a  $\Delta s$  push, are the derivatives of the velocity  
 2178 vector [16, Sect. 1.2] and may take substantial values if  $\mathbf{v}(s)$  changes quickly. In  
 2179 such case, taking too large a  $\Delta s$  value makes the high order terms significant and  
 2180 the Taylor series truncation [16, Eq. 1.2.4] is fatal to the accuracy (regardless of a  
 2181 possible additional issue of radius of convergence of the series).

2182 (f) Numerical convergence:  $\frac{\delta R}{R}(\Delta s)$

2183 Issues faced are the following:

- 2184 - the increase of  $\delta R(\Delta s)/R$  at large  $\Delta s$  has been addressed above;
- 2185 - a small  $\Delta s$  is liable to cause an increase of  $\delta R(\Delta s)/R$ , due to computer accuracy:  
 2186 truncation of numerical values at a limited number of digits may cause a  $\Delta s$  push to  
 2187 result in no change in  $\mathbf{R}(M_1)$  (position) and  $\mathbf{u}(M_1)$  (normed velocity) quantities [16,  
 2188 Eq. 1.2.4].

2189 A detailed answer to the question, including graphs, is left to the reader, the  
2190 method is the same as in (e).

### 2191 3.2 Modeling a Cyclotron Dipole: Using an Analytical Field Model

2192

2193 This exercise introduces the analytical modeling of a dipole, using DIPOLE [16,  
2194 *lookup* INDEX], and compares outcomes to the field map case of exercise 3.1. The  
2195 exercise is not entirely solved, however all the material needed for that is provided,  
2196 and indications are given to complete it.

2197 (a) Analytical modeling.

2198 DIPOLE keyword provides an analytical model of the field to simulate a sector  
2199 dipole with index, namely [16, *lookup* INDEX]

$$B_Z = \mathcal{F}(\theta)B_0 \left[ 1 + k \left( \frac{R - R_0}{R_0} \right) + k' \left( \frac{R - R_0}{R_0} \right)^2 + k'' \left( \frac{R - R_0}{R_0} \right)^3 \right] \quad (3.35)$$

2200  $R_0$  is a reference radius,  $B_0 = B_Z(R_0)|_{\mathcal{F}=1}$  is a reference field value,  $k$  is the field  
2201 index and  $k'$ ,  $k''$  are homogeneous to its first and second derivative with respect to  
2202  $R$  (Eq. 3.11).  $\mathcal{F}(\theta)$  is an azimuthal form factor, defined by the fringe field model,  
2203 presumably taking the value 1 in the body of the dipole. In the present case a  
2204 hard-edge field model is considered, so that

$$\mathcal{F} = \begin{cases} 1 & \text{inside} \\ 0 & \text{outside} \end{cases} \text{ the dipole magnet} \quad (3.36)$$

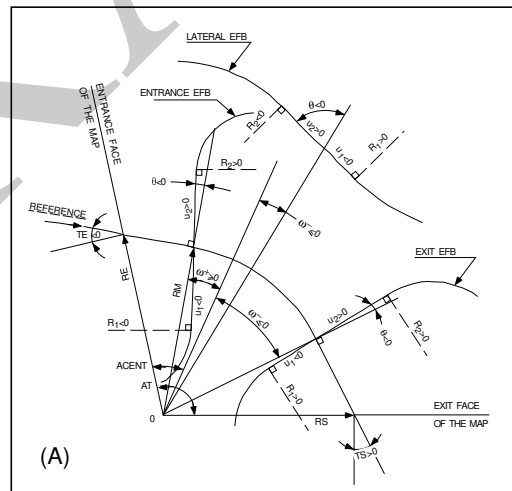


**Fig. 3.24** Parameters used to define the geometry of a dipole magnet with index, using DIPOLE. In the text, ACENT is noted ACN [16, Fig. 9]

2205 Setting up the input data list under DIPOLE (Table 3.6) requires close inspection  
 2206 of Fig. 3.24, which details the geometrical parameters such as the full angular  
 2207 opening of the field region that DIPOLE comprises, AT; a reference angle ACN  
 2208 to allow positioning the effective field boundaries at  $\omega^+$  and  $\omega^-$ ; field and indices;  
 2209 fringe field regions at  $ACN - \omega^+$  (entrance) and  $ACN - \omega^-$  (exit); wedge angles,  
 2210 etc.

2211 A 60 deg sector is used here for convenience, it is detailed in Table 3.6 (Table 3.7  
 2212 provides the definition of a 180 deg sector, for possible comparisons with the present  
 2213 three-sector assembly).

2214 In setting up DIPOLE data the following values have been accounted for:

2215 -  $R_0 = 50$  cm, an arbitrary value (consistent with other exercises), more or less  
 2216 half the dipole extent,

2217 -  $B_0 = B_Z(R_0) = 5$  kG, as in the previous exercise. Note in passing,  $R_0 = 50$  cm  
 2218 thus corresponds to  $BR = 0.25$  T m,  $E_k = 2.988575$  MeV proton kinetic energy,

2219 - radial field index  $k = 0$  for the time being (constant field at all  $(R, \theta)$ ),

2220 - a hard-edge field model for  $\mathcal{F}$  (Eq. 3.36). In that manner for instance, two  
 2221 consecutive 60 deg sectors form a continuous 120 deg sector.

2222 A graph of  $B_Z(R, \theta)$  can be produced by computing constant radius orbits, for a  
 2223 series of energies ranging in 0.12 – 5.52 MeV for instance. DIPOLE[IL=2] causes  
 2224 logging of step by step particle data in zgoubi.plt, including particle position and  
 2225 magnetic field vector; these data can be read and plotted, to yield similar results to  
 2226 Fig. 3.20.

2227 (b) Concentric trajectories in the median plane.

2228 The optical sequence of Exercise 3.1-b (Tab. 3.4) can be used, by just changing  
 2229 the INCLUDE to account for a 180° DIPOLE (instead of TOSCA), namely

```
2230 ' INCLUDE'
2231 1
2232 3* 60degSector.inc[#S_60degSectorUnifB:#E_60degSectorUnifB]
```

2233 wherein 60degSector.inc is the name of the data file of Tab. 3.6 and

```
2234 [#S_60degSectorUnifB:#E_60degSectorUnifB]
```

2235 is the DIPOLE segment as defined in the latter. Note that the segment represents a  
 2236 60° DIPOLE, thus it is included 3 times.

2237 The additional keywords in that modified version of the Tab. 3.4 file include

2238 - FIT, which finds the circular orbit for a particular momentum,

2239 - FAISTORE to print out particle data once FIT is completed,

2240 - REBELOTE, which repeats the execution of the sequence (REBELOTE sends  
 2241 the execution pointer back to the top of the data file) for a new momentum value  
 2242 which REBELOTE itself defines.

2243 For the rest, follow the same procedure as for exercise 3.1-b. The results are the  
 2244 same, Fig. 3.21.

2245 (c) Energy and rigidity dependence of orbit radius and time-of-flight.

2246 The orbit radius  $R$  and the revolution time  $T_{\text{rev}}$  as a function of kinetic energy  $E_k$   
 2247 and rigidity  $BR$  are obtained by a similar scan to exercise (b). The procedure is the  
 2248 same as in exercise 3.1-c. Results are expected to be the same as well (Fig. 3.22).

2249 A comparison of revolution periods can be made using the simulation file of  
 2250 Table 3.6 which happens to be set for a momentum scan and yields Fig. 3.25, to  
 2251 be compared to Fig. 3.22: DIPOLE and TOSCA produce the same results as long  
 2252 as both methods are converged, from the integration step size stand point (small  
 2253 enough), and regarding TOSCA from field map mesh density stand point in addition  
 2254 (dense enough).

2255 (d) Numerical convergence: integration step size;  $\frac{\delta R}{R}(\Delta s)$ .

2256 This question concerns the dependence of the numerical convergence of the  
 2257 solution of the differential equation of motion upon integration step size.

2258 Follow the procedure of exercise 3.1-e: a similar outcome to Fig. 3.23 is expected  
 2259 - ignoring mesh density with the present analytical modeling using DIPOLE.

2260 The  $\frac{\delta R}{R}$  dependence upon the integration step size  $\Delta s$  is commented in exer-  
 2261 cise 3.1-e and holds regardless of the field modeling method (field map or analytical  
 2262 model).

2263 (e) Pros and cons.

2264 Using a field map is a convenient way to account for complicated one-, two- or  
 2265 three-dimensional field distributions.

2266 However, using an analytical field model rather, ensures greater accuracy of the  
 2267 integration method.

2268 CPU-time wise, one or the other method may be faster, depending on the problem.

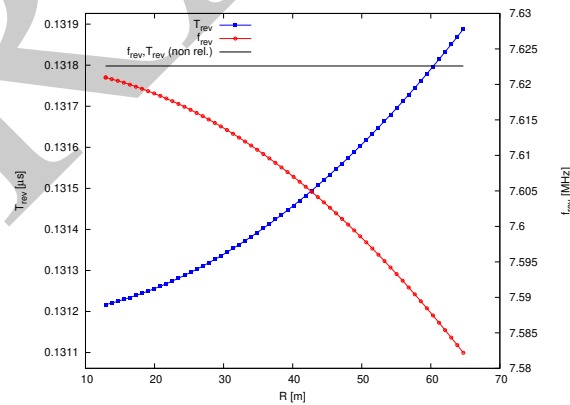


**Fig. 3.25** A scan of radius-dependent revolution frequency. An analytical model of a cyclotron dipole is used, featuring uniform field (no radial gradient, at this point)

**Table 3.6** Simulation input data file 60degSector.inc: analytical modeling of a dipole magnet, using DIPOLE. That file defines the labels (LABEL1 type [16, Sect. 7.7]) #S\_60degSectorUnifB and #E\_60degSectorUnifB, for INCLUDEs in subsequent exercises. It also realizes a 60-sample momentum scan of the cyclotron orbits, from 200 keV to 5 MeV, using REBELOTE

Note: this file is available in zgoubi sourceforge repository at

[https://sourceforge.net/p/zgoubi/code/HEAD/tree/branches/exemples/book/zgoubiMaterial/cyclotron\\_classical/ProbMdlAnal/](https://sourceforge.net/p/zgoubi/code/HEAD/tree/branches/exemples/book/zgoubiMaterial/cyclotron_classical/ProbMdlAnal/)

```
60degSector.inc
! Cyclotron, classical. Analytical model of dipole field. File name: 60degSector.inc
'MARKER' ProbMdlAnal_S ! Just for edition purposes.
'OBJET'
64.62444403717985 ! 200keV proton.
2
1 1 ! Just one ion.
12.9248888074 0. 0. 0. 1. 'm' ! Closed orbit coordinates for D=p_0-1
1 ! => 200keV proton. R=Brho/B=64.624444037[kG.cm]/5[kG].
'PARTICUL' ! Optioanl - using PARTICUL is a way to get the time-of-flight computed.
PROTON ! otherwise, by default \zgoubi\ only requires rigidity.
'FAISCEAU' ! Local particle coordinates.
'MARKER' #S_60degSectorUnifB ! Label should not exceed 20 characters.
'DIPOLE' ! Analytical modeling of a dipole magnet.
2 ! IL=2, only purpose is to logged trajectories in zgoubi.plt, for further plotting.
60. 50. ! Sector angle AT; reference radius R0.
30. 5. 0. 0. 0. ! Reference azimuthal angle ACN; BM field at R0; indices, N, N', N''.
0. 0. ! EFB 1 is hard-edge.
4. .1455 2.2670 -.6395 1.1558 0. 0. 0. ! hard-edge only possible with sector magnet.
30. 0. 1.E6 -1.E6 1.E6 1.E6 ! Entrance face placed at omega+=30 deg from ACN.
0. 0. ! EFB 2.
4. .1455 2.2670 -.6395 1.1558 0. 0. 0.
-30. 0. 1.E6 -1.E6 1.E6 1.E6 ! Exit face placed at omega=-30 deg from ACN.
0. 0. ! EFB 3 (unused).
0. 0. 0. 0. 0. 0. 0. 0.
0. 0. 1.E6 -1.E6 1.E6 1.E6 0.
2 10 ! '2' is for 2nd degree interpolation. Could also be '25' (5*5 points grid) or 4 (4th degree).
1. ! Integration step size. Small enough for orbits to close accurately.
2 0. 0. 0. 0. ! Magnet positioning RE, TE, RS, TS. Could be instead non-zero, e.g.,
! 2 RE=50. 0. RS=50. 0., as long as Yo is amended accordingly in OBJET.
'MARKER' #E_60degSectorUnifB ! Label should not exceed 20 characters.
'FAISCEAU' ! Local particle coordinates.
'FIT' ! Adjust Yo at OBJET so to get final Y = Y0 -> a circular orbit.
1 nfinal
2 30 0 [12.,.65.] ! Variable : Yo.
1 2e-12 199 ! constraint; default penalty would be 1e-10; maximu 199 calls to function.
3.1 1 2 #End 0. 1. 0 ! Constraint: Y_final=Yo.
'FAISTORE' ! Log particle data here, to zgoubi.fai.
zgoubi.fai ! for further plotting (by gnuplot, below).
1
'REBELOTE' ! Momentum scan, 60 samples.
60 0.2 0 1 60 different rigidities; log to video ; take initial coordinates as found in OBJET.
1 ! Change parameter(s) as stated next lines.
OBJET 35 1:5.0063899693 ! Change relative rigity (35) in OBJET; range (0.2 MeV to 5 MeV).
'SYSTEM'
1 ! 2 SYSTEM commands follow.
/usr/bin/gnuplot < ./gnuplot_TOF.gnu & ! Launch plot by ./gnuplot_TOF.gnu.
'MARKER' ProbMdlAnal_E ! Just for edition purposes.
'END'
```

A gnuplot script, gnuplot\_TOF.gnu, to obtain Fig. 3.25:

```
# gnuplot_TOF.gnu
set xlabel "R [m]"; set ylabel "T_{rev} [Symbol m]s"; set y2label "f_{rev} [MHz]"
set xtics nomirror; set ytics nomirror; set y2tics nomirror; set key t l ; set key spacin 1.2
nSector=6; Hz2MHz=1e-6; M=938.272e6; c=2.99792458e8; B=0.5; freqNonRel(x)= Hz2MHz* c**2*B/M/(2.*pi)
set y2range [7.58:7.63] ; set yrange[1/7.63:1/7.58]
plot \
"zgoubi.fai" u 10:($15 *nSector) axes x1y1 w lp pt 5 ps .6 lw 2 linecolor rgb "blue" tit "T_{rev}" ,\
"zgoubi.fai" u 10:(1/($15*nSector)) axes x1y2 w lp pt 6 ps .6 lw 2 linecolor rgb "red" tit "f_{rev}" ,\
freqNonRel(x) axes x1y2 w l lw 2. linecolor rgb "black" tit "f_{rev},T_{rev} (non rel.)" ; pause 1
```

**Table 3.7** A  $180^\circ$  version of a DIPOLE sector, where the foregoing quantities  $AT = 60^\circ$ ,  $ACN = \omega^+ = -\omega^- = 30^\circ$  have been changed to  $AT = 180^\circ$ ,  $ACN = \omega^+ = -\omega^- = 90^\circ$  - a file used under the name 180degSector.inc in further exercises

Note: this file is available in zgoubi sourceforge repository at

[https://sourceforge.net/p/zgoubi/code/HEAD/tree/branches/exemples/book/zgoubiMaterial/cyclotron\\_classical/ProbMdlAnal/](https://sourceforge.net/p/zgoubi/code/HEAD/tree/branches/exemples/book/zgoubiMaterial/cyclotron_classical/ProbMdlAnal/)

```
! 180degSector.inc
'MARKER' #S_180degSectorUnifB          ! Label should not exceed 20 characters.
'DIPOLE'                                ! Analytical modeling of a dipole magnet.
2
180. 50.                                ! Sector angle 180deg; reference radius 50cm.
90. 5. 0. 0. 0.                          ! Reference azimuthal angle; Bo field at R0; indices, N, N', N''.
0. 0.                                    ! EFB 1 is hard-edge,
4 .1455 2.2670 -.6395 1.1558 0. 0. 0.    ! hard-edge only possible with sector magnet.
90. 0. 1.E6 -1.E6 1.E6 1.E6
0. 0.                                    ! EFB 2.
4 .1455 2.2670 -.6395 1.1558 0. 0. 0.
-90. 0. 1.E6 -1.E6 1.E6 1.E6
0. 0.                                    ! EFB 3.
0. 0. 0. 0. 0. 0. 0. 0.
0. 0. 1.E6 -1.E6 1.E6 1.E6 0.
2 10.
0.5                                     ! Integration step size. Small enough for orbits to close accurately.
2 0. 0. 0. 0.                          ! Magnet positioning RE, TE, RS, TS. Could be instead non-zero, e.g.,
! 2 RE=50. 0. RS=50. 0., as long as Yo is amended accordingly in OBJET.
'MARKER' #E_180degSectorUnifB          ! Label should not exceed 20 characters.
```

### 2269 3.3 Resonant Acceleration

2270 The field map and TOSCA [16, *lookup* INDEX] model of a  $180^\circ$  sector is used  
 2271 here (an arbitrary choice, the analytical field modeling DIPOLE would do as well),  
 2272 the configuration is that of Fig. 3.5 with a pair of sectors.

2273 An accelerating gap between the two dees is simulated using CAVITE[IOPT=3],  
 2274 PARTICUL is added in the sequence in order to specify ion species and data,  
 2275 necessary for CAVITE to operate. Acceleration at the gap does not account for the  
 2276 particle arrival time in the IOPT=3 option: whatever the later, CAVITE boost will  
 2277 be the same as longitudinal motion is an unnecessary consideration, here).

2278 The input data file for this simulation is given in Tab. 3.8. It is resorted to  
 2279 INCLUDE, twice in order to create a double-gap sequence, using the field map model  
 2280 of a  $180^\circ$  sector. The INCLUDE inserts the magnet itself, *i.e.*, the #S\_halfDipole to  
 2281 #E\_halfDipole TOSCA segment of the sequence of Tab. 3.3. Note: the theoretical  
 2282 field model of Tab. 3.6, segment #S\_60degSectorUnifB to #E\_60degSectorUnifB  
 2283 (to be INCLUDED 3 times, twice), could be used instead: exercise 3.2 has shown  
 2284 that both methods, field map and analytical field model, deliver the same results.

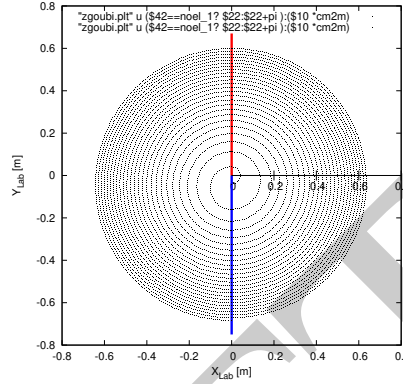
2285 Particle data are logged in zgoubi.fai at both occurrences of CAVITE, under the  
 2286 effect of FAISTORE[LABEL=cavity], Tab. 3.8. This is necessary in order to access  
 2287 the evolution of parameters as velocity, time of flight, etc. at each half-turn, given  
 2288 that each half-turn is performed at a different energy

2289 (a) Accelerate a proton.

2290 A proton with initial kinetic energy 20 keV is launched on its closed orbit radius,  
 2291  $R_0 = p/qB = 4.087013$  cm. It accelerates over 25 turns due to the presence to  
 2292 REBELOTE[NPASS=24], placed at the end of the sequence. The energy range,  
 2293 20 keV to 5 MeV, and the acceleration rate: 0.1 MeV per cavity, 0.2 MeV per turn,  
 2294 determine the number of turns,  $NPASS+1 = (5 - 0.02)/0.2 \approx 25$ . The accelerated

2295 trajectory spirals out in the fixed magnetic field, it is plotted in Fig. 3.26, reading  
2296 data from zgoubi.plt.

**Fig. 3.26** Twenty five turn spiral trajectory of a proton accelerated in a uniform 0.5 T field from 20 keV to 5 MeV at a rate of 200 kV per turn (a 100 kV gap voltage). The vertical thick line materializes the gap, the upper half (red) corresponds to the first occurrence of CAVITE in the sequence (Tab. 3.8), the lower half (blue) corresponds to the second occurrence of CAVITE



2297 (b) Momentum and energy.

2298 Proton momentum  $p$  and total energy  $E$  as a function of kinetic energy, from  
2299 raytracing (turn-by-turn particle data are read from zgoubi.fai, filled up due to FAI-  
2300 STORE) are displayed in Fig. 3.27, together with theoretical expectations, namely,  
2301  $p(E_k) = \sqrt{E_k(E_k + 2M)}$  and  $E = E_k + M$ .

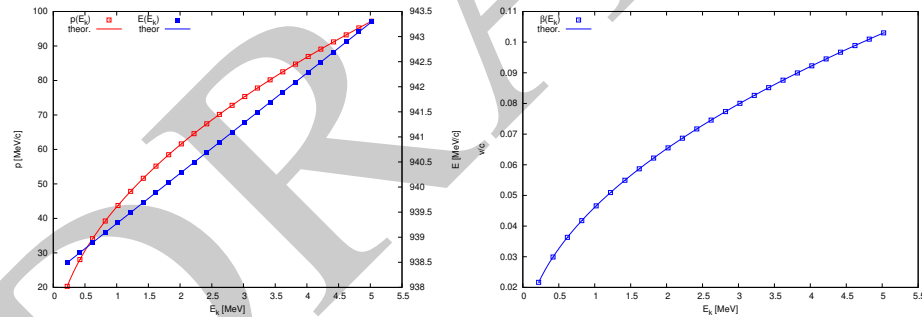


**Fig. 3.27** Energy dependence of, left: proton momentum  $p$  (left axis) and total energy  $E$  (right axis) and of, right: proton normalized velocity  $\beta = v/c$ . Markers: from raytracing; solid lines: theoretical expectation

2302 (c) Velocity.

2303 Proton normalized velocity  $\beta = v/c$  as a function of kinetic energy from raytracing  
2304 is displayed in Fig. 3.27, together with theoretical expectation, namely,  $\beta(E_k) =$   
2305  $p/(E_k + M)$ .

**Table 3.8** Simulation input data file: accelerating a proton in a double-dee cyclotron, from 20 keV to 5 MeV, at a rate of 100 kV per gap, independent of RF phase (longitudinal motion is frozen - see question (e) dealing with CAVITE[IOPT=7] for unfrozen motion). Note that particle data are logged in zgoubi.fai (under the effect of FAISTORE) at both occurrences of CAVITE. The INCLUDE file FieldMapSector.inc is taken from Tab. 3.3

```

Cyclotron, classical. Acceleration: 20 keV -> 6 MeV.
'MARKER' ProbAccelGap_S                               ! Just for edition purposes.
'OBJET'
64.6244403717985                                     ! Reference Brho ("BORO" in the users' guide) -> 200keV proton.
2
1 1                                                    ! Just one ion.
4.087013 0. 0. 0. 0. 0.3162126 'o'                  ! D=0.3162126 => Brho[kG.cm]= 20.435064, kin-E[keV]= 20.
1
'PARTICUL'                                           ! Usage of CAVITE requires partical data,
PROTON                                               ! otherwise, by default \zgoubi\ only requires rigidity.
'FAISTORE'                                           ! Store particle data, turn-by-turn.
zgoubi.fai cavity                                    ! Log coordinates at any occurrence of LABEL=cavity, in zgoubi.fai.
1
'INCLUDE'                                           ! Insert a 180 deg sector field map.
1
FieldMapSector.inc[#S_halfDipole:#E_halfDipole]
'FAISCEAU'                                           ! Particle coordinates before RF gap.
'CAVITE' cavity                                     ! Accelerating gap.
3                                                    ! dW = qVsin(phi), independent of time (phi forced to constant).
0. 0.                                               ! Unused.
100e3 1.57079632679                                  ! Peak voltage 100 kV; RF phase = pi/2.
'INCLUDE'                                           ! Insert a 180 deg sector field map.
1
FieldMapSector.inc[#S_halfDipole:#E_halfDipole]
'FAISCEAU'                                           ! Particle coordinates before RF gap.
'CAVITE' cavity                                     ! Accelerating gap.
3                                                    ! dW = qVsin(phi), independent of time (phi forced to constant).
0. 0.                                               ! Unused.
100e3 1.57079632679                                  ! Peak voltage 100 kV; RF phase = pi/2.
'REBELOTE'                                           ! Repeat NPASS=24 times, for a total of 25 turns; K = 99: coordinates at end of
24 0.1 99                                           ! previous pass are used as initial coordinates for the next pass.
'FAISCEAU'                                           ! Local particle coordinates logged in zgoubi.res.

'SYSTEM'
2                                                    ! 2 SYSTEM command follow:
/usr/bin/gnuplot < ./gnuplot_Zplt_XYLab.gnu &        ! plot trajectories;
/usr/bin/gnuplot < ./gnuplot_awk_Zfai_dTT.gnu &      ! dC/C, dbta/bta, dT/T graph.

'MARKER' ProbAccelGap_E                               ! Just for edition purposes.
'END'

```

Two gnuplot scripts, to obtain respectively Fig. 3.26: and Fig. 3.28:

The awk command in gnuplot\_awk\_Zfai\_dTT.gnu takes care of a 1-row shift so to subtract next turn data from currant turn ones.

```

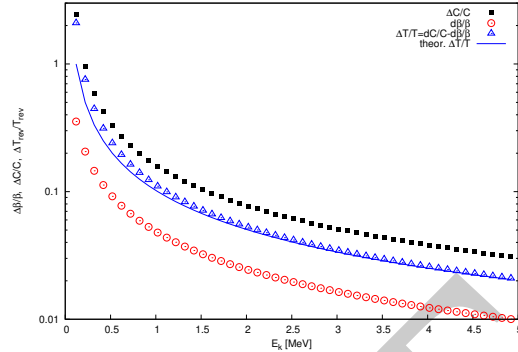
# gnuplot_Zplt_XYLab.gnu
set xtics ; set ytics ; set xlabel "X_{Lab} [m]" ; set ylabel "Y_{Lab} [m]"
set size ratio 1 ; set polar ; cm2m = 0.01 ; pi = 4.*atan(1.)
set arrow from 0, 0 to 0, 0.67 nohead lc "red" lw 6; set arrow from 0, -0.75 to 0, 0 nohead lc "blue" lw 6
noel_1=6 ; noel_2=11 # 1st CAVITE is element noel_1; 2nd CAVITE is noel_2. Col. $42 in zgoubi.plt is element numb.
plot for [nl=noel_1:noel_2:5] "zgoubi.plt" u ($42==noel_1? $22:$22+pi):($10 *cm2m) w p pt 5 ps .2 lc rgb "black"

# gnuplot_awk_Zfai_dTT.gnu
set xtics nomirror; set ytics mirror; set xlabel "E_k [MeV]";
set ylabel "{/Symbol Db}/{/Symbol b}, {/Symbol D}C/C, {/Symbol D}T_{rev}/T_{rev}"; set logscale y; set yrange [:3]
# zgoubi.fai columns: $25: energy; $14: path length; $23: kinetic E; $29: mass; $15: tim
plot "< awk '/#/{next}; { if(prev14>0 && prev25>0) print prev24, ($14 -prev14)/prev14 , prev24} \
{ prev14 = $14; prev24 = $24; prev25=$25 }' < zgoubi.fai" u 1:2 w p pt 5 lc rgb "black" tit "{/Symbol D}C/C" , \
"< awk '/#/{next}; { if(prev14>0 && prev25>0) print prev24, (-sqrt(prev25**2-$29**2)/prev25 + \
sqrt($25**2-$29**2)/$25 )/(sqrt(prev25**2-$29**2)/prev25) , prev24} { prev14 = $14; prev24 = $24; prev25=$25 }' \
< zgoubi.fai" u 1:2 w p pt 6 ps 1.5 lc rgb "red" tit "d{/Symbol b}/{/Symbol b}" , \
"< awk '/#/{next}; { if(prev14>0 && prev25>0) print prev24, ($14 -prev14)/prev14- (-sqrt(prev25**2-$29**2)/prev25 \
+ sqrt($25**2-$29**2)/$25 )/(sqrt(prev25**2-$29**2)/prev25) , prev24} { prev14 = $14; prev24 = $24; prev25=$25 }' \
< zgoubi.fai" u 1:2 w p pt 8 ps 1.5 lc rgb "blue" tit "{/Symbol D}T/T=dC/C-d{/Symbol b}/{/Symbol b}" , \
"< awk '/#/{next}; { if(prev14>0 && prev15>0) print prev24, ($15-prev15)/prev15 , prev24} { prev14 = $14; \
prev24 = $24; prev15=$15 }' < zgoubi.fai" w l lw 2 lc rgb "blue" tit "theor. {/Symbol D}T/T"

```



**Fig. 3.28** Relative variation of velocity  $\Delta\beta/\beta$  (empty circles), circumference  $\Delta C/C$  (solid disks) and revolution time  $\Delta T/T$  (triangles), as a function of energy, from raytracing. Theoretical expectation for the latter is also displayed (solid line), for comparison



2306 (d) Relative velocity, orbit length and time of flight.

2307 The relative increase in velocity is smaller than the relative increase in orbit length  
 2308 as energy increases (this is what Fig. 3.28 shows). Thus the relative variation of the  
 2309 revolution time, Eq. 3.23, is positive; in other words the revolution time increases  
 2310 with energy, the revolution frequency decreases. Raytracing outcomes are displayed  
 2311 in Fig. 3.28, they are obtained using the gnuplot script given in Tab. 3.8. Note that  
 2312 the path length difference (taken as the difference of homologous quantities in a  
 2313 common line) is always between the two CAVITEs (particle data are logged at the  
 2314 two occurrences of CAVITE), crossed successively, which is half a turn. Same for  
 2315 the difference between homologous velocity data on a common line, it corresponds  
 2316 to two successive crossings of CAVITE, *i.e.*, half a turn. The graph includes the  
 2317 theoretical  $\delta T_{\text{rev}}/T_{\text{rev}}$  (Eq. 3.23) for comparison with raytracing; some difference  
 2318 appears in the low velocity regime, this may be due to the large  $\Delta\beta$  step imparted by  
 2319 the 100 kV acceleration at the gaps.

2320 (e) Harmonic  $h=3$  RF.

2321 The input data file for this simulation is given in Tab. 3.9. The RF is on harmonic  
 2322  $h=3$  of the revolution frequency. It has been tuned to ensure acceleration up to 3 MeV.  
 2323 The accelerating gap between the two dees is simulated using CAVITE[IOPT=7]: by  
 2324 contrast with the previous exercise (where CAVITE[IOPT=3] is used), the RF phase  
 2325 at ion arrival at the gap is now accounted for.

2326 Repeating questions (b-d) is straightforward, changing what needs be changed in  
 2327 Tab. 3.9 input data file.

**Table 3.9** Simulation input data file: accelerating a proton in a double-dee cyclotron, from 20 keV to 5 MeV, using harmonic 3 RF. The INCLUDE file is taken from Tab. 3.6

```

Cyclotron, classical. Analytical model of dipole field.
'OBJET'
64.62444403717985                                ! 200keV proton.
2
1 1                                                ! Just one ion.
12.924888 0. 0. 0. 1. 'm'                        ! D=1 => 200keV proton. R=Brho/B=64.624444037[kG.cm]/5[kG].
1
'PARTICUL'                                       ! This is required for spin motion to be computed,
PROTON                                           ! otherwise, by default \zgoubi\ only requires rigidity.
'INCLUDE'
1                                                ! Include a first 180 deg sector.
./180degSector.inc[#S_180degSectorUnifB:#E_180degSectorUnifB]
'CAVITE'
7
0 22862934.0
285e3 -0.5235987755982988
'INCLUDE'
1                                                ! Include a second 180 deg sector.
./180degSector.inc[#S_180degSectorUnifB:#E_180degSectorUnifB]
'CAVITE'
7
0 22862934.0                                       ! RF = 3/T_rev.
285e3 -3.665191429188092                         ! Peak voltage; synchronous phase.
'REBELOTE'
26 0.4 99                                         ! 26+1 turn tracking.
'END'

```

### 2328 3.4 Spin Dance

2329 The DIPOLE analytical field model of exercise 3.2 (Tab. 3.6) is used here, as  
 2330 opposed to using a field map and TOSCA, as it allows more straightforward changes  
 2331 in the field, if desired.

2332 (a) Spin transport.

2333 Spin transport is obtained by adding SPNTRK. PARTICUL is necessary in order  
 2334 to get the Thomas-BMT equation of motion solved [16, Sect. 2]. This results in  
 2335 the input data file given in Tab. 3.10 (excluding FIT and REBELOTE keywords,  
 2336 introduced for the purpose of the following question (b)).

2337 The use of SPNTRK results in the following outcome (an excerpt from zgoubi.res  
 2338 execution listing):

```

2339 4 Keyword, label(s) : SPNTRK
2340 Spin tracking requested.
2341 Particle mass = 938.2721 MeV/c2
2342 Gyromagnetic factor G = 1.792847
2343 Initial spin conditions type 1 :
2344 All particles have spin parallel to X AXIS
2345 PARAMETRES DYNAMIQUES DE REFERENCE :
2346 BORO = 64.624 kG*cm
2347 beta = 0.02064411
2348 gamma = 1.00021316
2349 gamma*G = 1.7932295094
2350 POLARISATION INITIALE MOYENNE DU FAISCEAU DE 1 PARTICULES :
2351 <SX> = 1.000000
2352 <SY> = 0.000000
2353 <SZ> = 0.000000
2354 <S> = 1.000000

```

2355 Spin coordinates are logged in zgoubi.res execution listing using SPNPRT. Five  
 2356 sample passes around the cyclotron (four iterations by REBELOTE) result in the  
 2357 following outcomes in zgoubi.res, under SPNPRT:

```

2358 26 Keyword, label(s) : SPNPRT
2359 INITIAL
2360 SX SY SZ |S| SX SY SZ |S| GAMMA
2361 m 1 1.000000 0.000000 0.000000 1.000000 0.268269 0.963344 0.000000 1.000000 1.0002
2362 m 1 1.000000 0.000000 0.000000 1.000000 0.268599 0.963252 0.000000 1.000000 1.0002
2363 m 1 1.000000 0.000000 0.000000 1.000000 0.268949 0.963154 0.000000 1.000000 1.0003
2364 m 1 1.000000 0.000000 0.000000 1.000000 0.269319 0.963051 0.000000 1.000000 1.0003
2365 m 1 1.000000 0.000000 0.000000 1.000000 0.269710 0.962942 0.000000 1.000000 1.0003

```

**Table 3.10** Simulation input data file: add spin to the cyclotron simulation of Tab. 3.6. The present input file INCLUDEs six copies of the 60 degree sector DIPOLE defined therein

```

Cyclotron, classical. Analytical model of dipole field. Spin transport.
'MARKER' ProbAddSpin_S ! Just for edition purposes.
'OBJET'
64.62444403717985 ! Reference Brho ("BORO" in the users' guide) -> 200keV proton.
2
1 1 ! Just one ion.
12.9248888074 0. 0. 0. 1. 'm' ! D=1 => 200keV proton. R=Brho/B=64.624444037[kG.cm]/5[kG].
1
'PARTICUL' ! This is required to get the time-of-flight,
PROTON ! otherwise, by default \zgoubi\ only requires rigidity.
'SPNTRK' ! Request spin tracking.
1 ! All spins launched longitudinal (parallel to OX axis).
'INCLUDE'
1
6* ./60degSector.inc[#5_60degSectorUnifB:#E_60degSectorUnifB] ! 6 * 60 degree sector.
'FAISCEAU' ! Local particle coordinates.
'FIT' ! Adjust Yo at OBJET so to get final Y = Y0 -> a circular orbit.
1 nofinal ! Variable : Yo.
2 30 0 [12.,65.] ! constraint; default penalty would be 1e-10; maximu 199 calls to function.
1 2e-12 199 ! Constraint: Y_final=Yo.
3.1 1 2 #End 0. 1. 0 ! Allows checking that Y = Y0 and T = T0 = 0, here.
'FAISCEAU' ! Local spin data, logged in zgoubi.res.
'SPNPRT' ! Log particle data here, to zgoubi.fai.
'FAISTORE' ! for further plotting of spin coordinates (by gnuplot, below).
zgoubi.fai
1
'REBELOTE' ! Momentum scan, 60 samples.
60 0.2 0 ! 60 different rigidities; log to video ; take initial coordinates as found in OBJET.
1 ! Change parameter(s) as stated next lines.
OBJET 35 1:5.0063899693 ! Change relative rigity (35) in OBJET; Range (0.2 MeV to 5 MeV).
'SYSTEM' ! 2 SYSTEM commands follow.
1
/usr/bin/gnuplot < ./gnuplot_Zfai_spin.gnu &
'MARKER' ProbAddSpin_E ! Just for edition purposes.
'END'

```

A *gnuplot* script to obtain Fig. 3.29:

The file *zgoubi.lcm* is a copy of *zgoubi.fai* obtained for a  $\Delta s = 1$  cm run; *zgoubi.fai* is for  $\Delta s = 0.5$  cm.

```

# gnuplot_Zfai_spin.gnu
set xlabel "G/(Symbol q)"; set ylabel "Spin precession angle {/Symbol q}_{sp} / 2{/Symbol p}"
set y2label "relative difference num./theor"; set logscale y2
set xtics; set ytics nomirror; set y2tics; am = 938.27208; G = 1.79284735; pi = 4.*atan(1.); set key t c spacin 1.5
plot \
"zgoubi.fai" u ($31*$25/$29):(((4.*pi -atan($21/$20)))/(2.*pi)) w lp pt 4 ps .7 tit "{/Symbol q}_{sp}/2{/Symbol p}" , \
"zgoubi.lcm" u ($31*$25/$29):(abs((4.*pi -atan($21/$20))/pi*180-$31*$25/$29*360.)) axes xly2 w lp pt 8 ps .7 tit "1 cm", \
"zgoubi.fai" u ($31*$25/$29):(abs((4.*pi -atan($21/$20))/pi*180-$31*$25/$29*360.)) axes xly2 w lp pt 8 ps .7 tit "5 mm"

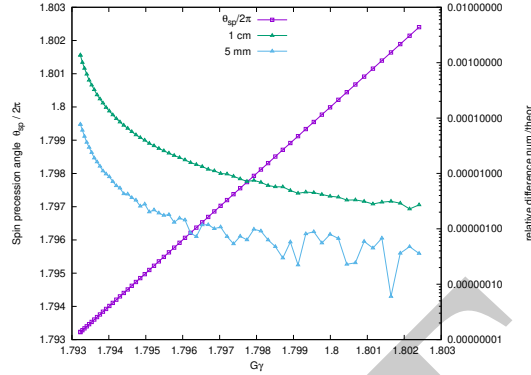
```

2366 (b) Spin precession.

2367 Proton case is considered, simulation is performed using Tab. 3.10 input data file.  
 2368 Initial spin is parallel to the X axis (longitudinal). The particle is raytraced on the  
 2369 circular closed orbit over one revolution, for a particular momentum. Particle data  
 2370 resulting from a FIT (FIT forces orbit closure, by varying the initial  $Y_0$ ) are logged  
 2371 in *zgoubi.fai*, by FAISTORE. The computation is repeated using REBELOTE in the  
 2372 very manner that the energy scan was done in exercise 3.2, over an energy range  
 2373 12 keV  $\rightarrow$  5 MeV.

2374 Figure 3.29 (obtained using the *gnuplot* script given in Tab. 3.10) displays the  
 2375 resulting energy dependence of the spin precession,  $\theta_{sp}(E)$ , together with its differ-  
 2376 ence to theoretical expected  $\theta_{sp}(E) = G \frac{E}{M} \times 2\pi = G\gamma \times 2\pi$  (proton gyromagnetic  
 2377 anomaly  $G = 1.792847$ ).

**Fig. 3.29**  $G\gamma$  dependence of the spin precession angle over a revolution around the cyclotron, in the moving frame (left axis), and relative difference to  $G\gamma$  for the two integration step sizes  $\Delta s = 0.5$  and 1 cm (right axis). Markers are from raytracing, solid lines are to guide the eye



2378 (c) Spin tune.

2379 Two protons are injected with longitudinal initial spin  $S_z \parallel OX$  axis and respective  
 2380 energies 12 keV and 5.52 MeV, thus the following OBJET (a slight modification to  
 2381 Tab. 3.10 data):

```

2382 'OBJET'
2383 64.62444403717985 ! Reference Brho ("BORO" in the users' guide) -> 200keV proton.
2384 2
2385 2 1
2386 12.9248888074 0. 0. 0. 1. 'm' ! D=1 => 200keV proton, R=Brho/B=64.624444037[kG.cm]/5[kG].
2387 67.997983 0. 0. 0. 5.2610112 'o' ! p[MeV/c]=101.926, Brho[kG.cm]=339.990, kin-E[MeV]=5.52.
2388 1 1
    
```

2389 FAISCEAU following FIT (Tab. 3.10) allows to control that momentum and  
 2390 trajectory radius are matched, which means coordinates at OBJET and current co-  
 2391 ordinates at FAISCEAU are equal. Inspection of zgoubi.res execution listing shows  
 2392 for instance, after 4 turns:

	OBJET					FAISCEAU						
	D	Y(cm)	T(mr)	Z(cm)	P(mr)	S(cm)	D-1	Y(cm)	T(mr)	Z(cm)	P(mr)	S(cm)
2393	1.0000	12.925	0.000	0.000	0.000	0.0000	0.0000	12.925	0.000	0.000	0.000	3.248379E+02
2394	5.2610	67.998	0.000	0.000	0.000	0.0000	4.2610	67.998	-0.000	0.000	0.000	1.708976E+03

2397 A graphic of the projection of the spin motion on the longitudinal axis, over a  
 2398 few turns, from the ray tracing, is given in Fig. 3.30, together with the longitudinal  
 2399 component as of the parametric equations of motion

$$\begin{cases} S_x = \hat{S} \cos(G\gamma\theta) \\ S_y = \hat{S} \sin(G\gamma\theta) \end{cases} \quad (3.37)$$

2400 The motion amplitude is  $\hat{S} = \sin \phi$ , with  $\phi$  the angle that the spin vector makes with  
 2401 the vertical precession axis. In this simulation  $\mathbf{S}$  is launched parallel to  $OX$ , thus  
 2402  $\phi = \pi/2$  and  $\hat{S} = 1$ .

2403 Now, checking the spin precession:

2404 Placing both FAISCEAU and SPNPRT commands right after the first dipole  
 2405 sector allows checking the spin precession and its relationship to particle rotation,  
 2406 for simplicity right after the first pass through that first sector, as follows. FAISCEAU  
 2407 and SPNPRT (Tab. 3.10) yield, respectively:

	OBJET					FAISCEAU						
	D	Y(cm)	T(mr)	Z(cm)	P(mr)	S(cm)	D-1	Y(cm)	T(mr)	Z(cm)	P(mr)	S(cm)
2408	1.0000	12.925	0.000	0.000	0.000	0.0000	0.0000	12.925	0.000	0.000	0.000	3.248379E+02
2409	5.2610	67.998	0.000	0.000	0.000	0.0000	4.2610	67.998	-0.000	0.000	0.000	1.708976E+03

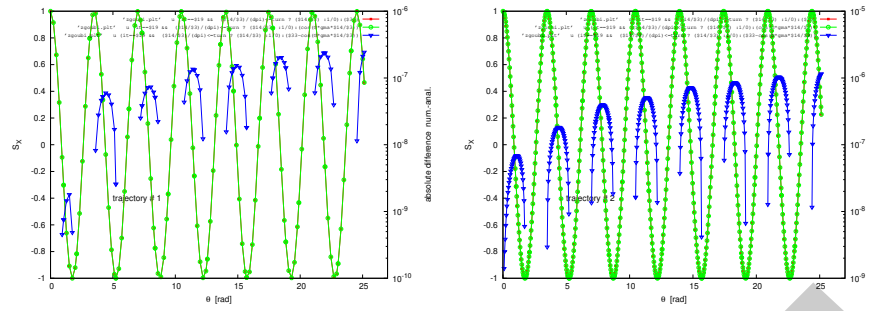


**Fig. 3.30** Longitudinal spin component motion (left vertical axis), observed in the moving frame, case of 0.2 MeV energy,  $R=12.924888$  cm (left graph), and of 5.52 MeV energy,  $R=67.998$  cm (right graph). Markers are from ray tracing, the solid line is the theoretical expectation (Eq. 3.37). The right vertical axis (triangle markers; solid line is to guide the eye) shows the absolute difference between both. The oscillation is as expected slightly faster at 5.52 MeV: frequencies are in the ratio  $\gamma(5.52 \text{ MeV})/\gamma(0.2 \text{ MeV}) = 1.00566$

		INITIAL				FINAL				--- angles ---			
		SX	SY	SZ	S	SX	SY	SZ	S	GAMMA	Si, Sf  (deg.)	(Z, Sf) (deg.)	
2412	m	1	1.000000	0.000000	0.000000	1.000000	-0.302266	-0.953224	0.000000	1.000000	1.0002	-107.594	90.000
2413	o	1	1.000000	0.000000	0.000000	1.000000	-0.312396	-0.949952	0.000000	1.000000	1.0059	-108.204	90.000

2417 SPNPRT tells that,

2418 - case of the first particle, tagged 'm' above; its energy is 200 keV,  $\gamma = 1.00021315$ ,

2419 its spin tune is  $\nu_{sp} = G\gamma = 1.793229$

2420 The computed value of the ' $(S_i, S_f)$ ' angle between initial and final spin vectors is

2421  $-107.594$  (truncated), negative as spin precession has the sign of proton rotation.

2422 Theoretical expectation is  $G\gamma\alpha = -107.59377$  deg. The resulting spin components

2423 are, as above,  $S_X = \cos(-107.59377) = -0.302266$  and  $S_Y = \sin(-107.59377) =$

2424  $-0.9532235$ .

2425 - case of the second particle, tagged 'o'; its energy is 5.52 MeV,  $\gamma = 1.00588315$ ,

2426 its spin tune is  $\nu_{sp} = G\gamma = 1.803394$

2427 The computed value of ' $(S_i, S_f)$ ' is  $-108.204$  (truncated). Theoretical expectation is

2428  $G\gamma\alpha = -108.20370$  deg.

2429 Now, accounting for particle rotation in order to get spin coordinates in the

2430 laboratory frame:

2431 - the FAISCEAU outcome above shows that, after crossing the 60 deg sector the

2432 angles of the two particles have the value  $T = 0$ , which is expected as they are

2433 launched with zero incidence, and as DIPOLE uses a polar coordinate system [16]

2434 with particle coordinates computed in the moving (rotating) frame. The latter has

2435 also undergone a  $-60$  deg rotation, clockwise, which is therefore the implicit rotation

2436 of the particles in the laboratory frame. The spin precession in the laboratory frame

2437 results, namely,

2438 - case of the first particle:  $(1 + G\gamma)\alpha = -167.59377$  deg.

2439 - case of the second particle:  $(1 + G\gamma)\alpha = -168.20370$  deg.

2440 (d) Spin dance.

2441 A 200 keV proton is injected with its initial spin vector at 80 degrees from the  
 2442 vertical axis. The input data file for this simulation is given in Tab. 3.11, together  
 2443 with a gnuplot script for the animation. The latter plots three things, concurrently:

2444 - the circular trajectory of the particle in the (X,Y) plane: this is the curve at Z=0  
 2445 in Fig. 3.31, a set of points  $\{(R \cos(-X), R \sin(-X), 0)\}$  resulting from the step by  
 2446 step integration. Note that X is counted positive clockwise in zgoubi.fai (consistently  
 2447 with the definition of DIPOLE parameters, Fig. 9 in [16]), hence “-X” the rotation  
 2448 angle;

2449 - the spin vector: its foot is attached to the particle (the previous set of points),  
 2450 whereas its tip is at  $\{(S_X \cos(-X) - S_Y \sin(-X), S_X \sin(-X) + S_Y \cos(-X), S_Z)\}$ ,  
 2451 with  $S_X, S_Y, S_Z$  the spin vector components in the moving frame as read from  
 2452 zgoubi.fai.  $S_Z$  is constant as the precession axis is parallel to the Z axis. The  
 2453  $\begin{pmatrix} \cos(-X) & -\sin(-X) \\ \sin(-X) & \cos(-X) \end{pmatrix}$  rotation applied to the  $(S_X, S_Y)$  vector accounts for the trans-  
 2454 formation from the moving frame to the laboratory frame;

2455 - the cycloidal shape trajectory of the tip of the spin vector (the previous set of  
 2456 points).

2457 A frozen view of that spin dance, over about 2.5 proton revolutions around the  
 2458 ring, is given in Fig. 3.31.

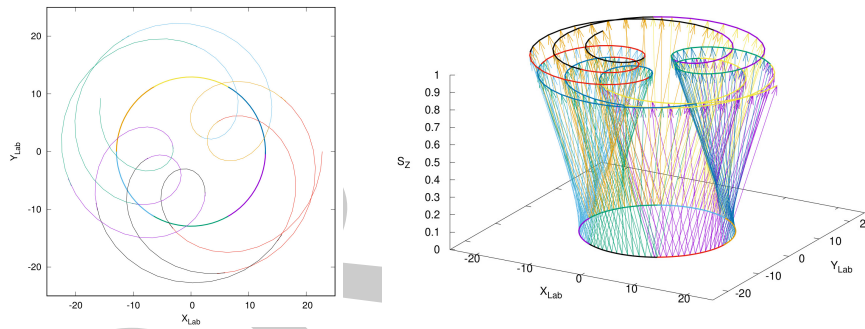


**Fig. 3.31** Dance - frozen, here - of the spin of a 200 keV proton over 2.5 turns around the cyclotron. The circle on the left, or bottom closed curve on the right, is the trajectory of the proton. The cycloidal curve represents the motion of the spin vector tip in the moving frame

**Table 3.11** Simulation input data file: spin dance, 20 turns around a uniform field cyclotron. The INCLUDE file 60degSector.inc is taken from Tab. 3.6

Note: this animation (input data file & gnuplot script) is available in zgoubi sourceforge repository at

[https://sourceforge.net/p/zgoubi/code/HEAD/tree/branches/exemples/book/zgoubiMaterial/cyclotron\\_classical/ProbAddSpin/spinDance/](https://sourceforge.net/p/zgoubi/code/HEAD/tree/branches/exemples/book/zgoubiMaterial/cyclotron_classical/ProbAddSpin/spinDance/)

```
Cyclotron, classical. Spin dance.
'MARKER' ProbAddSpinDance_S ! Just for edition purposes.
'OBJET'
64.62444403717985 ! Reference Brho ("BORO" in the users' guide) -> 200keV proton.
2
1 1 ! Just one ion.
12.9248888074 0. 0. 0. 1. 'm' ! D=1 => 200keV proton. R=Brho/B=64.624444037[kG.cm]/5[kG].
1
'PARTICUL' ! This is required to get the time-of-flight,
PROTON ! otherwise, by default \zgoubi\ only requires rigidity.
'SPNTRK' ! Request spin tracking.
4.1 ! All spins are initially
0.984807753012 0. 0.173648177667 ! at 10 degrees to X axis.
'FAISCEAU'
'INCLUDE'
1
6* ./60degSector.inc[#S_60degSectorUnifB:#E_60degSectorUnifB] ! 6 * 60 degree sector.
'REBELOTE' ! Multiturn:
19 0.2 99 ! 19 additional passes.
'SYSTEM'
1
gnuplot < ./gnuplot_Zplt_SDance.gnu
'MARKER' ProbAddSpinDance_E ! Just for edition purposes.
'END'
```

A gnuplot script to obtain the spin dance in Fig. 3.31. Note a “mag” factor, aimed at artificially increasing the amplitude of the vector tip oscillation in this graphic:

```
set xlabel "X_{Lab}"; set ylabel "Y_{Lab}"; set zlabel "S_Z"; set xtics; set ytics; set ztics #unset ztics
set xrange [-25:25]; set xrange [-25:25]; set yrange [-25:25]; set xyplane 0
dip1=7; dip2=22; dd=3 # positining of 1st and last dipoles in zgoubi.dat sequence, and increment
# magnifies apparent spin tilt speedUp graphic pi/3 z norm
mag = 10. ; speedUp=1 ; pi3 = 4.*atan(1.)/3 ; nz=0.18

# JUST 2D, PROJECTED IN (X,Y) PLANE, FIRST:
set size ratio -1
do for [i=1:239]{ plot \
for [dip=dip1:dip2:dd] "zgoubi.plt" every 1:::speedUp*i u ($i9==1 && $42==dip? $i0*cos(-$22-pi3*(dip-6.)/3.):1/0): \
($i0*sin(-$22-pi3*(dip-6.)/3.)) w l lw 3 notit , \
for [dip=dip1:dip2:dd] "zgoubi.plt" every 1:::speedUp*i u ($i9==1 && $42==dip? $i0*cos(-$22-pi3*(dip-6.)/3.) \
+mag*(cos(-$22-pi3*(dip-6.)/3.)*$33-sin(-$22-pi3*(dip-6.)/3.)*$34) :1/0): \
($i0*sin(-$22-pi3*(dip-6.)/3.) +mag*(sin(-$22-pi3*(dip-6.)/3.)*$33+cos(-$22-pi3*(dip-6.)/3.)*$34) w l lw 3 notit }
unset size

# 3D, NEXT:
do for [i=1:239]{ splot \
for [dip=dip1:dip2:dd] "zgoubi.plt" every speedUp*i:::speedUp*i u ($i9==1&& $42==dip? $i0*cos(-$22-pi3*(dip-6)/3):1/0): \
($i0*sin(-$22-pi3*(dip-6)/3)):(($i0*(mag*(cos(-$22-pi3*(dip-6)/3)*$33-sin(-$22-pi3*(dip-6)/3)*$34): \
(mag*(sin(-$22-pi3*(dip-6)/3)*$33+cos(-$22-pi3*(dip-6)/3)*$34)):(($35/nz) w vectors notit , \
for [dip=dip1:dip2:dd] "zgoubi.plt" every 1:::speedUp*i u ($i9==1 && $42==dip? $i0*cos(-$22-pi3*(dip-6)/3) :1/0): \
($i0*sin(-$22-pi3*(dip-6)/3)):(($i0*(mag*(cos(-$22-pi3*(dip-6)/3)*$33-sin(-$22-pi3*(dip-6)/3)*$34):1/0): \
($i0*sin(-$22-pi3*(dip-6)/3.)):(($i0*(mag*(sin(-$22-pi3*(dip-6)/3.)*$33+cos(-$22-pi3*(dip-6)/3.)*$34)):(($35/nz) w l lw 3 notit }
for [dip=dip1:dip2:dd] "zgoubi.plt" every 1:::speedUp*i u ($i9==1 && $42==dip? $i0*cos(-$22-pi3*(dip-6)/3)+mag*( \
cos(-$22-pi3*(dip-6)/3)*$33-sin(-$22-pi3*(dip-6)/3)*$34):1/0):($i0*sin(-$22-pi3*(dip-6)/3)+mag*(sin(-$22-pi3*(dip-6)/3) \
*$33+cos(-$22-pi3*(dip-6)/3)*$34):($35/nz):($i9==1&&$42==dip? $i0*cos(-$22-pi3*(dip-6)/3 +mag*(cos(-$22-pi3*(dip-6)/3) \
*$33 -sin(-$22-pi3*(dip-6)/3)*$34) :1/0): ($i0*sin(-$22-pi3*(dip-6)/3) +mag*(sin(-$22-pi3*(dip-6)/3)*$33+cos(-$22-pi3* \
(dip-6)/3)*$34)):(($35/nz) w l lw 3 notit }
```

2459 (e) Deuteron.

2460 The input data file set up for questions (b-e) can be used *mutatis mutandis*, as  
2461 follows.

2462 Raytracing a different particle requires changing the reference rigidity, BORO,  
2463 under OBJET, and changing particle data, under PARTICUL. That reference rigidity  
2464 is to be determined from the field value in the dipole model (namely,  $B_0 = 5$  kG).

Particle data for these two particles are (respectively mass (MeV/c<sup>2</sup>), charge (C), G factor):

$$\text{deuteron} : \quad 1875.612928 \quad 1.602176487 \times 10^{-19} \quad -0.14301$$

$${}^3\text{He}^{2+} : \quad 2808.391585 \quad 3.204352974 \times 10^{-19} \quad -0.14301$$

### 2465 3.5 Synchronized Spin Torque

2466 The simulation input data file of exercise 3.4-(d) can be used here, with a few  
2467 addenda or modifications, as follows:

2468 (i) the initial ion coordinate D (rigidity relative to the reference BORO=64.6244440)  
2469 under OBJET has to be calculated for the four energies concerned;

2470 (ii) the closed orbit radius at 0.2, 108.412, 118.878 and 160.746 MeV has to be  
2471 found; calculation is straightforward given that the field considered here is vertical,  
2472 uniform, namely,  $B_z = \text{constant} = 5 \text{ kG}$ ,  $\forall R$ , so that  $R = B\rho/B_z$ ; otherwise a FIT  
2473 procedure can be used to find the orbit radius, given the rigidity, as done already  
2474 in various exercises [16, lookup “closed orbit”], that could help for instance in the  
2475 presence of a radial index, or field defects;

2476 (iii) initial spins are set vertical for convenience, but this is not mandatory;

2477 (iv) the multiturn tracking is set to a few 10s of turns, in order to allow a few spin  
2478 precessions;

2479 (v) particle data through DIPOLes are saved step-by-step all the way in zgoubi.plt  
2480 by means of IL=2 (the integration step size is 1 cm (Tab. 3.6), thus zgoubi.plt may  
2481 end up bulky);

2482 (vi) turn-by-turn data are saved in zgoubi.fai by means of FAISTORE;

2483 (vii) SPINR is added at the end of the sequence, to impart on spins the requested  
2484 X-tilt.

2485 This results in the updated simulation input data file given in Tab. 3.12.

2486 The oscillatory motion of the vertical spin component as the ion orbits around the  
2487 ring, is displayed in Fig. 3.32. The spin points upward, parallel to the vertical axis at  
2488 start; SPINR kick is 10 deg in the present case. At  $G\gamma = 2$  the spin always finds itself  
2489 back in the (Y,Z) transverse plane after one proton orbit, this synchronism causes  
2490 the cumulated spin tilt at SPINR to take the value  $N \times 10 \text{ deg}$  (with N the number of  
2491 orbits). Thus after 18 proton orbits, 36 spin precessions, the spin points downward;  
2492 it takes 36 orbits, or 226.194 rad, to complete an oscillation. If  $G\gamma$  moves away from  
2493 an integer, the spin tilts with bounded amplitude, within the limits of a cone.

2494 Additional graphs and details are obtained using the simulation file of Tab. 3.13.  
2495 This file simulates spin motion in three different cases,  $G\gamma = 1.79322$ ,  $G\gamma = 2$ ,  
2496 integer, yielding an integer number of spin precessions over one proton orbit around  
2497 the cyclotron, and  $G\gamma = 2.5$ , half-integer, yielding a half-integer number of spin  
2498 precessions over one proton orbit. Outcomes are given in Fig. 3.33 which shows the  
2499 spin motion projected on the (X,Y) plane (horizontal), and on a sphere, step-by-step.  
2500 The spin kick by SPINR is 20 deg in this case. If  $G\gamma = 1.793229$ , far from an integer,  
2501 **S**, initially vertical, remains at a bounded angle to the vertical axis, X-kicked from  
2502 one circle to another, turn after turn; if  $G\gamma = 2$  the spin vector flips by 20 degree in  
2503 the (Y,Z) plane at SPINR, turn after turn; if  $G\gamma = 2.5$ , half-integer, the spin vector



**Table 3.12** Simulation input data file: superimposition of a turn-by-turn localized 10 deg X-rotation of the spin (using SPINR[ $\phi = 0, \mu = 10$ ]), on top of Thomas-BMT  $2\pi G\gamma$  Z-precession. The INCLUDE file 60degSector.inc is taken from Tab. 3.6

```

Cyclotron, classical. Synchronous spin kick.
'MARKER' ProbAddSpinTorque_S ! Just for edition purposes.
'OBJET'
64.62444403717985 ! Reference Brho ("BORO" in the users' guide) -> 200keV proton.
2
4 1
12.9248888074 0. 0. 0. 1. 'm' ! D=1 => 200keV proton. R=Brho/B=64.624444037[kG.cm]/5[kG].
3.0947295453790e2 0. 0. 0. 0. 23.9439548880185 'm' ! Ggamma=2
3.2492145208941e2 0. 0. 0. 0. 25.1392067607172 'm' ! Ggamma=2.02
3.8177333586897e2 0. 0. 0. 0. 29.5378429599586 'm' ! Ggamma=2.1
1 1 1 1
'PARTICUL' ! This is required for spin motion to be computed,
PROTON ! otherwise, by default \zgoubi\ only requires rigidity.
'SPNTRK' ! Request spin tracking.
4.1 ! Request spin tracking.
0. 0. 1. ! Initial spin vector is defined here.

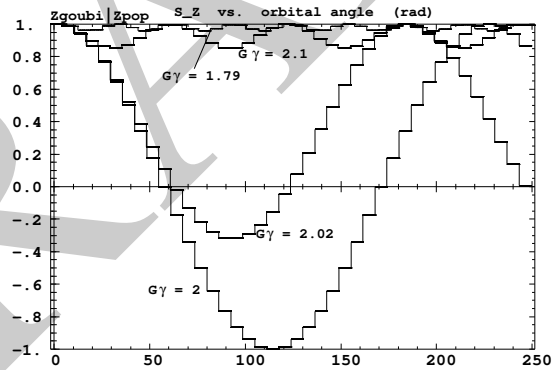
'FAISTORE'
zgoubi.fai
1

'INCLUDE'
1
6* ./60degSector.inc[#S_60degSectorUnifB:#E_60degSectorUnifB] ! 6 * 60 degree sector.
'FAISCEAU'
'SPINR' ! Spin rotation,
1 ! about the X-axis, by 10 or 20 degrees as the case may be.
0. 10. ! Multiturn ray-tracing.

'REBELOTE'
39 0.2 99
'SYSTEM'
1
gnuplot < ./gnuplot_Zplt_spinTilt.gnu
'MARKER' ProbAddSpinTorque_E ! Just for edition purposes.
'END'

```

**Fig. 3.32**  $S_Z$  motion versus orbital angle, while the ion orbits on a circle.  $S_Z$  is constant over a turn and then undergoes a discontinuity upon the 10 deg X-tilt, hence the step function. At  $G\gamma = 2$  it takes 36 turns, or 226.194 rad, to complete an oscillation. A graph obtained using zpop: menu 7; 1/1 to open zgoubi.plt; 2/[6,23] for  $S_Z$  versus  $\theta$ ; 7 to plot



2504 undergoes a half-integer number of precessions over one orbit around the cyclotron,  
 2505 it jumps and alternates between vertical, and the surface of the 20 degree Z-axis  
 2506 cone.

**Table 3.13** Simulation input data file: a similar simulation to 3.12, for different  $G\gamma$  values, namely 1.79322, 2 and 2.5. The spin kick at SPINR has been changed to 20 deg. Regarding the use of OBJE[T|IEX] option: IEX=-9 allows inhibiting the tracking for the particle(s) concerned, all the rest left unchanged; it is necessary here to have at least one particle with IEX=1, for proper operation of the gnuplot scripts. The INCLUDE file 60degSector.inc is taken from Tab. 3.6

```
Cyclotron, classical. Synchronized spin kick in a uniform field
'MARKER' ProbAddSpinSphere_S ! Just for edition purposes.
'OBJET'
64.62444403717985 ! Reference Brho ("BORO" in the users' guide) -> 200keV proton.
2
3 1
12.924889 0. 0. 0. 1. 'o' ! Ggamma=1.793229 -> 0.200MeV;
309.47295 0. 0. 0. 23.943951797 'i' ! Ggamma=2 -> 108.411628MeV;
608.30878 0. 0. 0. 47.064911290 'h' ! Ggamma=2.5 -> 370.082556MeV.
1 1 1 ! For any particle: set to 1 to enable ray-tracing, or to -9 to ignore.
'PARTICUL' ! This is required for spin motion to be computed.
PROTON ! otherwise, by default \zgoubi\ only requires rigidity.
'SPNTRK' ! Request spin tracking.
4.1 ! All initial spins taken parallel to Z axis.
0. 0. 1.

'SPNPRT' PRINT

'INCLUDE'
1
6* ./60degSector.inc[#S_60degSectorUnifB:#E_60degSectorUnifB] ! 6 * 60 degree sector.
'FAISCEAU'
'SPINR'
1 ! Spin rotation,
0. 20. ! about the X-axis, by 20 degree here.

'REBELOTE' ! REBELOTE[K=99] for multiturn ray-tracing,
39 0.2 99 ! 39+1 turns total.
'SYSTEM'
3
gnuplot <./gnuplot_Zspnprt_spinOscillation.gnu
gnuplot <./gnuplot_Zplt_spinTilt.gnu
gnuplot <./gnuplot_Zplt_spinTilt_3D.gnu
'END'
'MARKER' ProbAddSpinSphere_E ! Just for edition purposes.
'END'
```

A gnuplot script to produce spin components versus turn, reading from zgoubi.SPNPRT.Out, Fig. 3.33:

```
# gnuplot_Zspnprt_spinOscillation.gnu
set xlabel "turn"; set ylabel "S_X, S_Y, S_Z"; set key b l ; nbrtrj=3 # number of trajectories tracked
do for [it=1:nbrtrj] { unset label; set label sprintf("particle %3.5g",it) at 10, 0.8
plot [] [-1:1] \
'zgoubi.SPNPRT.Out' every nbrtrj::(it+2) u ($22):($13) w lp lw .3 pt 4 ps .8 lc rgb "red" , \
'zgoubi.SPNPRT.Out' every nbrtrj::(it+2) u ($22):($14) w lp lw .3 pt 6 ps .8 lc rgb "blue" , \
'zgoubi.SPNPRT.Out' every nbrtrj::(it+2) u ($22):($15) w lp lw .3 pt 8 ps .8 lc rgb "black" ; pause .5
set terminal postscript eps blacktext color enh
set output sprintf('gnuplot_Zspnprt_spinOsc_trj%i.eps',it); replot; set terminal X11; unset output }
```

A gnuplot script to produce 2D spin motion projection of Fig. 3.33:

```
# gnuplot_Zplt_spinTilt.gnu
set xlabel "S_X"; set ylabel "S_Y"; set size ratio -1; set xrange [-1:1]; set yrange [-1:1]; set key t l
nbrtrj=3 # number of trajectories tracked
do for [it=1:nbrtrj] { unset label; set label sprintf("particle %i",it) at -.9, .8
plot 'zgoubi.plt' u ($19==it? $33 :1/0):($34):($35) w lp lw .3 ps .2 lc rgb "blue" ; pause .5
set terminal postscript eps blacktext color enh
set output sprintf('gnuplot_Zplt_SX-SY_trj%i.eps',it); replot; set terminal X11; unset output }
```

A gnuplot script to produce the projection on a sphere of Figs. 3.33:

```
# gnuplot_Zplt_spinTilt_3D.gnu
set xlabel "X"; set ylabel "Y"; set zlabel "Z"; set xrange [-1:1]; set yrange [-1:1]; set zrange [-1:1]
set xyplane 0; set view equal xyz; set view 49, 339; unset colorbox
set urange [-pi/2:pi/2]; set vrange [0:2*pi]; set parametric; R = 1. # radius of sphere
nbrtrj=3 # number of trajectories tracked
do for [it=1:nbrtrj] { unset label; set label sprintf(" particle %i",it) at -1, .9, 1.
splot R*cos(u)*cos(v),R*cos(u)*sin(v),R*sin(u) w l lw .2 lc rgb "cyan" notit , \
'zgoubi.plt' u ($19==it? $33 :1/0):($34):($35) w lp lw .2 ps .4 lc palette ; pause .5
set terminal postscript eps blacktext color enh
set output sprintf('gnuplot_Zplt_S3D_trj%i.eps',it); replot; set terminal X11; unset output }
```

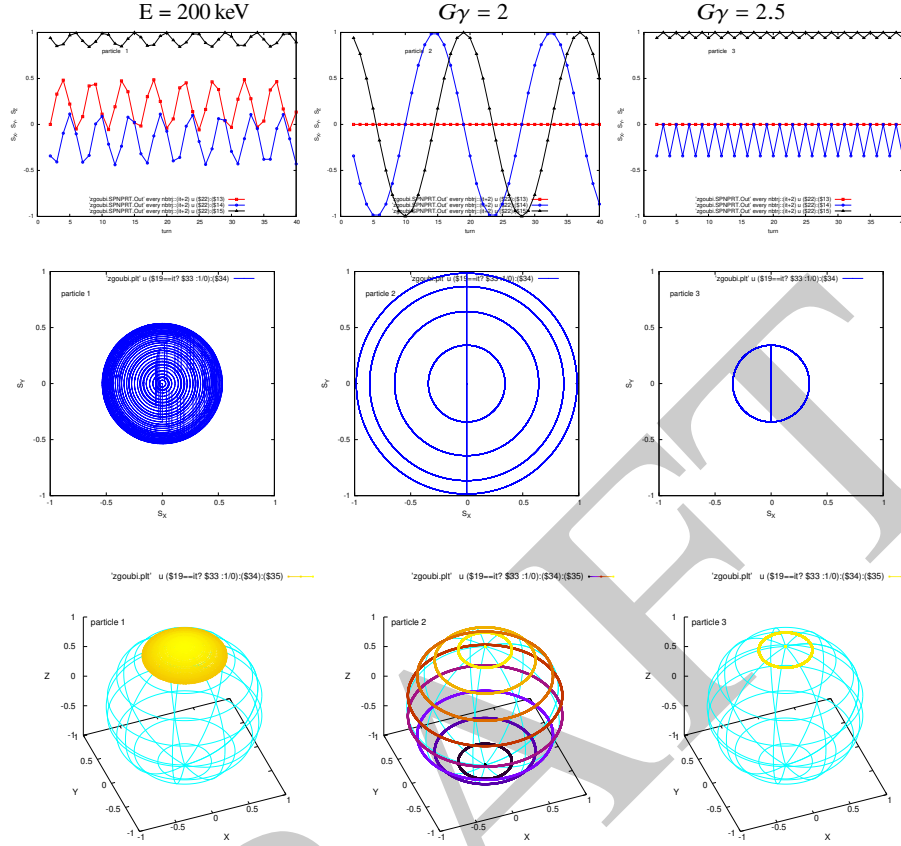


**Fig. 3.33** Top row: spin coordinates versus turn; middle row: projection in the median plane (the segment between two consecutive circles materializes the location of the X-kick by SPINR); bottom row: projection on a sphere.  $G\gamma = 1.793229$ : far from an integer,  $\mathbf{S}$  remains within a cone of reduced aperture.  $G\gamma = 2$ : the spin vector oscillates between up and down orientations, by 20 deg steps; it takes  $180/20=9$  orbits for the X-precession at SPINR to flip the spin;  $G\gamma = 2.5$ : the spin vector finds itself back in the (Y,Z) plane at the location of SPINR, after one orbit and a half-integer number of precessions; it alternates between vertical and 20 deg from vertical, after each orbit around the cyclotron

2507 **3.6 Weak Focusing**

2508 (a) Add a field index.

2509 To the first order in  $R$ , in the median plane ( $Z=0$ ) and noting  $R = R_0 + dR$ ,  
 2510  $B_Z(R_0) = B_0$ ,  $B_Z(R) = B$ , the field writes (Sect. 3.2.2)  $B(R) = B_0 + dR \left. \frac{\partial B}{\partial R} \right|_{R_0}$ . With  
 2511  $k = \frac{R_0}{B_0} \frac{\partial B}{\partial R}$  (Eq. 3.11) this yields

$$B(R) = B_0 + \frac{B_0}{R_0} k dR \tag{3.38}$$

2512 Assume the earlier 200 keV conditions as a reference, thus take

2513  $R_0 = 12.9248888$  cm as the 200 keV radius, whereas  $B_0 = B(R_0) = 5$  kG.

2514 Take  $k = -0.03$ , a slow decrease of the field with  $R$  - proper to ensure appropriate  
2515 vertical focusing with marginal impact on the radial extent of the cyclotron. For  
2516 instance, with that index value the 5 MeV orbit is at a radius of 75.75467 cm (see  
2517 OBJET in Tab. 3.3) (giving  $B = 0.3235$  T along the orbit), whereas if  $k=0$  then  
2518  $R = 75.75467$  cm is the 6.8463 MeV orbit radius ( $B = 0.3788$  T).

2519 The field map is generated using a similar Fortran program to that of exercise 3.1  
2520 (see Tab. 3.1), *mutatis mutandis*, namely, introducing a reference radius  $R_0$  and  
2521 field index  $k$ . The resulting program is given in Tab. 3.14, it can be compiled and  
2522 executed, as is, excerpts of the field data file so obtained are given in Tab. 3.15, a  
2523 graph  $B_Z(R, \theta)$  is given in Fig. 3.34. The orbit radius is assessed for three different  
2524 energies, and appears to be in accord with theoretical expectation (Fig. 3.34-right).  
2525 Comparison with Fig. 3.20-right shows the effect of the negative index on the radial  
2526 distribution of the orbits, including a radius about 20% greater in the 5 MeV range.  
2527 The input data file to find these trajectories is given in Tab. 3.16:

2528 - the file defines an INCLUDE segment, #S\_60degSectorIndx to #E\_60degSectorIndx,  
2529 used in subsequent exercises;

2530 - the file is set to allow a preliminary test regarding the field map geneSector  
2531 MapIndex.out (as produced by the program given in Tab. 3.14), by computing  
2532 three circular trajectories centered on the center of the map, at respectively 20 keV,  
2533 200 keV (the reference energy for the definition of the gradient index  $k$ ) and 5 MeV  
2534 (a large radius);

2535 - note that once the FIT procedure is completed, zgoubi continues in sequence,  
2536 so raytracing the 3 ions through the field map with, this time, IL set to 2 under  
2537 TOSCA for stepwise particle data to be logged in zgoubi.plt.

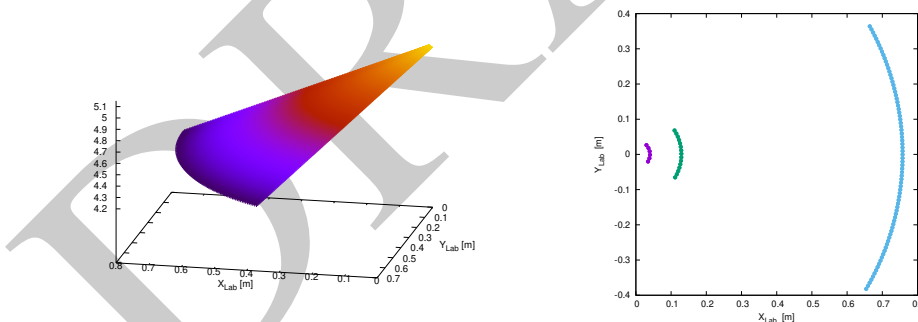


**Fig. 3.34** Left: field map of a 60 deg magnetic sector with radial index, 76 cm radial extent. The field decreases from the center of the ring (at  $(X_{Lab}, Y_{Lab}) = (0, 0)$ ). Right: three circular arc of trajectories over a sextant, at respectively from left to right: 0.02 MeV, 0.2 MeV (energy on the reference radius) and 5 MeV

**Table 3.14** A Fortran program which generates a  $60^\circ$  mid-plane field map with non-zero transverse field  $k$ . The field map it produces is logged in geneSectorMapIndex.out

```

C geneSectorMapIndex.f program
implicit double precision (a-h,o-z)
parameter (pi=4.d0*atan(1.d0), BY=0.d0, BX=0.d0, Z=0.d0)

open(unit=2,file='geneSectorMapIndex.out')           ! Field map storage file.

C----- Hypotheses :
AT = 60.d0 /180.d0*pi           ! Angular extent of field map. Can be changed 360, 60 deg, etc.).
B0 = 5.d0 ;R0 = 12.9248888074d0  ! field at R0 (kG); 200keV radius (cm), B(R0)=B0=5kG.
ak = -0.03d0                    ! Field index, defined at R0.
Rmi=1.d0; Rma=76.d0; RM=50.d0  ! cm. Radial extent of field map; reference radius to define mesh.
dR = 0.5d0 ; NR = NINT((Rma - Rmi)/dR)+1  ! R-distance between nodes in mesh. Number of R-nodes.
C                                     RdA=RM*dA is the distance between two nodes along R=RM arc.
RdA = 0.5d0 ! given angle increment dA (dA is the "Delta theta" quantity in the main text).
NX= NINT(RM*AT /RdA) +1 ; RdA= RM*AT / DBLE(NX -1) ! exact mesh step at RM, corresponding to NX.
dA = RdA / RM ; A1 = 0.d0 ; A2 = AT           ! corresponding delta_angle.
C-----
write(2,*) Rmi,dR,dA/pi*180.d0,dZ,
>'      ! Rmi/cm, dR/cm, dA/deg, dZ/cm'
write(2,*) '# Field map generated using geneSectorMapIndex.f '
write(2,fmt='(a)') '# AT/rd, AT/deg, Rmi/cm, Rma/cm, RM/cm,'
>/' NR, dR/cm, NX, RdA/cm, dA/rd : '
write(2,fmt='(a,1p,5(e16.8,1x),2(i3,1x,e16.8,1x),e16.8)')
>' # 'AT, AT/pi*180.d0,Rmi, Rma, RM, NR, dR, NX, RdA, dA
write(2,*) '# For TOSCA: ',NX,NR,' 1 22.1 1. !IZ=1 -> 2D ; '
>/'MOD=22 -> polar map ; .MOD2=.1 -> one map file'
write(2,*) '# '
write(2,*) '#      R*cosA          Z=0,          R*sinA'
>/'      BY          BZ          BX      ix jr'
write(2,*) '#      cm          cm          cm '
>/'      kG          kG          kG '
do jr = 1, NR
  R = Rmi + dble(jr-1)*dR
  BZ = B0 + B0/R0 * ak * (R - R0)
  do ix = 1, NX
    A = A1 + dble(ix-1)*dA ; X = R * sin(A) ; Y = R * cos(A)
    write(2,fmt='(1p,6(e16.8),2(1x,i0))') Y,Z,X,BY,BZ,BX,ix,jr
  enddo
enddo
stop ' Job complete ! Field map stored in geneSectorMapIndex.out.'
end

```

**Table 3.15** First and last few lines of the field map file `geneSectorMapIndex.out`. The file starts with an 8-line header, the first one of which is effectively used by `zgoubi`, the following 7 are just comments

```

1.      0.5      0.57142857142857140      0.      ! Rmi/cm, dR/cm, dA/deg, dZ/cm
# Field map generated using geneSectorMapIndex.f
# AT/rd, AT/deg, Rmi/cm, Rma/cm, R0/cm, NR, dR/cm, NX, RdA/cm, dA/rd :
# 1.04719755E+00 6.0E+01 1.0E+00 7.60E+01 1.29248888E+01 151 5.0E-01 106 4.98665501E-01 9.97331001E-03
# For TOSCA:      106      151 1 22.1 1. !IZ=1 -> 2D ; MOD=22 -> polar map ; .MOD2=-1 -> one map file
#
# R*cosA      Z=0,      R*sinA      BY      BZ      BX      ix jr
# cm          cm          cm          kG      kG      kG
1.00000000E+00 0.00000000E+00 0.00000000E+00 0.00000000E+00 5.13839448E+00 0.00000000E+00 1 1
9.99950267E-01 0.00000000E+00 9.97314468E-03 0.00000000E+00 5.13839448E+00 0.00000000E+00 2 1
9.99801073E-01 0.00000000E+00 1.99452974E-02 0.00000000E+00 5.13839448E+00 0.00000000E+00 3 1
9.99552432E-01 0.00000000E+00 2.99154662E-02 0.00000000E+00 5.13839448E+00 0.00000000E+00 4 1
9.99204370E-01 0.00000000E+00 3.98826594E-02 0.00000000E+00 5.13839448E+00 0.00000000E+00 5 1
.....
4.05947602E-01 0.00000000E+00 6.42500229E+01 0.00000000E+00 4.26798081E+00 0.00000000E+00 102 151
3.99519665E-01 0.00000000E+00 6.46516850E+01 0.00000000E+00 4.26798081E+00 0.00000000E+00 103 151
3.93051990E-01 0.00000000E+00 6.50469164E+01 0.00000000E+00 4.26798081E+00 0.00000000E+00 104 151
3.86545219E-01 0.00000000E+00 6.54356779E+01 0.00000000E+00 4.26798081E+00 0.00000000E+00 105 151
3.80000000E-01 0.00000000E+00 6.58179307E+01 0.00000000E+00 4.26798081E+00 0.00000000E+00 106 151

```

A `gnuplot` script to obtain Fig. 3.34:

```

# PLOT THE FIELD MAP:
set xtics mirror ; set ytics mirror ; set xlabel "X_{Lab} [m]" ; set ylabel "Y_{Lab} [m]" ; cm2m = 0.01
set zrange [:5.15] ; set view 66, 192 ; unset colorbox
splot "geneSectorMapIndex.out" u ($1 *cm2m):($3 *cm2m):($5) w p lc palette notit ; pause 1

# PLOT THREE TRAJECTORIES
set xtics ; set ytics ; set xlabel "X_{Lab} [m]" ; set ylabel "Y_{Lab} [m]" ; cm2m = 0.01 ; set size ratio 1
plot for [trj=1:3] \
"zgoubi.plt" u ($19==trj ? $10*cm2m*cos($22) :1/0):($10*cm2m*sin($22)) w p pt 7 ps .6 notit ; pause 1

```

**Table 3.16** Simulation input data file FieldMapSectorIndex.inc: a file to test trajectories for a field map with radial index. This file also defines the INCLUDE segment between the LABEL\_1s #S\_60degSectorIdx and #E\_60degSectorIdx

```

FieldMapSectorIndex.inc
! Uniform field sector with index. INCLUDE file FieldMapSectorIndex.inc
'MARKER' FieldMapSectorIdx_S ! Just for edition purposes.
'OBJET'
64.62444403717985 ! Reference Brho ("BORO" in the users' guide) -> 200keV proton.
2
3 1
4.003593 0. 0. 0. 0.3162126 'o' ! p[MeV/c]= 6.126277, Brho[kG.cm]=20.435, kin-E[MeV]=-0.02.
12.92488 0. 0. 0. 1. 'o' ! Reference ; p[MeV/c]=193.739, Brho[kG.cm]=BORO, kin-E[MeV]=-0.2.
75.75467 0. 0. 0. 5.0063900 'o' ! p[MeV/c]=969.934, Brho[kG.cm]=323.535, kin-E[MeV]=5.
1 1 1
'MARKER' #S_60degSectorIdx
'TOSCA'
0 2 ! IL=2 to log step-by-step coordinates, spin, etc., in zgoubi.plt (avoid, if CPU time matters).
1. 1. 1. 1. ! Normalization coefficients, for B, X, Y and Z coordinate values read from the map.
HEADER_8 ! The field map file starts with an 8-line header.
106 151 1 22.1 1. ! IZ=1 for 2D map; MOD=22 for polar frame; .MOD2=.1 if only one map file.
geneSectorMapIndex.out
0 0 0 0 ! Possible vertical boundaries within the field map, to start/stop stepwise integration.
2
2 ! Integration step size. Small enough for orbits to close accurately.
! Magnet positioning option.
0. 0. 0. 0. ! Magnet positioning.
'MARKER' #E_60degSectorIdx
'FIT2' ! This matching procedure finds the closed orbit radius.
3 nofinal
2 30 0 [2.,10.] ! Variable : Y_0, trajectory 1
2 40 0 [10.,15.] ! Variable : Y_0, trajectory 2
2 50 0 [50.,80.] ! Variable : Y_0, trajectory 3
3 1e-20 9999 ! Penalty; max numb of calls to function
3.1 1 2 #End 0. 1. 0 ! Constraint : Y_final=Y_0, trajectory 1
3.1 2 2 #End 0. 1. 0 ! Constraint : Y_final=Y_0, trajectory 2
3.1 3 2 #End 0. 1. 0 ! Constraint : Y_final=Y_0, trajectory 3

! Carry on with coordinates as found, yet with IL=2 under TOSCA so to log trajectories in zgoubi.plt.
'TOSCA'
0 2 ! IL=2: log step-by-step coordinates, spin, etc., in zgoubi.plt (avoid if CPU time matters).
1. 1. 1. 1. ! Normalization coefficients, for B, X, Y and Z coordinate values read from the map.
HEADER_8 ! The field map file starts with an 8-line header.
106 151 1 22.1 1. ! IZ=1 for 2D map; MOD=22 for polar frame; .MOD2=.1 if only one map file.
geneSectorMapIndex.out
0 0 0 0 ! Possible vertical boundaries within the field map, to start/stop stepwise integration.
2
2 ! Integration step size. Small enough for orbits to close accurately.
! Magnet positioning option.
0. 0. 0. 0. ! Magnet positioning.
'FAISCEAU' ! Local particle coordinates logged in zgoubi.res.
'SYSTEM' ! This SYSTEM command runs gnuplot, for a graph of the two trajectories.
1
gnuplot <./gnuplot_Zplt.gnu
'MARKER' FieldMapSectorIdx_E ! Just for edition purposes.
'END'

```

2538 (b) R-dependence of orbit rigidity.

2539 The method is similar to exercise 3.1-(b) (see Tab. 3.4.): FIT finds the closed orbit  
 2540 radius  $R$  for a given ion rigidity, and REBELOTE is used to repeat for a series of  
 2541 different momenta, 20 here. The input data file for this exercise is given in Tab. 3.17,  
 2542 it includes a 21 ion 1-turn raytracing, in sequence with the previous 21-orbit finding.

2543 Raytracing outcomes for  $k = -0.03$ ,  $R_0 = R(E = 200 \text{ keV}) = 12.924888 \text{ cm}$ ,  
 2544  $B_0 = B(R_0) = 0.5 \text{ T}$  are given in Fig. 3.35, together with theoretical expectation  
 2545 (with  $B(R)$  from Eq. 3.7)

$$\text{Rigidity } BR(R) = B_0 \left( 1 + \frac{R - R_0}{R_0} k \right) R \quad (3.39)$$

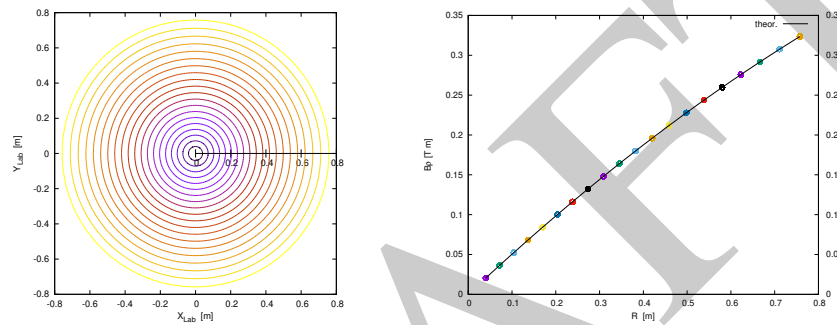


**Fig. 3.35** Case of field index  $k=-0.03$ . Left: closed orbits at a series of different rigidities. Right: comparison of  $B\rho(R)$  from raytracing outcomes (markers) and from theory (solid line, Eq. 3.39)

2546 (c) Paraxial motion.

2547 A proton with energy 1 MeV is considered, here. DIPOLE [16, *lookup* INDEX]  
 2548 is used rather than a field map, so to allow to freely change the  $k$  index value (using  
 2549 TOSCA instead would require computing a new field map when changing  $k$ ).

2550 The input data for a 60 deg sector are given in Tab. 3.18, essentially a copy of  
 2551 the uniform dipole field case of Tab. 3.6 in which the index value  $k = -0.03$  has  
 2552 been added (line 3 under DIPOLE). The input data sequence for multiturn trajectory  
 2553 computation around the cyclotron is given in Tab. 3.19: in a first stage, orbit finding  
 2554 is performed by FIT, for 1 MeV energy; in a subsequent second stage, 4 protons with  
 2555 their initial horizontal coordinates taken on the closed orbit, and differing by their  
 2556 initial vertical take-off angle, are tracked over 120 sectors, *i.e.*, 20 turns around the  
 2557 ring.

2558 Fig. 3.36 displays the vertical sine motion. Stronger index ( $k$  closer to -1) results  
 2559 in stronger vertical focusing, hence more oscillations as expected from Eq. 3.18 and  
 2560 smaller motion amplitude as expected from Eq. 3.17. The latter can be written



**Table 3.17** Simulation input data file: scan orbits for momentum dependence. Two problems are stacked, executed in sequence: in a first stage FIT finds a closed orbit, whose coordinates are logged in initialRs.fai file when FIT is completed, following what REBELOTE repeats for an additional 20 momenta; in a second stage OBJET grabs the 21-set of ion coordinates from initialRs.fai and these ions are raytraced over 6 sectors, *i.e.*, one full turn. The INCLUDE file FieldMapSectorIndex.inc is taken from Tab. 3.16

```
Uniform field sector with index. Scan orbits.
'MARKER' scanSectorIdx_S ! Just for edition purposes.
'OBJET'
64.62444403717985 ! Reference Brho ("BORO" in the users' guide) -> 200keV proton.
2
1 1 ! Just one ion.
4.0039 0. 0. 0. 0. 0.3162126 'o' ! p[MeV/c]= 6.126277, Brho[kG.cm]=20.435, kin-E[MeV]=-0.02.
1
'FAISCEAU' ! Local particle coordinates logged in zgoubi.res.
'INCLUDE'
1
./FieldMapSectorIndex.inc[#S_60degSectorIdx:#E_60degSectorIdx]
'FIT' ! This matching procedure finds the closed orbit radius.
1 nofinal
2 30 0 [3.,80.] ! Variable : Y_0
1 1e-15 99 ! Penalty; max numb of calls to function
3.1 1 2 #End 0. 1. 0 ! Constraint : Y_final=Y_0
'FAISTORE'
initialRs.fai ! Log coordinates in initialRs.fai.
1
'REBELOTE' ! A do-loop. Repeat the above, after changing particle rigidity to a new value.
20 0.2 0 1 ! 20 diffrnt rigidities; I/O options; coordinates as from OBJET; changes follow:
1 ! Parameter 35 to be changed, in OBJET: relative momentum, namely,
OBJET 35 0.3162126:5.0063900 ! for energy scan from 0.02 MeV to 5 MeV.

'OBJET'
64.62444403717985 ! Reference Brho ("BORO" in the users' guide) -> 200keV proton.
3
1 999 1
1 999 1
1. 1. 1. 1. 1. 1. 1. '*'
0. 0. 0. 0. 0. 0. 0.
0
initialRs.fai
'FAISCEAU' ! Local particle coordinates logged in zgoubi.res.
'INCLUDE'
1
6* ./FieldMapSectorIndex.inc[#S_60degSectorIdx:#E_60degSectorIdx] ! INCLUDE 6 times.
'SYSTEM'
2
gnuplot <./gnuplot_Zplt_orbits.gnu ! Plot orbits around the cyclotron.
gnuplot <./gnuplot_Zplt_scanBrho.gnu ! Plot R(Brho).
'MARKER' scanSectorIdx_E ! Just for edition purposes.
'END'
```

A *gnuplot* script to obtain orbits, Fig. 3.35:

```
set xtics ; set ytics ; set xlabel "X_{Lab} [m]" ; set ylabel "Y_{Lab} [m]" ; cm2m = 0.01; set polar; set size ratio 1
unset colorbox; pi = 4.*atan(1.); TOSCA1=12; dT=3 # number of 2nd TOSCA & increment in zgoubi.plt listing
plot for [trj=2:21] \
"zgoubi.plt" u ($19==trj ? $22+($42-TOSCA1)/dT*pi/3 : 1/0):($10*cm2m):( $19) w l lw 2 lc palette notit ; pause 1
```

A *gnuplot* script to obtain  $B\rho(R)$ , Fig. 3.35:

```
set xtics ; set ytics nomirror ; set y2tics; set xlabel "R [m]" ; set ylabel "B{Symbol r} [T m]"
B0=0.5; R0=12.924888e-2; k=-0.03; Brho(x)= B0*(1.+ (x-R0)/R0^k )^x ; kGcm2Tm=1e-3; cm2m = 0.01
plot for [trj=2:21] \
"zgoubi.plt" u ($19==trj? $10*cm2m :1/0):($40*(1.+ $2)*kGcm2Tm) w p pt 6 ps 1.2 notit \
Brho(x) axes xly2 w l lw 2 lc rgb "black" tit "theor." ; pause 1
```

**Table 3.18** Simulation input data file sectorWithIndex.inc: definition of a dipole with index, case of analytical field modeling, namely here  $k=-0.03$  and reference radius  $R_0 = 50$  cm. Definition of the [#S\_60degSectorWIdx:#E\_60degSectorWIdx] segment

```
# sectorWithIndex.inc
'MARKER' #S_60degSectorWIdx ! Label should not exceed 20 characters.
'DIPOLE' ! Analytical modeling of a dipole magnet.
2 ! IL=2, only purpose is to logged trajectories in zgoubi.plt, for further plotting.
60. 50. ! Sector angle AT; reference radius.
30. 5. -0.03 0. 0. ! Reference azimuthal angle ACN; BM field at R0; indices, N (-k=-0.03) at R0=50cm.
0. 0. ! EFB 1 is hard-edge,
4 .1455 2.2670 -.6395 1.1558 0. 0. 0. ! hard-edge only possible with sector magnet.
30. 0. 1.E6 -1.E6 1.E6 1.E6 ! EFB 2.
0. 0. ! EFB 3 (unused).
4 .1455 2.2670 -.6395 1.1558 0. 0. 0.
-30. 0. 1.E6 -1.E6 1.E6 1.E6
0. 0.
0. 0. 0. 0. 0. 0. 0.
0. 0. 1.E6 -1.E6 1.E6 1.E6 0.
4 10.
0.5 ! Integration step size. Small enough for orbits to close accurately.
2 0. 0. 0. 0. ! Magnet positioning RE, TE, RS, TS.
'MARKER' #E_60degSectorWIdx ! Label should not exceed 20 characters.
'END'
```

$$Z(s) = P_0 \frac{R_0}{\sqrt{-k}} \sin \frac{\sqrt{-k}}{R_0} (s - s_0) \quad \text{and} \quad \hat{Z} = P_0 \frac{R_0}{\sqrt{-k}} \quad (3.40)$$

2561 Note that this vertical oscillation results in a modulation of the field along the  
 2562 trajectory (see question (d) of this exercise) which results in a radial oscillation, a  
 2563 second order Y-Z coupling effect (extremely weak), displayed in Fig. 3.37.

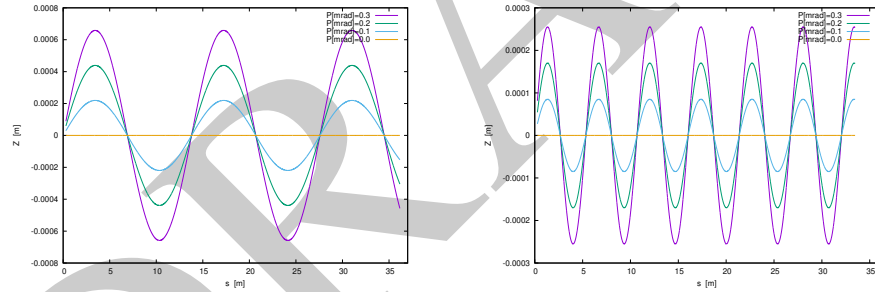


**Fig. 3.36** Vertical sine motion over a few turns around the cyclotron, at 1 MeV. Vertical take-off angles are  $P_0 = 0, 0.1, 0.2, 0.3$  mrad. Left:  $k=-0.03$ ,  $\nu_Z = \sqrt{0.03} \approx 0.173$  oscillations per turn; right: for  $k=-0.2$ ,  $\nu_Z = \sqrt{0.2} \approx 0.447$  oscillations per turn

2564 (d) Magnetic field.

2565 The magnetic field experienced by 1 MeV protons with four different take-off  
 2566 angles  $P_0$  (Fig. 3.36), along their respective trajectories, case of an index value  
 2567  $k = -0.03$ , is displayed in Fig. 3.38. It is essentially constant as expected.

**Table 3.19** Simulation input data file: scan orbits for momentum dependence; the file actually stacks two simulations, executed in sequence; the second simulation uses data produced by the first one, as follows. The first part of the file finds the closed orbits, they depend on the vertical excursion and are not exactly zero, due to the field index; closed orbit coordinates so found are logged in initialRs.fai when FIT is completed. The second part of the file starts at the second occurrence of OBJET which reads initial particle coordinates from initialRs.fai and tracks these particles through a sequence of 120 sector dipoles, *i.e.*, 20 turns. The [#S\_60degSectorWIdx:#E\_60degSectorWIdx] segment of Tab. 3.18 is INCLUDED, here

```

Uniform field sector with index. Scan orbits.
'MARKER' 1MeVVMotion_S ! Just for edition purposes.
! First stage: find closed orbit at 1 MeV, for some k value.
'OBJET'
64.62444403717985 ! Reference Brho ("BORO" in the users' guide) -> 200keV proton.
1.1
1 1 1 4 1 1
0. 1. 0. 0.1 0. 1.
30.107900 0. 0. 0. 2.2365445724 'm' ! 1 MeV proton -> Brho/Brho_ref = 2.2365445724.
'INCLUDE'
1
./sectorWithIndex.inc[#S_60degSectorWIdx:#E_60degSectorWIdx] ! DIPOLE case R0=50cm k=-0.03.
'FIT' ! This matching procedure finds the closed orbit radius.
1 nofinal
2 40 0 .9 ! Variable : Y_0. Variation can be up to 90%.
1 1e-15 99 ! Penalty; max numb of calls to function.
3.1 1 2 #End 0. 1. 0 ! Constraint : Y_final=Y_0.
'FAISTORE'
initialRs.fai ! Log coordinates in initialRs.fai.
1
! Second stage: raytrace the four particles over 20 turns.
'OBJET'
64.62444403717985 ! Reference Brho ("BORO" in the users' guide) -> 200keV proton.
3
1 999 1
1 999 1
1. 1. 1. 1. 1. 1. 1. '*'
0. 0. 0. 0. 0. 0. 0.
0
initialRs.fai
'FAISCEAU' ! Local particle coordinates logged in zgoubi.res.
'INCLUDE'
1
120 * sectorWithIndex.inc[#S_60degSectorWIdx:#E_60degSectorWIdx] ! INCLUDE 120 sectors (20 turns).
'FAISCEAU' ! Local particle coordinates logged in zgoubi.res.
'SYSTEM'
2
gnuplot <./gnuplot_Zplt_1MeVVMotion.gnu
gnuplot <./gnuplot_Zplt_1MeVBFfield.gnu
'MARKER' 1MeVVMotion_E ! Just for edition purposes.
'END'

```

A *gnuplot* script to obtain Figs. 3.36, 3.37:

```

# gnuplot_Zplt_1MeVVMotion.gnu
set xtics ; set ytics ; set xlabel "s [m]" ; set ylabel "Z [m]" ; cm2m = 0.01; unset colorbox ; set xrange [:36]
plot for [trj=4:1:-1] \
"zgoubi.plt" u ($19==trj && $42>10? $14*cm2m :1/0):($12*cm2m ):($19) w l lw 2 tit "P[mrad]=0.". (trj-1) ; pause 1

```

A *gnuplot* script to obtain Fig. 3.38:

```

# gnuplot_Zplt_1MeVBFfield.gnu
set xtics; set ytics; set xlabel "s [m]"; set ylabel "Y [m]"; cm2m = 0.01; unset colorbox
plot for [trj=4:1:-1] \
"zgoubi.plt" u ($19==trj && $42>10? $14*cm2m :1/0):($10*cm2m ):($19) w l lw 2 tit "P[mrad]=0.". (trj-1) ; pause 1

```

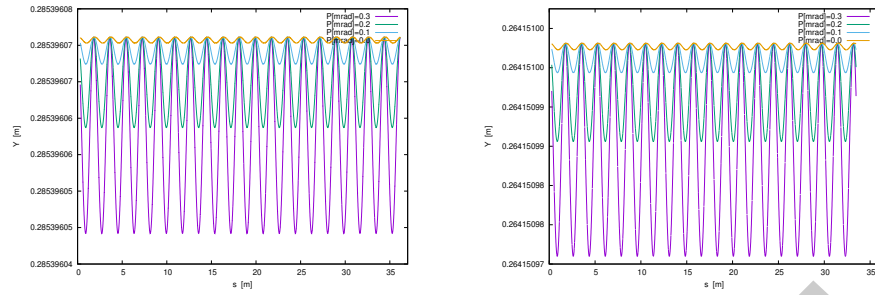
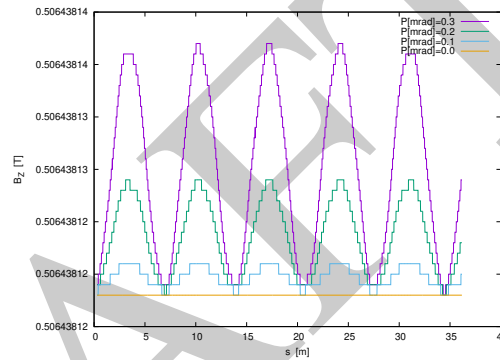


**Fig. 3.37** Horizontal motion at 1 MeV, 20 turns around the cyclotron, for vertical take-off angles  $P_0 = 0, 0.1, 0.2, 0.3$  mrad. Left:  $k = -0.03$ ,  $\nu_R = \sqrt{1 + 0.03} \approx 1.015$  oscillations per turn; right: for  $k = -0.2$ ,  $\nu_R = \sqrt{1 + 0.2} \approx 1.095$  oscillations per turn

**Fig. 3.38** Magnetic field experienced by 1 MeV protons with four different take-off angles  $P_0$  (Fig. 3.36), along their respective trajectories. Case  $k = -0.03$ . The stepwise structure of these  $B_Z(s)$  curves is due to the fact that field variations are at the limit of computer truncation related accuracy



### 2568 3.7 Loss of Isochronism

2569 In order to scan  $T_{\text{rev}}(R)$  for different  $k$  values, DIPOLE [16, *lookup* INDEX] is  
 2570 used here, as it allows to easily vary  $k$  and subsequently find the closed orbit using  
 2571 FIT. The method of exercise 3.6 is employed to obtain a scan. The input data file  
 2572 of Tab. 3.17 is a good starting point to do this exercise, changing the INCLUDE  
 2573 to account for DIPOLE instead of a field map modeling using TOSCA: the proper  
 2574 INCLUDE formatting can be reproduced from Tab. 3.19. IL under DIPOLE may  
 2575 be set at IL=0 as zgoubi.plt is not used here. Introduce FAISTORE to store local  
 2576 particle data after FIT (that includes time of flight, the quantity of interest here,  
 2577 which requires PARTICUL[PROTON] following OBJET).

2578 The new input data file so built for this simulation, is given in Tab. 3.20.

2579 This input data file is run for four different  $k$  values, namely, under DIPOLE (*cf.*  
 2580 Tab. 3.18), the line “30. 5. -0.03 0. 0.” is successively changed to  $\begin{cases} 30. 5. 0. 0. 0. \\ 30. 5. -0.5 0. 0. \\ 30. 5. -0.95 0. 0. \end{cases}$

2581 The corresponding zgoubi.fai files are saved under dedicated copies for plotting, see  
 2582 “gnuplot script gnuplot\_Zfai\_scanTrev.gnu” at the bottom of Tab. 3.20.

2583 The results of these  $T_{\text{rev}}$  scans are displayed in Fig. 3.39. In the case  $k = 0$  the  
 2584 loss of isochronism is only due to the relativistic change of the mass, a non-zero  $k$

**Table 3.20** Simulation input data file: scan revolution time. The [#S\_60degSectorWIdx:#E\_60degSectorWIdx] segment of Tab. 3.18 is INCLUDED, here

```
Uniform field sector with index. Scan orbits.
'MARKER' isoChroLoss_S ! Just for edition purposes.
'OBJET'
64.62444403717985 ! Reference Brho ("BORO" in the users' guide) -> 200keV proton.
2
1 1 ! Just one ion.
4.0039 0. 0. 0. 0.3162126 'o' ! p[MeV/c]= 6.126277, Brho[kG.cm]=20.435, kin-E[MeV]=0.02.
1
'PARTICUL' ! Necessary as time of flight computation is needed,
PROTON ! otherwise, by default \zgoubi\ only requires rigidity.
'INCLUDE'
1
./sectorWithIndex.inc[#S_60degSectorWIdx:#E_60degSectorWIdx] ! DIPOLE case R0=50cm k=-0.03.
'FIT2' ! This matching procedure finds the closed orbit radius.
1 nofinal
2 30 0 [0.5,80.] ! Variable : Y_0
1 1e-15 99 ! Penalty; max numb of calls to function
3.1 1 2 #End 0. 1. 0 ! Constraint : Y_final=Y_0
'FAISCEAU' ! Local particle coordinates logged in zgoubi.res.
'FAISTORE'
zgoubi.fai
1
'REBELOTE' ! A do-loop. Repeat the above, after changing particle rigidity to a new value.
20 0.2 0 1 ! 20 diffrent rigidities; I/O options; coordinates as from OBJET; changes follow:
1 ! Parameter 35 to be changed, in OBJET: relative momentum, namely,
OBJET 35 0.3162126:5.00639 ! Acceleration to 5MeV. Commented here, for use in subsequent exercises.
! OBJET 35 0.3162126:2.2365445724 ! Substitute to previous, for energy scan from 0.02 MeV to 1 MeV.
'SYSTEM'
1
gnuplot <./gnuplot_Zfai_scanTrev.gnu ! Plot revolution time.
'MARKER' isoChroLoss_E ! Just for edition purposes.
'END'
```

A *gnuplot* script to obtain Fig. 3.39:

```
# gnuplot_Zfai_scanTrev.gnu
set xtics ; set ytics nomirror ; set y2tics ; set xlabel "R [m]" ; set ylabel "T_{rev} [1/Symbol m]s]"
cm2m = 0.01; nSec=6; set y2label "T_{rev} at k=0[1/Symbol m]s]" ; set key c r
plot "zgoubi_k0.fai" u ($10 *cm2m):($15 * nSec) w lp pt 4 ps 1.2 lc rgb "black" tit "k=0" ,\
"zgoubi_k0.fai" u ($10 *cm2m):($15 * nSec) axes xly2 w lp pt 4 ps 1.2 lc rgb "black" notit ,\
"zgoubi_k0.03.fai" u ($10 *cm2m):($15 * nSec) w lp pt 7 ps 1.2 tit "k=-03" ,\
"zgoubi_k0.5.fai" u ($10 *cm2m):($15 * nSec) w lp pt 8 ps 1.2 tit "k=-5" ,\
"zgoubi_k0.95.fai" u ($10 *cm2m):($15 * nSec) w lp pt 9 ps 1.2 tit "k=-95" ; pause 1
```

2585 augments the effect. The loss of isochronism is the cause of the  $\approx 20$  MeV proton  
2586 energy limit of the classical cyclotron.

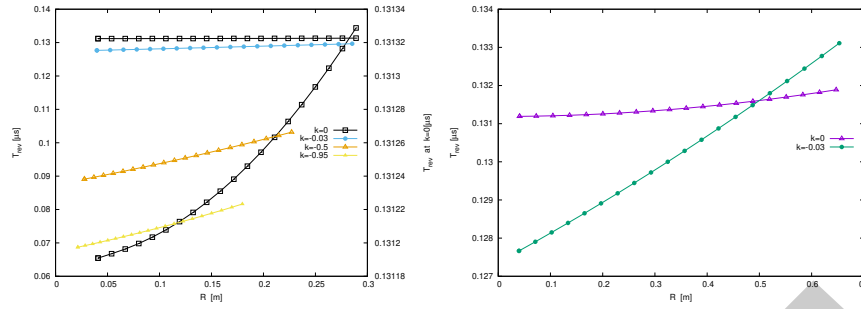


**Fig. 3.39** A scan of the revolution time, from 0.02 to 1 MeV, and its dependence on the field index  $k$ . The right vertical axis only concerns the case  $k = 0$  where the change in revolution time is weak and only due to the mass increase (in  $T_{\text{rev}} = 2\pi\gamma m_0/qB$ ). The right graph shows, up to 5 MeV, the relatively important contribution of the focusing index, even a weak  $k=-0.03$ , compared to the effect of the mass increase ( $k=0$  curve). Markers are from raytracing, solid lines are from theory

### 2587 3.8 Ion Trajectories

2588 A zgoubi data file is set up for computation of particle trajectories, taking a  
 2589 field value on reference radius of  $B_0(R_0) = 0.5 \text{ T}$ , and reference energy 200 keV  
 2590 (proton). These hypotheses determine the reference radius value. DIPOLE [16,  
 2591 *lookup* INDEX] is used (Tab. 3.21), for its greater flexibility in changing magnet  
 2592 parameters, field and radial field index amongst other, compared to using TOSCA  
 2593 and a field map.

2594 (a) Transverse motion.

2595 It first has to be checked that there is consistency between initial orbital radius  
 2596  $Y_0$  in OBJET at 200 keV proton energy and the value of the reference radius  $R_0$  in  
 2597 DIPOLE (Eq. 3.35). Its theoretical value is  $R_0 = BORO/5[kG] = 12.924889 \text{ cm}$ , a  
 2598 closed orbit finding using FIT can be performed, or it can be referred to the solutions  
 2599 of earlier exercises, to check agreement with raytracing outcomes.

2600 (b) Wave numbers at 1 and 5 MeV.

2601 These considerations result in the input data file given in Tab. 3.22, to compute  
 2602 multiturn trajectories. ; note that  $R_0 = 12.924889 \text{ cm}$  therein, whereas a value of  
 2603  $R_0 = 50 \text{ cm}$  may be taken instead in other exercises. Field index derivatives  $k'$ ,  $k''$ , ...  
 2604 are taken null in the present exercise.

2605 Three particles with paraxial radial and axial motions are raytraced over a few  
 2606 turns. Their starting radius is the closed orbit radius for the respective energies, while  
 2607 a 0.1 mrad take-off angle is imparted to each particle both vertically and horizontally.

The value of the focusing index  $k_E$  at an energy  $E$  can be expressed in terms of DIPOLE data which are, the index value  $k$  at  $R_0$  (Eq. 3.11), reference radius  $R_0$ , and field  $B_0 = B_Z(R_0)$ , namely,

$$k_E = \frac{R_E}{B_E} \frac{\partial B}{\partial R} = \frac{R_0 + \Delta R}{B_0 + \Delta B} \frac{\partial B}{\partial R} \approx k \frac{1 + \Delta R/R_0}{1 + k\Delta R/R_0} \approx k \left[ 1 + (1 - k) \frac{\Delta R}{R_0} \right]$$

**Table 3.21** Input data file 60DegSectorR200.inc: it defines DIPOLE as a sequence segment comprised between the “LABEL\_1” type labels [16, Sect. 7.7] #S\_60DegSectorR200 and #E\_60DegSectorR200. DIPOLE here, has an index  $k = -0.03$ , reference radius  $R_0 \equiv R_0(E_k = 200 \text{ keV}) = 12.924888 \text{ cm}$  and  $B_0 = B(R_0) = 0.5 \text{ T}$ . Note that (i) this file can be run on its own: it has been designed to provide the transport MATRIX of that DIPOLE; (ii) for the purpose of some of the exercises, IL=2 under DIPOLE, optional, causes the printout of particle data in zgoubi.plt, at each integration step (this is at the expense of CPU time, and memory volume)

```
60DegSectorR200.inc
'OBJET'
64.62444403717985 ! 200keV proton.
5
0.01 0.001 0.01 0.001 0. 0.0001
12.924888074 0. 0. 0. 0. 1. ! 200keV. R=Brho/B=*/.5.
'DIPOLE' #S_60DegSectorR200 ! Analytical modeling of a dipole magnet.
2 ! IL=2, purpose: log stepwise particle data in zgoubi.plt. Avoid if unused: I/Os take CPU time.
60. 12.924888 ! Sector angle AT; reference radius R0.
30. 5. -0.03 0. 0. ! Reference azimuthal angle ACN; BM field at R0; indices, N, N', N''.
0. 0. ! EFB 1 is hard-edge,
4 .1455 2.2670 -.6395 1.1558 0. 0. 0. ! hard-edge only possible with sector magnet.
30. 0. 1.E6 -1.E6 1.E6 1.E6
0. 0. ! EFB 2.
4 .1455 2.2670 -.6395 1.1558 0. 0. 0.
-30. 0. 1.E6 -1.E6 1.E6 1.E6
0. 0. ! EFB 3 (unused).
0 0. 0. 0. 0. 0. 0. 0.
0. 0. 1.E6 -1.E6 1.E6 1.E6 0. 0.
4 10.
0.5 ! Integration step size. Small enough for orbits to close accurately.
2 0. 0. 0. 0. ! Magnet positioning RE, TE, RS, TS.
'FAISCEAU' #E_60DegSectorR200
'MATRIX'
1 0
'END'
```

**Table 3.22** Simulation input data file: raytrace a few turns around the cyclotron, three particles with different momenta, and 0.1 mrad horizontal and vertical take-off angles. The INCLUDE segment is taken from Tab. 3.21

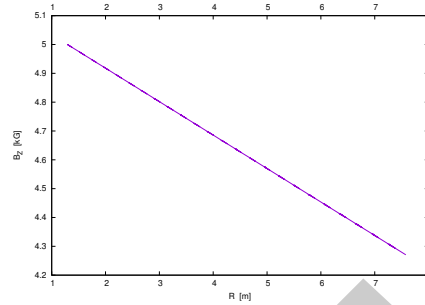
```
'MARKER' ProbProjTraj_S
'OBJET'
64.62444403717985 ! Reference Brho ("BORO" in the users' guide) -> 200keV proton.
2
3 1
12.924888 0.1 0. 0.1 0. 1. 'o' ! A particle with kin-E=0.2 MeV and 0.1 mrad take-off angles.
30.107898 0.1 0. 0.1 0. 2.2365445 'm' ! p[MeV/c]=433.306, Brho[kG.cm]=144.535, kin-E[MeV]=1.
75.754671 0.1 0. 0.1 0. 5.0063900 'o' ! p[MeV/c]=969.934, Brho[kG.cm]=323.535, kin-E[MeV]=5.
1 1 1
'INCLUDE'
1
6* 60DegSectorR200.inc[#S_60DegSectorR200:#E_60DegSectorR200] ! 6 sectors for an overall 360 deg.
'REBELOTE'
9 0.1 99 ! There will be a total of 9+1=10 turns.
'SYSTEM'
1
gnuplot < ./gnuplot_Zplt_traj.gnu ! Plot the projected Y(s) and Z(s) motions.
'MARKER' ProbProjTraj_E
'END'
```

A gnuplot script to obtain Fig. 3.41:

```
# gnuplot_Zplt_traj.gnu
set xtics nomirror; set x2tics; set ytics; set xlabel 's /C_E'; set ylabel 'Y [cm]'
set palette defined ( 1 "red", 2 "blue", 3 "black" ); unset colorbox
array R[3]; R[1]=0.12924888; R[2]=0.301078986; R[3]=0.75754671; pi = 4.*atan(1.); cm2m = 0.01
sector=3 # number (NOEL) of 1st DIPOLE in \zgoubi.res (col. 42 in zgoubi.plt)
# in zgoubi.plt, col. 19: particle number; col. 42: keyword number; col. 14: distance; col. 10: Y; col. 12: YZ
plot for [sector=1:6] for [trj=1:3] 'zgoubi.plt' u ($19==trj && $42==sector1+2*(sector-1)? $14*cm2m/(2.*pi*R[$19]):1/0) \
:($10*cm2m-R[trj]):($19) w p ps .2 lc palette notit ; pause 1

set ylabel 'Z [cm]'; plot for [sector=1:6] for [trj=1:3] 'zgoubi.plt' u ($19==trj && $42==sector1+2*(sector-1)? $14*cm2m \
/(2.*pi*R[$19]):1/0):($12):($19) w p ps .2 lc palette notit ; pause 1
```

**Fig. 3.40** In DIPOLE field model (Eq. 3.35),  $\frac{\partial B}{\partial R}$  is constant: this graph shows the linear decrease of the field  $B_Z(R)$  (Eq. 3.38), obtained from the raytracing of particles circulating in the median plane on orbits spanning a 0.2 to 5 MeV energy range



2608 with  $\Delta R$  assumed small,  $\partial B/\partial R = kB/R_E$  an energy independent quantity, and the  
 2609 index E denoting a quantity taken at the reference energy. The latter property is  
 2610 illustrated in Fig. 3.40, produced using the input data file of Tab. 3.23.

**Table 3.23** Simulation input data file for a magnetic field scan. The INCLUDE segment is taken from Tab. 3.21

```
Field and derivative dB/dR, as a function of R
'MARKER' ProbProjTrajB_S
'OBJET'
64.62444403717985 ! Reference Brho ("BORO" in the users' guide) -> 200keV proton.
2
1 1 ! Just one ion.
12.924888 0.1 0. 0.1 0. 1. 'o' ! A particle with kin-E=0.2 MeV and 0.1 mrad take-off angles.
1
'INCLUDE'
1 ! IL=2 is necessary under DIPOLE, for step-by-step log of particle data in zgoubi.plt.
60DegSectorR200.inc[#_5_60DegSectorR200:#E_60DegSectorR200] ! One sector is enough.
'FIT'
1
2 30 0 [12,80] ! Vary particle's Y0 at OBJET, to have it match its D (=Brho/BORO).
1 1e-20
3.1 1 2 #End 0. 1. 0 ! Constrain Y_final=Y0.
'REBELOTE'
25 0.1 0 1 ! Scan parameter 35 (relative rigidity, D) in OBJET.
1
OBJET 35 1:5.00639 ! Scan relative rigidity D from 1 (200 keV) to 5.0063900 (5 MeV).
'SYSTEM'
1
gnuplot < ./gnuplot_Zplt_field.gnu ! Plot B(R), as read from zgoubi.plt.
'MARKER' ProbProjTrajB_E
'END'
```

A gnuplot script to obtain Fig. 3.40:

```
# gnuplot_Zplt_field.gnu
set xtics nomirror; set x2tics; set ytics; set xlabel 's /C_E'; set ylabel 'Y [cm]'
set palette defined ( 1 "red", 2 "blue", 3 "black" ); unset colorbox
array R[3]; R[1]=0.12924888; R[2]=0.301078986; R[3]=0.75754671; pi = 4.*atan(1.); cm2m = 0.01
sector1=3 # number (NOEL) of 1st DIPOLE in \zgoubi,res (col. 42 in zgoubi.plt)
# in zgoubi.plt, col. 19: particle number; col. 42: keyword number; col. 14: distance; col. 10: Y; col. 12: YZ
plot for [i=1:6] for [trj=1:3]
'zgoubi.plt' u ($19==trj && $42==sector1 +2*(i-1) ? $14*cm2m / (2.*pi*R[$19]) : 1/0) \
:($10*cm2m-R[trj]):($19) w p ps .2 lc palette notit ; pause 1

set ylabel 'Z [cm]' ;
plot for [i=1:6] for [trj=1:3]
'zgoubi.plt' u ($19==trj && $42==sector1 +2*(i-1) ? $14*cm2m \
/(2.*pi*R[$19]) : 1/0):($12):($19) w p ps .2 lc palette notit ; pause 1
```



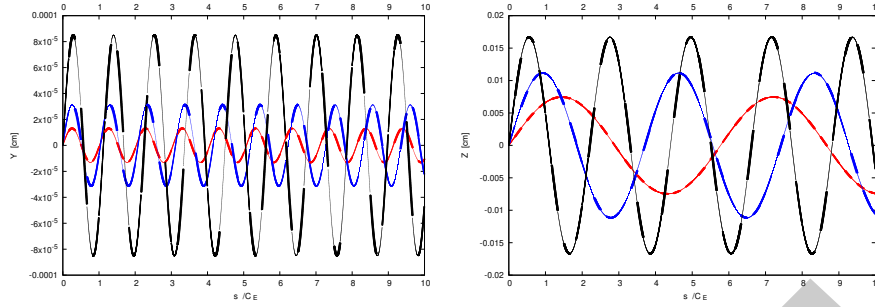


**Fig. 3.41** Radial (left) and axial (right) paraxial motion around respectively the 200 keV (smallest amplitude), 1 MeV (intermediate) and 5 MeV (greatest amplitude) closed orbit (the latter is circular, in the median plane, with radius respectively  $R_{200\text{ keV}} = 12.924888\text{ cm}$ ,  $R_{1\text{ MeV}} = 30.107898\text{ cm}$  and  $R_{5\text{ MeV}} = 75.754671\text{ cm}$ ). The horizontal axis in this graph is  $s/C_E$ : path length over closed orbit circumference at energy  $E$ , the vertical axis is the motion excursion

2611 The resulting radial and axial motions over 10 turns are displayed in Fig. 3.41,  
 2612 which also illustrates, for paraxial motion at some reference energy, the energy  
 2613 dependence of the focusing strength (or wave number) and of the motion amplitude.

**Table 3.24** Wave numbers, from numerical raytracing (columns denoted “ray-tr.”), from theory, and from discrete Fourier transform (‘DFT’ cols.) from a multi-turn tracking

E (MeV)	$k_E$	ray-tr.	$\nu_R =$		$\nu_Z =$		DFT
			ray-tr.	$\sqrt{1+k}$	ray-tr.	$\sqrt{-k}$	
0.2	-0.03	0.98520	0.9849	0.98513	0.17320	0.1732	0.17321
1	-0.07279	0.96187	0.96292	0.96291	0.26980	0.26979	0.26981
5	-0.20586	0.89083	0.89115	0.89115	0.45326	0.45371	0.45371

An estimate of the wave numbers can be obtained as the inverse of the number of turns per oscillation, namely,

$$\nu_R = \left. \frac{C_E}{\Delta s_M} \right|_E \quad \text{and} \quad \nu_Z = \left. \frac{C_E}{\Delta s_M} \right|_E$$

2614 with  $\Delta s_M$  the measured distance between two consecutive maxima in the sinusoid  
 2615 of concern in Fig. 3.41,  $C_E$  the closed orbit length for the energy of concern. Both  
 2616 quantities are obtained from motion records in zgoubi.plt. This yields the values  
 2617 of Tab. 3.24, where they are compared with the theoretical expectations, namely  
 2618 (Eq. 3.18),  $\nu_R = \sqrt{1+k}$  and  $\nu_Z = \sqrt{-k}$ .

2619 The maximum amplitude of the oscillation is obtained from zgoubi.plt records as  
 2620 well, this yields the results of Tab. 3.25. For comparison, the theoretical values are  
 2621 (Eqs. 3.16, 3.17 with respectively  $x_0 = 0$ ,  $x'_0 = T_0$  and  $y_0 = 0$ ,  $y'_0 = P_0$ )  $\hat{Y} = T_0 \frac{R_E}{\sqrt{1+k}}$   
 2622 and  $\hat{Z} = P_0 \frac{R_E}{\sqrt{-k}}$ , wherein  $R_E$  denotes the closed orbit radius at energy  $E$  (for the  
 2623 record:  $R_E \equiv R_0$  at energy  $E = 200\text{ keV}$ , in the foregoing).

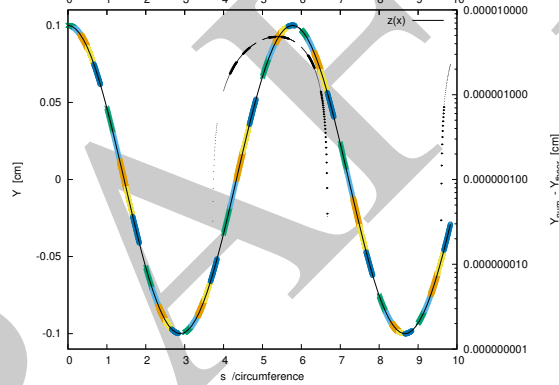
**Table 3.25** Maximum amplitude of the oscillation, from raytracing (columns denoted “ray-tr.”) and from theory.  $R_E$  is the closed orbit radius for the energy of concern,  $T_0 = P_0 = 0.1$  mrad is the trajectory angle at the origin, positions at the origin are zero

E (MeV)	k	$\hat{Y}$		$\hat{Z}$	
		ray-tr. $T_0 \frac{R_E}{\sqrt{1+k}}$ ( $\times 10^{-5}$ )	$1.3125$	ray-tr. $P_0 \frac{R_E}{\sqrt{-k}}$ ( $\times 10^{-5}$ )	$7.4624$
0.2	-0.03	1.3123	1.3125	7.4622	7.4624
1	-0.072787	3.1270	3.1267	1.1160	1.1160
5	-0.20586	8.5010	8.5008	1.6697	1.6697

2624 (c) Comparison with theory.

2625 Figure 3.42 shows the difference between numerical and theoretical vertical motion  
 2626 excursion, using an *ad hoc* gnuplot script. An integration step size  $\Delta s = 2$  cm is  
 2627 used in the numerical integration.

**Fig. 3.42** Vertical excursion of a 1 MeV trajectory over 20 turns (left vertical axis), and difference with theoretical expectation as per Eq. 3.17 (right vertical axis). The plot shows two sinusoidal curves: a segmented one, thicker, from numerical integration, and a thinner one, superimposed, from Eq. 3.17



2628 (d) A scan of energy dependence of wave numbers.

2629 A scan of the wave numbers over 200 keV–5 MeV energy range, computing tunes  
 2630 with MATRIX, is performed using the input data file given in Tab. 3.26 (essentially  
 2631 a copy of the input data file of Tab. 3.23, with an INCLUDE accounting for 6  
 2632 DIPOLES [16, *lookup* INDEX]).

2633 OBJET[KOBJ=5] generates 13 particles with paraxial horizontal, vertical and  
 2634 longitudinal sampling, proper to allow the computation of the first order transport  
 2635 coefficients and wave numbers by MATRIX. REBELOTE repeats MATRIX computation  
 2636 for a series of different particle rigidities. It is preceded by FIT which finds the  
 2637 closed orbit. MATRIX includes a PRINT command, which causes the transport  
 2638 coefficients (and various other outcomes of MATRIX computation) to be logged  
 2639 in zgoubi.MATRIX.out. This allows producing the graphic in Fig. 3.43 - using the  
 2640 gnuplot script given at the bottom of Tab. 3.26.

**Table 3.26** Simulation input data file: for this wave number scan, the INCLUDE segment is taken from Tab. 3.21

```

Field and derivative dB/dR, as a function of R
'MARKER' ProbMATRIX_S
'OBJET'
64.62444403717985          ! Reference Brho ("BORO" in the users' guide) -> 200keV proton.
5                          ! Define 13 particles for MATRIX computation.
.001 .01 .001 .01 .001 .00001          ! Sampling of the initial coordinates.
12.924888 0. 0. 0. 1.          ! Reference: p[MeV/c]=193.739, Brho[kG.cm]=BORO, kin-E[MeV]=0.2.
'INCLUDE'
1          ! IL=2 is necessary under DIPOLE, for step-by-step log of particle data in zgoubi.plt.
6* 60DegSectorR200.inc[#S_60DegSectorR200:#E_60DegSectorR200]          ! Six 60 degree sectors.
'FIT'
1
2 30 0 [12,80]          ! Vary particle's Y0 at OBJET, to have it match its D (=Brho/BORO).
1 1e-10
3.1 1 2 #End 0. 1. 0          ! Constrain Y_final=Y0.
'MATRIX'
1 11 PRINT          ! PRINT: log computation outcome data to zgoubi.MATRIX.out, for further plotting.
'REBELOTE'
25 0.1 0 1          ! Scan parameter 35 (particle 1's D) in OBJT.
1
OBJET 35 1:5.00639
'SYSTEM'
1
gnuplot < ./gnuplot_MATRIX_Qxy.gnu
'MARKER' ProbMATRIX_E
'END'

```

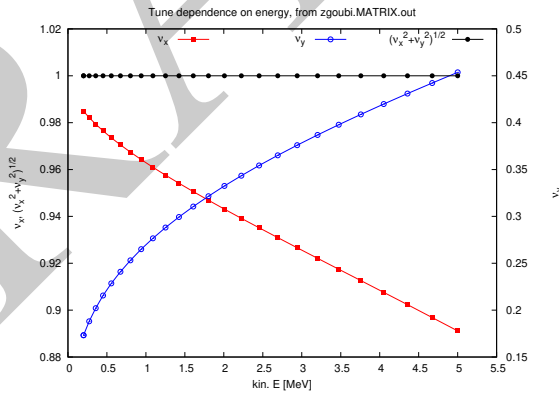
A gnuplot script to obtain Fig. 3.43:

```

# gnuplot_MATRIX_Qxy.gnu
set xlab "kin. E [MeV]"; set ylab "{/Symbol n}_x, ({/Symbol n}_x^2+{/Symbol n}_y^2)^{1/2}"; set y2label "{/Symbol n}_y"
set key t l maxrow 1; set xtics; set ytics nomirror; set y2tics nomirror
BORO = 64.62444403717985; am = 938.27203e6; c = 2.99792458e8; BrhoRef = BORO *1e-3; eV2MeV = 1e-6
plot "zgoubi.MATRIX.out" u ((sqrt(($47*BrhoRef*c)**2 + am*am)-am)*eV2MeV):(556) w lp pt 5 lt 1 lw .5 lc rgb "red" \
tit "{/Symbol n}_x " , \
"zgoubi.MATRIX.out" u ((sqrt(($47*BrhoRef*c)**2 + am*am)-am)*eV2MeV):(557) axes x1y2 w lp \
pt 6 lt 3 lw .5 lc rgb "blue" tit "{/Symbol n}_y " , \
"zgoubi.MATRIX.out" u ((sqrt(($47*BrhoRef*c)**2 + am*am)-am)*eV2MeV):(sqrt($56**2+$57**2)) \
w lp pt 7 lt 1 lw .5 lc rgb "black" t " ({/Symbol n}_x^2+{/Symbol n}_y^2)^{1/2}"; pause 1

```

**Fig. 3.43** A scan of the energy dependence of the horizontal and vertical wave numbers. Markers are from raytracing, solid lines are from theory (Eq. 3.18). The figure also shows that the raytracing yields  $\nu_R^2 + \nu_y^2 = 1$ ,  $\forall E$ , as expected



2641 **3.9 RF Phase at the Accelerating Gap**

2642 According to Sect. 3.2.3 (Fig. 3.13), the RF is taken about half-way of the ac-  
 2643 celerating range, namely, referring to Fig. 3.39,  $T_{\text{REV}} = 0.131 \mu\text{s}$  and  $f_{\text{rf}} = 1/T_{\text{REV}} =$   
 2644  $7.633 \text{ MHz}$ .

2645 An input data file for this simulation is given in Tab. 3.27.

2646 In a similar way to the diagrams in Fig. 3.13, the resulting  $B(R)$  curve is given in  
 2647 Fig. 3.44, the resulting  $\Delta W(\phi)$  curve in Fig. 3.45.

**Table 3.27** Simulation input data file: accelerating a proton to get the evolution of RF phase The [#S\_60degSectorWIdx:#E\_60degSectorWIdx] segment of Tab. 3.18 is INCLUDED, here

```

Cyclotron, classical. Acceleration to 6.02 MeV.
'MARKER' ProbRFFPhase_S                               ! Just for edition purposes.
'OBJET'
64.62444403717985                                     ! Reference: 200keV (assuming proton).
2
1 1                                                    ! Just one ion.
12.629892 0. 0. 0. 0. 1. 'm'                          ! Injection energy 200keV, proton.
1
'PARTICUL'                                           ! Particle data are necessary as CAVITE is used,
PROTON                                                ! otherwise, by default \zgoubi\ only requires rigidity.
'INCLUDE'
1
3* sectorWithIndex.inc[#S_60degSectorWIdx:#E_60degSectorWIdx] ! Three 60 deg sectors. R0=50cm, k=-0.03.
'FAISTORE'                                           ! Log particle coordinates at each turn.
zgoubi.fai
1
'CAVITE' GAPI
7 PRINT                                              ! PRINT: log CAVITE computational dat to zgoubi.CAVITE.out.
0.00 7.63358778626e6                                  ! f_rf= 1/T_rev, T_rev at about middle of acceleration range.
100e3 -1.57079632679                                  ! Peak voltage;, relative phase of 1st cavity.
'INCLUDE'
1
3* sectorWithIndex.inc[#S_60degSectorWIdx:#E_60degSectorWIdx] ! Three 60 deg sectors. R0=50cm, k=-0.03.
'CAVITE' GAPI
7 PRINT                                              ! PRINT: log CAVITE computational dat to zgoubi.CAVITE.out.
0.00 7.63358778626e6                                  ! f_rf= 1/T_rev, T_rev at about middle of acceleration range.
100e3 +1.57079632679                                  ! Peak voltage;, relative phase of 1st cavity.
'FAISCEAU'                                           ! Local particle coordinates logged in zgoubi.res.
'REBELOTE'                                           ! K = 99 : coordinates at end of previous pass are used as initial
42 1.1 99                                           ! coordinates for the next pass ; idem for spin components.
'SYSTEM'
1                                                    ! 1 SYSTEM command follows.
/usr/bin/gnuplot < ./gnuplot_CAVITE.gnu &           ! Plot phase, as read from zgoubi.CAVITE.out.
'MARKER' ProbRFFPhase_E                               ! Just for edition purposes.
'END'

```

A *gnuplot* to obtain the accelerated orbit of Fig. 3.45:

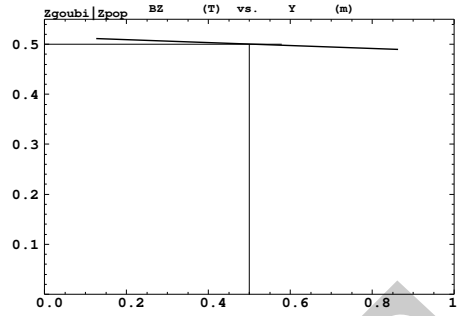
```

# gnuplot_CAVITE.gnu
set xlabel "RF phase [rad]" ; set ylabel "{Symbol D}W [MeV]" ; set xtics ; set ytics mirror
plot 'zgoubi.CAVITE.Out' u ($11):(52 - (56-50)/10000.) w lp notit ; pause 2

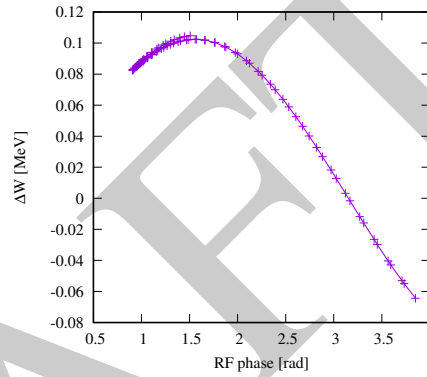
```

2648 More turns are performed by changing the arguments under REBELOTE in the  
 2649 input data file (Tab. 3.27), from 42 to 75 in the present case. The resulting energy gain  
 2650 of the proton as a function of RF phase is shown Fig. 3.46. A first graph in Fig. 3.47  
 2651 shows the evolution of its relative rigidity, namely  $D-1$  as a function of distance, with  
 2652  $D = B\rho(s)/BORO$  and  $BORO=64.624444 \text{ kG cm}$  the reference rigidity as defined  
 2653 under OBJET; a second graph shows its orbital radius as a function of distance.

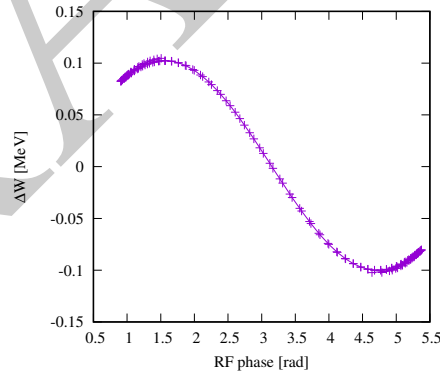
**Fig. 3.44** Radial dependence of the magnetic field over the acceleration range. The field is 0.5 T at a reference radius  $R_0 = 0.5$  m, the slope results from the index  $k = -0.03$ . A graph obtained using zpop: menu 7; 1/1 to open zgoubi.plt; 2/[2,32] for  $B_Z$  versus  $Y$ ; 7 to plot



**Fig. 3.45** Span in phase of the energy gain  $\Delta W = q\hat{V} \sin \phi$  over the acceleration range 200 keV to 5 MeV. The vertical separation of the two  $\Delta W(\phi)$  branches on the left ( $\Delta\phi < 0$  above and  $\Delta\phi > 0$  underneath) is artificial (a “ $-(5-5)/10000$ .” “trick” in the gnuplot script of Tab. 3.27), for the sake of clarity - they actually superimpose



**Fig. 3.46** Span in phase of the energy gain  $\Delta W = q\hat{V} \sin \phi$  over an acceleration and deceleration cycle, starting from 200 keV. The vertical separation of  $\Delta W(\phi)$  branches at the left and right ends is artificial



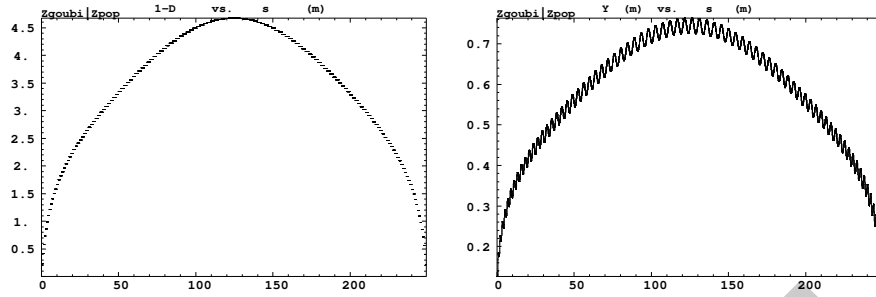


**Fig. 3.47** Left: relative rigidity offset of the proton as a function of distance around the ring, accelerating over half the path, and subsequently decelerating back to the initial energy, under the effect of the cumulated phase-shift. Right: increase first and decrease next of the orbital radius as a function of azimuthal distance

### 2654 3.10 The Cyclotron Equation

2655 Cyclotron model settings of exercise 3.3 are considered in questions (a) to (c),  
 2656 first: two dees, double accelerating gap, uniform field  $B = 0.5$  T. The analytical field  
 2657 modeling DIPOLE [16, *lookup* INDEX] is used.

2658 (a) Simulation data file.

2659 Acceleration is over the energy range  $[0.2, 20]$  MeV, the maximum of  $\cos(\phi)$   
 2660 (Fig. 3.14) is placed at  $E_k = E_{k,m} = 10$  MeV.

2661 The cyclotron equation (Eq. 3.26) can be written under the form

$$\cos \phi = \cos \phi_i - \frac{\pi}{q\hat{V}} \left[ \frac{\omega_{rf}}{2M\omega_{rev}} (E^2 - E_i^2) - (E - E_i) \right] \quad (3.41)$$

2662 where the index  $i$  denotes injection parameters,  $\phi$  is the phase of the RF at particle  
 2663 arrival at the accelerating gap,  $\hat{V}$  is the peak gap voltage,  $E = E_k + M$  is the total  
 2664 energy with  $M$  the rest mass. The value of  $E_k$  at the maximum of  $\cos \phi$  is drawn  
 2665 from  $d(\cos \phi)/dE_k = 0$ , namely

$$E_{k,m} = \left( \frac{\omega_{rev}}{\omega_{rf}} - 1 \right) M \quad (3.42)$$

Taking  $E_{k,m} = 10$  MeV one gets

$$\frac{\omega_{rev}}{\omega_{rf}} \approx 1 + 0.106578, \quad f_{rf} \approx 0.989454\omega_{rev}/2\pi = 7.542209 \text{ MHz}$$

The corresponding input data file is given in Tab. 3.28. Figure 3.48 shows the case of two particles accelerated at a rate of 400 kV per turn, one resulting from an initial phase at the gap of  $\phi_i = \pi/2$  and reaches 20 MeV in about 52 turns, the other resulting from an initial phase  $\phi_i = 3\pi/4$  and reaches 20 MeV in about 64 turns. In the latter case, the  $\pi/4$  phase shift results from an initial path length offset

**Table 3.28** Simulation input data file: the cyclotron equation (Eq. 3.26). This requires a uniform field, for that the [#S\_60degSectorUnifB:#E\_60degSectorUnifB] segment of Tab. 3.6 is INCLUDED, here. Note the PRINT instruction under CAVITE: it causes a print out of CAVITE computational data in zgoubi.CAVITE.out, during the ray tracing, including RF phase and ion energy which can then be plotted (gnuplot script below, called by SYSTEM, and Fig. 3.48). The second particle under OBJET is launched on the closed orbit, its initial phase at the voltage gap is  $\pi/2$ . The first and third particles leave with an initial longitudinal shift  $\delta s = \mp 10.26647$  cm at OBJET resulting in  $\pi/4$  and  $3\pi/4$  initial phase at the voltage gap

```
Cyclotron, classical. Acceleration to 6.02 MeV.
'MARKER' ProbCycloEq_S                               ! Just for edition purposes.
'OBJET'
64.62444403717985                                     ! Reference: 200keV (assuming proton).
2
3 1                                                     ! A single particle.
12.924888 0. 0. 0 -10.266476 1. '2' ! Path length offset +pi/4, initial phase at gap: phi_rf=pi/2-pi/4.
12.924888 0. 0. 0. 0. 1. '1' ! Initial phase at gap is phi_rf=pi/2.
12.924888 0. 0. 0. 10.266476 1. '2' ! Path length offset +pi/4, initial phase at gap: phi_rf=pi/2+pi/4.
1 1 1
'PARTICUL' ! Particle data are necessary as CAVITE is used,
PROTON ! otherwise, by default \zgoubi\ only requires rigidity.
'INCLUDE'
1
3 * ./60degSector.inc[#S_60degSectorUnifB:#E_60degSectorUnifB] ! Uniform field, no index.
'CAVITE' GAP1
7 PRINT ! PRINT: log CAVITE computational dat to zgoubi.CAVITE.out.
0.00 7.54220925334568e6 ! f_rf= 1/T_rev, T_rev at about middle of acceleration range.
200e3 -1.57079632679 ! Peak voltage;, relative phase of 1st cavity.
'INCLUDE'
1
3 * ./60degSector.inc[#S_60degSectorUnifB:#E_60degSectorUnifB] ! Uniform field, no index.
'CAVITE' GAP1
7 PRINT ! PRINT: log CAVITE computational dat to zgoubi.CAVITE.out.
0.00 7.54220925334568e6 ! f_rf= 1/T_rev, T_rev at about middle of acceleration range.
200e3 +1.57079632679 ! Peak voltage;, relative phase of 1st cavity.
'FAISTORE' ! Log particle coordinates at each turn.
zgoubi.fai
1
'REBELOTE' ! K = 99 : coordinates at end of previous pass are used as initial
135 1.1 99 ! coordinates for the next pass ; idem for spin components.
'SYSTEM'
1 ! 1 SYSTEM command follows.
/usr/bin/gnuplot < ./gnuplot_CAVITE.gnu & ! Plot Ek versus phase, as read from zgoubi.CAVITE.out.
'MARKER' ProbCycloEq_E ! Just for edition purposes.
'END'
```

A gnuplot script to obtained Fig. 3.49:

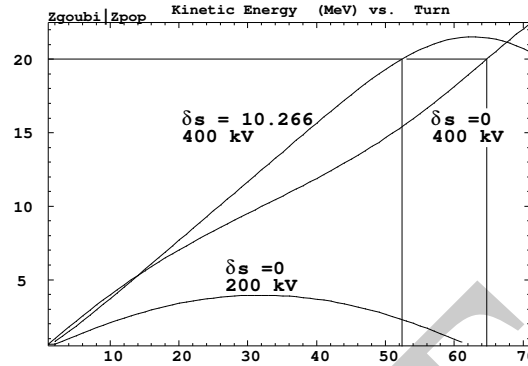
```
# gnuplot_CAVITE.gnu
set xlabel "E_k [MeV]" ; set ylabel "cos({/Symbol f})"; set xtics; set ytics mirror
pi = 4. * atan(1.); E0 = 938.2720813; qV=400e-3; Ei=0.2; E_km = 10 # locate max of cos(phi) at 10 MeV
omgR = 1. / (1. + E_km/E0); mxTurn=80
plot [0.2:20] [-1.1:1.8] for [i=2:1:-1] \
'zgoubi.CAVITE.Out' u ($5=i && $6<mxTurn? $10 :1/0):(cos($11)) w pt i+4 ps .5 notit \
cos(pi/2.) +pi*(1.-omgR*(1.+(x+Ei)/(2*E0))) *(x-Ei)/(.*qV) w l lw 2 lc rgb "blue" \
tit "V/gap=200kV, {/Symbol f}_0={/Symbol p}/2" \
cos(3*pi/4.)+pi*(1.-omgR*(1.+(x+Ei)/(2*E0))) *(x-Ei)/(.*qV) w l lw 2 lc rgb "red" \
tit "{/Symbol f}_0={/Symbol 3p}/4" \
```

$$\delta s = \beta c T_{\text{rf}} / 4 = 10.26647 \text{ cm}$$

2666 as specified under OBJET ( $\beta c = 0.020648c$  is the proton velocity at  $E_i = 200$  keV),  
 2667 yielding  $\delta\phi = \omega_{\text{rf}}\delta s / \beta c = \pi/4$ . A third curve in the figure is for to 200 kV voltage  
 2668 and initial phase at gap  $\phi = \pi/2$ , in that case  $\cos(\phi)$  reaches the value of 1 at about  
 2669 4 MeV, 32 turns, and the particle starts decelerating.

2670 (b) Energy-phase relationship.

**Fig. 3.48** Proton energy versus turn, case of (Tab. 3.28) voltage 400 kV/turn, two protons with initial phase respectively  $\pi/2$  ( $\delta s = 0$ ) and  $3\pi/4$  ( $\delta s = 10.26647$  cm), which make it up to 20 MeV and beyond. The third case case, voltage 200 kV/turn, initial phase  $\pi/2$  ( $\delta s = 0$ ), features a maximum energy of 4 MeV and deceleration from there on. A graph obtained using zpop: menu 7; 1/5 to read from zgoubi.fai; 2/[39,2] for Y versus turn



2671 A graph of the energy-phase relationship obtained by ray tracing, for  $\phi_i = \frac{3\pi}{4}$  and  
 2672  $\frac{\pi}{2}$  at the three different gap voltages  $\hat{V} = 100, 200$  and  $400$  kV, is given in Fig. 3.49,  
 2673 together with theoretical expectations (Eq. 3.26).

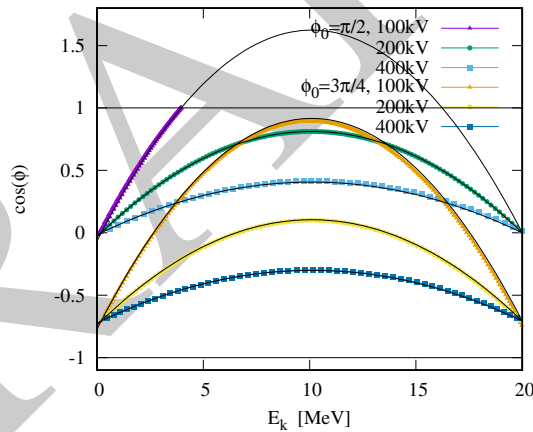


**Fig. 3.49** A graph of the energy dependence of the arrival phase at the voltage gap, for a few different values of gap voltage  $\hat{V}$  and initial phase  $\phi_i$ . Markers are from raytracing, using the input data file of Tab. 3.28 repeatedly for the various values of  $\hat{V}$  and  $\phi_i$ . Superimposed solid lines are from theory (Eq. 3.26 and Fig. 3.14)

### 2674 3.11 Cyclotron Extraction

2675 (a) Distance between turns.

2676 Simulation input data of exercise 3.3, Tab. 3.8, can be referred to as a guidance  
 2677 to build the present simulation file.

2678 A proton is accelerated in 26 turns, in a uniform field  $B_0 = 0.5$  T, from 20 keV  
 2679 (rigidity  $BORO \times D = 0.064624444 \times 0.3162126 = 0.0204350634608$  T m, injection  
 2680 radius  $Y_0 = BR/B_0 = 4.08701269216$  cm) to 5.02 MeV. The RF phase is ignored



2681 thus CAVITE[IOPT=3] is used, with a 100 kV gap voltage. The input data file for  
2682 this simulation is given in Tab. 3.29.

**Table 3.29** Simulation input data file: accelerating a proton to check evolution of  $\Delta R/R$ , in a dipole field with index. The #S\_180degSectorUnifB to #E\_180degSectorUnifB segment of Tab. 3.6 is INCLUDED

```

Cyclotron extraction. Uniform field.
'MARKER' ProbdRRUnifB_S ! Just for edition purposes.
'OBJET'
64.62444403717985 ! Reference: 200keV (assuming proton).
2
1 1 ! A single particle.
4.08791 0. 0. 0. 0.3162126 'o' ! p[MeV/c]= 6.126277, Brho[kG.cm]=20.435, kin-E[MeV]=0.02.
1
! 4.003593 0. 0. 0. 0.3162126 'o' ! Brho[kG.cm]=20.435, kin-E[MeV]=0.02, case of field with index.
'PARTICUL' ! Particle data are necessary as CAVITE is used,
PROTON ! otherwise, by default \zgoubi\ only requires rigidity.
'INCLUDE'
1
./180degSector.inc[#S_180degSectorUnifB:#E_180degSectorUnifB] ! one 180 deg sector, uniform field.
'FAISTORE'
zgoubi.fai ! Log current particle coordinates, in zgoubi.fai.
1
'CAVITE' cavity ! Accelerating gap.
3 ! In this option, dW = qVsin(phi_s), independent of time.
0. 0.
100e3 1.57079632679
'INCLUDE'
1
./180degSector.inc[#S_180degSectorUnifB:#E_180degSectorUnifB] ! one 180 deg sector, uniform field.
'FAISCEAU' ! Particle coordinates before gap.
'CAVITE' cavity ! Accelerating gap.
3 ! In this option, dW = qVsin(phi_s), independent of time.
0. 0.
100e3 1.57079632679
'REBELOTE' ! K = 99 : coordinates at end of previous pass are used as initial
25 1.1 99 ! coordinates for the next pass ; idem for spin components.
'FAISCEAU' ! Local particle coordinates logged in zgoubi.res.
'SYSTEM'
2 ! ! SYSTEM command follows.
/usr/bin/gnuplot < ./gnuplot_Zplt_UnifB.gnu & ! Plot accelerated orbits.
/usr/bin/gnuplot < ./gnuplot_Zfai_dRR.gnu & ! Plot delta_R(R).
'MARKER' ProbdRRUnifB_E ! Just for edition purposes.
'END'

```

A *gnuplot* script to obtain the accelerated orbit of Fig. 3.50:

```

# gnuplot_Zplt_UnifB.gnu
set xtics ; set ytics ; set xlabel "X_{Lab} [m]" ; set ylabel "Y_{Lab} [m]"
set size ratio 1 ; set polar ; cm2m = 0.01 ; pi = 4.*atan(1.)
set arrow from 0, 0 to 0.7, 0 nohead linecolor "red" lw 6 ; set arrow from 0, 0 to -0.65, 0 nohead linecolor "blue" lw 6
noel_1=5 ; noel_2=10 # 1st DIPOLE is element $42=noel_1; 4th DIPOLE is $42=noel_2. $42=column number in zgoubi.plt.
plot "zgoubi.plt" u ($42< noel_2? $22 +pi/3.*(($42-noel_1)/2) :1/0):($10 *cm2m) w p pt 5 ps .2 lc rgb "black" notit , \
"zgoubi.plt" u ($42->noel_2? $22+pi+pi/3.*(($42-noel_2)/2) :1/0):($10 *cm2m) w p pt 5 ps .2 lc rgb "black" notit; pause 1

```

A *gnuplot* script to obtain the turn separation curves of Fig. 3.50. In this script, *zgoubi.fai2* is a copy of *zgoubi.fai* (see exercise 3.3) in which the first particle data line (particle data at the first pass) has been removed. This allows drawing the difference  $\Delta R$  between two successive passes, using the "paste" command (see Tab. 3.8 for a similar 1-row shift using *awk* commands):

```

# gnuplot_Zfai_dRR.gnu
set xtics; set ytics mirror; set key maxrow 2 ; set xlabel "R [cm]" ; set ylabel "{/Symbol D}R [cm]"
set key r c; set logscale y; unset colorbox
plot [8:65] "paste zgoubi.fai2 zgoubi.fai" u ($10):($10-$63) w p pt 7 ps 1.5 lc rgb "black" tit "num." , \
"zgoubi.fai2" u ($10):($10./($38-1)) w l lc rgb "red" tit "theory" ; pause 1

```

2683 The accelerated orbit and the distance  $\Delta R$  between turns are displayed in Fig. 3.50.  
 2684 Theoretical expectation (Eq. 3.27) in the case of slow acceleration (typically, the fixed  
 2685 energy closed orbit configuration of Fig. 3.21) is also displayed, for comparison.

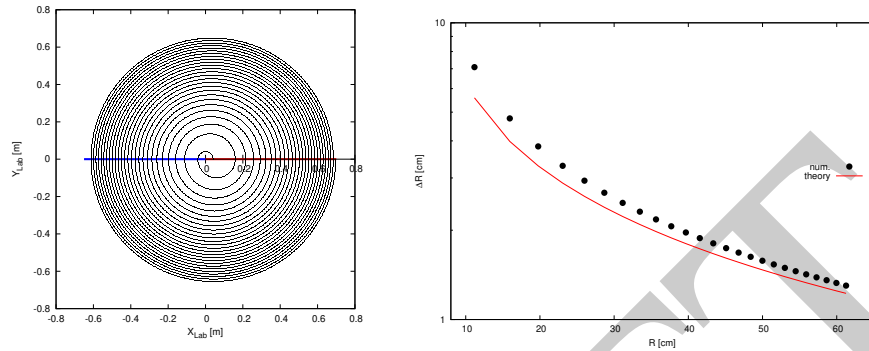


**Fig. 3.50** Left: accelerated orbit from 20 keV to 5.02 MeV, at a rate of 200 keV per turn over 26 turns, in a uniform field. The thick horizontal line (colored) figures the accelerating gap. Right: the resulting dependence of orbit separation  $\Delta R$  on radius, from raytracing (markers) and from theory (solid line); the theoretical curve assumes small  $dE$  (adiabatic acceleration, concentric orbits), which is not quite the case here with  $\Delta E = 200$  keV/turn

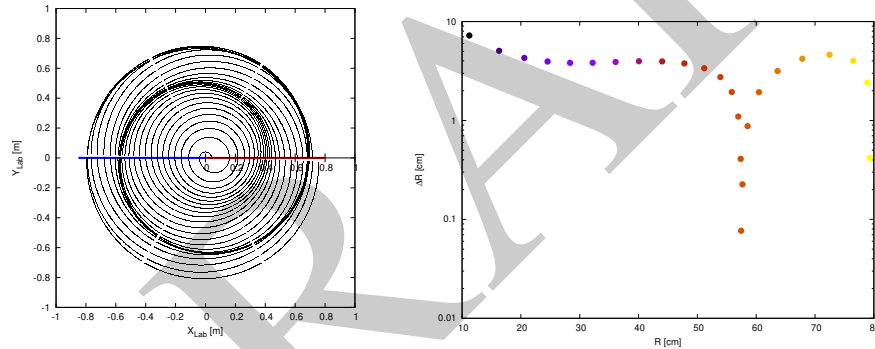


**Fig. 3.51** Left: accelerated orbit from 20 keV to 5.02 MeV, at a rate of 200 keV per turn over 26 turns, in a dipole field with index. The thick horizontal line (colored) figures the accelerating gap. Right: the resulting dependence of orbit separation  $\Delta R$  on radius, observed at the second gap

2686 (b) Beam losses.

2687 Indications to solve this exercise:

- 2688 - a beam with Gaussian momentum distribution and *rms* momentum spread  
 2689  $\delta p/p = 10^{-3}$  can be defined using MCOBJET,  
 2690 - use REBELOTE to accelerate over a given number of turns,  
 2691 - an extraction septum placed half-way between two successive turns can be  
 2692 simulated using COLLIMA, placed after REBELOTE (the execution pointer will

2693 quietly continue beyond REBELOTE do-loop once the latter is completed). COL-  
 2694 LIMA counts particles stopped. FAISTORE (or FAISCNL) can be placed after  
 2695 COLLIMA, to log particle data: particles stopped by COLLIMA have their IEX tag  
 2696 set to IEX=-4 [16, *lookup* COLLIMA].

2697 Change the value of NPASS under REBELOTE for a different number of accel-  
 2698 erated turns, and COLLIMA positioning data accordingly.

2699 (c) Change the field index.

2700 The cyclotron model of Tab. 3.21 is used here, reference field  $B_0 = 5$  kG on the  
 2701 200 keV orbit, and field index  $k=-0.03$ . A proton is accelerated over 26 turns, from  
 2702 20 keV to 5.02 MeV, as in question (a). The 20 keV closed orbit radius (taken as the  
 2703 injection radius) differs from question (a) due to the index  $k=-0.03$ , and can be found  
 2704 using a FIT procedure (Tab. 3.30); it comes out to be  $Y_0 = 4.0040586$  cm.

2705 The input data file for this exercise is given in Tab. 3.31.

**Table 3.30** Simulation input data file: finding the 20 keV injection radius in the presence of a non-zero index  $k$ , using FIT The INCLUDE segment is taken from Tab. 3.21

```

Cyclotron, classical. Find injection radius for k=-0.03
'OBJET'
64.62444403717985                                ! Reference: 200keV (assuming proton).
2
1 1                                                ! A single particle.
4.0040586 0. 0. 0. 0. 0.3162126 'o'                ! p[MeV/c]= 6.126277, Brho[kG.cm]=20.435, kin-E[MeV]=0.02.
1
! 4.003593 0. 0. 0. 0. 0.3162126 'o' ! Brho[kG.cm]=20.435, kin-E[MeV]=0.02, case of field with index.
'PARTICUL'
PROTON
'INCLUDE'
1
./60DegSectorR200.inc[#S_60DegSectorR200:#E_60DegSectorR200] ! One 60 deg sectors with index.
'FIT'
1                                                ! 1 variable:
1 30 0 1.                                         ! variable is Y0 (parameter 30) under OBJET (keyword 1 in the sequence).
2                                                ! 2 constraints:
3.1 1 2 #End 0. 1. 0                               ! constraint 1: final Y = Y0.
3 1 3 #End 0. 1. 0                               ! constraint 2: final T = 0.
'END'

```

2706 The resulting proton trajectory is displayed in Fig. 3.51 (the gnuplot script given in  
 2707 Tab. 3.31 is used). The greatly different accelerated orbit in this case, compared to the  
 2708 uniform field case in (a) (Fig. 3.50), results from a modulation of the distance between  
 2709 turns, which is an effect of the oscillation motion undergone by the accelerated orbit  
 2710 (around the local on-momentum half-circle orbit arc). This effect may be exploited  
 2711 to increase extraction efficiency, by causing such a radial modulation as to maximize  
 2712 turn separation at the location of the septum [17].

2713 (d) Optimize extraction.

2714 The modulation is minimized (or enhanced possibly, at the last turn, for minimized  
 2715 losses at extraction) by optimizing the injection conditions  $(x_0, x_0')$ .

**Table 3.31** Simulation input data file: accelerating a proton to check evolution of  $\Delta R/R$ , in a dipole field with index. The [#S\_60DegSectorR200:#E\_60DegSectorR200] segment of Tab. 3.21 is INCLUDED

```

Cyclotron extraction. Field with index.
'MARKER' ProbdRRIdx_S                                ! Just for edition purposes.
'OBJET'
64.62444403717985                                    ! Reference: 200keV (assuming proton).
2
1 1                                                    ! A single particle.
4.0040586 0. 0. 0. 0. 0.3162126 'o'                ! p[MeV/c]= 6.126277, Brho[kG.cm]=20.435, kin-E[MeV]=0.02.
1
! 4.003593 0. 0. 0. 0. 0.3162126 'o' ! Brho[kG.cm]=20.435, kin-E[MeV]=0.02, case of field with index.
'PARTICUL'                                           ! Particle data are necessary as CAVITE is used,
PROTON                                               ! otherwise, by default \zgoubi\ only requires rigidity.
'INCLUDE'
1
3* ./60DegSectorR200.inc[#S_60DegSectorR200:#E_60DegSectorR200] ! Three 60 deg sectors with index.

'FAISTORE'
zgoubi.fai                                           ! Log current particle coordinates, in zgoubi.fai.
1

'CAVITE' cavity                                     ! Accelerating gap.
3                                                    ! In this option, dW = qVsin(phi_s), independent of time.
0. 0.
100e3 1.57079632679
'INCLUDE'
1
3* ./60DegSectorR200.inc[#S_60DegSectorR200:#E_60DegSectorR200] ! Three 60 deg sectors with index.

'FAISCEAU'
'CAVITE' cavity                                     ! Accelerating gap.
3                                                    ! In this option, dW = qVsin(phi_s), independent of time.
0. 0.
100e3 1.57079632679

'REBELOTE'                                           ! K = 99 : coordinates at end of previous pass are used as initial
25 1.1 99                                           ! coordinates for the next pass ; idem for spin components.
'FAISCEAU'
'SYSTEM'
2                                                    ! 1 SYSTEM command follows.
/usr/bin/gnuplot < ./gnuplot_Zplt.gnu &             ! Plot accelerated orbits.
/usr/bin/gnuplot < ./gnuplot_Zfai_DR.gnu &          ! Plot delta_R(R).
'MARKER' ProbdRRIdx_E                                ! Just for edition purposes.
'END'

```

A gnuplot script to obtain the accelerated orbit of Fig. 3.51:

```

# gnuplot_Zplt.gnu
set xtics ; set ytics ; set xlabel "X_{Lab} [m]" ; set ylabel "Y_{Lab} [m]"
set size ratio 1 ; set polar ; cm2m = 0.01 ; pi = 4.*atan(1.)
set arrow from 0, 0 to 0.8, 0 nohead linecolor "red" lw 6 ; set arrow from 0, 0 to -0.85, 0 nohead linecolor "blue" lw 6
noel_1=4 ; noel_2=12 # 1st DIPOLE is element $42=noel_1; 4th DIPOLE is $42=noel_2. $42=column number in zgoubi.plt.
plot "zgoubi.plt" u ($42< noel_2? $22 -pi/3.*((($42-noel_1)/2):1/0):($10 *cm2m) w p pt 5 ps .2 lc rgb "black" notit , \
"zgoubi.plt" u ($42>noel_2? $22+pi+pi/3.*((($42-noel_2)/2) :1/0):($10 *cm2m) w p pt 5 ps .2 lc rgb "black" notit; pause 1

```

A gnuplot script to obtain the turn separation curves of Fig. 3.51. In this script, *zgoubi.fai2* is a copy of *zgoubi.fai* in which the first particle data line (particle data at the first pass) has been removed. This allows drawing the difference  $\Delta R$  between two successive passes, using the "paste" command - see Tab. 3.8 for a similar 1-row shift using *awk* commands:

```

# gnuplot_Zfai_DR.gnu
set xtics ; set ytics mirror ; set key maxrow 2 ; set xlabel "R [cm]" ; set ylabel "{Symbol D}R [cm]"
set key r c ; set logscale y ; unset colorbox
plot "<paste zgoubi.fai2 zgoubi.fai" u ($10):($10-$63):($10) w p pt 7 ps 1.5 lw .1 lc palette notit ; pause 1

```

### 2716 3.12 Acceleration and Extraction of a 6-D Polarized Bunch

2717 This simulation can be set up using material drawn from previous exercises. It is  
2718 not fully developed here, guidelines are given.

2719 The cyclotron simulation hypotheses of exercise 3.10-a are considered, the input  
2720 data file for this exercise can be built from that of Tab. 3.28, with a few modifications,  
2721 namely:

2722 - downstream of REBELOTE, add a 1 meter DRIFT: an embryo of an “high  
2723 energy line” into which the bunch is steered at extraction;

2724 - that DRIFT is preceded by CHANGREF to center the current reference frame on  
2725 the final coordinates  $Y$  and  $T$  of the accelerated orbit; the latter have to be determined  
2726 by prior raytracing;

2727 - add histograms (to be logged in zgoubi.res) for observation of transverse and  
2728 longitudinal particle coordinate densities in the bunch at extraction. This uses HISTO,  
2729 as many times as needed.

### 2730 References

- 2731 1. Sessler, A., Wilson, E.: Engines of Discovery. A century of particle accelerators. World  
2732 Scientific (2007)
- 2733 2. Lawrence, E.O., Livingston, M.S. Phys. Rev. 37, 1707 (1931), 1707; Phys. Rev. 38, 136,  
2734 (1931); Phys. Rev. 40, 19 (1932)
- 2735 3. Credit: Lawrence Berkeley National Laboratory. ©The Regents of the University of California,  
2736 Lawrence Berkeley National Laboratory
- 2737 4. Lawrence, E.O. and Livingston, M.S.: The Production of High Speed Light Ions Without the  
2738 Use of High Voltages. Phys. Rev. 40, 19-35 (1932)
- 2739 5. Livingston, M.S., McMillan, E.M.: History of the cyclotron. Physics Today, 12(10) (1959).  
2740 <https://escholarship.org/uc/item/29c6p35w>
- 2741 6. Bethe, H. E., Rose, M. E.: Maximum energy obtainable from cyclotron. Phys. Rev. 52 (1937)  
2742 1254
- 2743 7. Cole, F.T.: O Camelot ! A memoir of the MURA years (April 1, 1994).  
2744 <https://accelconf.web.cern.ch/c01/cyc2001/extra/Cole.pdf>
- 2745 8. Thomas, L.H.: The Paths of Ions in the Cyclotron. Phys. Rev. 54, 580, (1938).  
2746 Craddock, M.K.: AG focusing in the Thomas cyclotron of 1938. Proceedings of PAC09,  
2747 Vancouver, BC, Canada, FR5REP1
- 2748 9. Stambach, T.: Introduction to Cyclotrons. CERN accelerator school, cyclotrons, linacs and  
2749 their applications. IBM International Education Centre, La Hulpe, Belgium, 28 April-5 May  
2750 1994.
- 2751 Fig. 3.4: Stambach, T.: Introduction to Cyclotrons. CERN Yellow Re-  
2752 port 96-02 (1996), Figure 8, page 15. Copyright/License CERN CC-BY-3.0  
2753 <https://creativecommons.org/licenses/by/3.0>, no change to the material
- 2754 10. Baron, E., et al.: The GANIL Injector. Proceedings of the 7th International Conference on  
2755 Cyclotrons and their Applications, Zürich, Switzerland (1975).  
2756 <http://accelconf.web.cern.ch/c75/papers/b-05.pdf>
- 2757 11. Cohen, L.B.: Cyclotrons and Synchrocyclotrons. In Encyclopedia of Physics, Vol. XLIV,  
2758 Nuclear Instrumentation I. Editor S. Flügge. Springer-Verlag, 1959
- 2759 12. Le Duff, J.: Longitudinal beam dynamics in circular accelerators. CERN Accelerator School,  
2760 Jyväskylä, Finland, 7-18 September 1992
- 2761 13. Montague, B.W.: Polarized beams in high energy storage rings. Phys. Rep. (Rev. Sect. Phys.  
2762 Lett.) 113(1), 1-96 (1984)

- 2763 14. Thomas Roser, Anatoli Zelensky, private communication, BNL, June 2021.  
2764 Günther Clausnitzer: History of Polarized Ion Source Developments. In: International Work-  
2765 shop on Polarized Ion Sources and Polarized Gas Jets, February 12-17, 1990, KEK, Tsukuba,  
2766 Japan. KEK Report 90-15, November 1990, edited by Y. MORI.  
2767 [https://inis.iaea.org/collection/NCLCollectionStore/\\_Public/22/051/22051667.pdf](https://inis.iaea.org/collection/NCLCollectionStore/_Public/22/051/22051667.pdf)  
2768 15. Méot, F.: Spin Dynamics. In: Polarized Beam Dynamics and Instrumentation in Particle  
2769 Accelerators, USPAS Summer 2021 Spin Class Lectures, Springer Nature, Open Access  
2770 (2023).  
2771 <https://link.springer.com/book/10.1007/978-3-031-16715-7>  
2772 16. Méot, F.: Zgoubi Users' Guide. <https://www.osti.gov/biblio/1062013-zgoubi-users-guide>.  
2773 Sourceforge latest version: <https://sourceforge.net/p/zgoubi/code/HEAD/tree/trunk/guide/Zgoubi.pdf>  
2774 17. Stambach, T.: Introduction to Cyclotrons. CERN accelerator school, cyclotrons, linacs and  
2775 their applications. IBM International Education Centre, La Hulpe, Belgium, 28 April-5 May  
2776 1994.

DRAFT